Modelling the Late Devonian Climate: Implications for evolution and extinction

Claudia Mack

Wolfson College
Department of Physics and Earth Science

A thesis submitted for the degree of
Doctor of Philosophy

January 27, 2021

UNIVERSITY OF
OXFORD

Abstract

The Devonian period (419.2 - 358.9 Ma) was characterised by a warm greenhouse climate which transitioned towards glaciation throughout the Late Devonian. This period in Earth's history was punctuated by repeated environmental and biotic crises. A common feature accompanying these events was widespread ocean anoxia, typically recorded in the geological record by periodic organic-rich laminated shales. However, the relationship between climate, evolution and extinction in the Late Devonian remains unclear.

In the first part of this thesis, Late Devonian (375 Ma) boundary conditions are applied to an Ocean General Circulation Model (OGCM) forced by monthly atmospheric surface forcing to determine ocean circulation and likely regions of ocean anoxia. The model simulation oscillates between two quasi-stable states: (1) an unventilated phase where the ocean circulation is dominated by shallow tropical/sub-tropical cells; (2) a ventilated phase with globally strong deep ocean overturning. In the second part of this thesis, Late Devonian boundary conditions are applied to a Coupled Atmosphere-Ocean-Ice General Circulation Model (CGCM) and an Atmospheric Slab Ocean General Circulation Model (ASGCM). Comparisons of the atmospheric results highlight the importance of a dynamic ocean in transporting heat polewards. The CGCM ocean also exhibits two ocean states, although the 'unventilated' equivalent is termed the partly-ventilated state since there is a weak, deep overturning circulation restricted to the Northern Hemisphere.

In this state the deep ocean is anoxic globally, and subsequently during the ventilated state there is a global deep overturning circulation where the deep ocean is ventilated and oxic. Unlike the OGCM, the air-sea interactions of the CGCM mean the ocean stays ventilated, and there is no oscillation between states. The results of the CGCM are consistent with the geological record. The climate in which tetrapods evolved is discussed, and mechanisms for Late Devonian extinction considered with the aid of the CGCM. The results suggest that anoxia is plausible as a kill mechanism for Late Devonian extinctions. However, future work could consider other hypotheses of extinction, including changes in astronomical forcing and atmospheric pCO_2 concentration due to volcanic outgassing.

Acknowledgements

Firstly my thanks go to my supervisors Raymond Pierrehumbert and Helen Johnson, for their support, guidance and mentorship. Thank you for your enthusiasm, attention to detail and countless helpful discussions, ideas and suggestions. Thank you to the wider Devonian research group including Steve Balbus, Tomos David, Per Ahlberg, Mattias Green, Hannah Byrne and Hannah Davies for interesting discussions and insights into Devonian tides, tetrapods and tectonics. In particular thanks to Mattias Green for meeting with me on several occasions to discuss the tidal simulations and my results. Special thanks go to all current and past members of the Ocean Climate Group, who have always been friendly, and helpful.

My research, of course would not be possible without financial support from NERC, as well as access to to the UK national supercomputer ARCHER. I would like to thank Yavor Kostov for always being willing to help when trying to first setup MITgcm locally on the University of Oxford physics server, and then later both Yavor and David Ferreira for help setup the MITgcm coupled atmosphere-ocean-sea-ice model and resolve runtime issues on ARCHER.

I thank my parents, brother, sister and extended family for their love and unending support. Finally, I thank my husband, Josh, for encouraging me throughout my BSc, MSc, and DPhil, discussing my research with me, and for the exciting projects outside of work.

Contents

1 Introduction **1**

1.1 The Devonian Climate and Extinction 1

1.1.1 Devonian Continental Configuration 6

1.1.2 Evolution in the Devonian 8

1.1.3 Equatorial Ocean Dynamics 10

1.2 Energy and General Circulation in the Ocean 11

1.2.1 Mixing in the Ocean 13

1.2.2 Circum-navigating Currents 14

1.3 Thesis Aims and Outline 16

2 MITgcm Setup **20**

2.1 Resolution 21

2.2 MITgcm Ocean Model 21

2.2.1 Continent Outline and Bathymetry 23

2.2.2 Atmospheric Surface Forcing 25

2.2.3 Initial Conditions 27

2.2.4 Mixing Parameterisations 28

2.2.5 Biogeochemistry 28

2.2.6 Tidal Mixing 30

2.2.7 Model Performance 31

2.3 MITgcm Atmospheric Model 32

2.3.1 Convection 33

2.3.2 Large Scale Condensation . . . 33
2.3.3 Cloud Cover . . . 33
2.3.4 Shortwave Radiation . . . 33
2.3.5 Longwave radiation . . . 33
2.3.6 Surface fluxes of momentum and energy . . . 34
2.3.7 Vertical diffusion . . . 34
2.3.8 Ice Package . . . 34
2.3.9 Boundary Conditions . . . 34
2.4 Coupled Atmosphere-Ocean-Ice Model . . . 37
2.5 Summary . . . 38

3 Ocean General Circulation Model 39
3.1 Unventilated phase . . . 40
3.2 Ventilated phase . . . 51
3.3 Transition to Ventilated Phase . . . 53
3.4 Transition to Unventilated phase . . . 57
3.5 Discussion: Frasnian-Famennian Extinction . . . 59
3.6 Model Limitations . . . 64
3.7 Summary . . . 64

4 Ocean Circulation with variable mixing 66
4.1 Ocean General Circulation Model with vertically different diapycnal diffusivity (OGCMvert) . . . 68
4.2 Ocean General Circulation Model with spatially variable diapycnal diffusivity (OGCMmix) . . . 68
4.3 Summary . . . 73

5 Coupled Ocean-Atmosphere-Sea-Ice 74
5.1 Atmospheric Surface Conditions in the ASGCM, CGCM and De Vleeschouwer simulations . . . 75
5.2 Ocean . . . 78
5.2.1 Partly-ventilated State . . . 79

5.2.2 Ventilated State 83
5.2.3 Transition Partly-ventilated - Ventilated 87
5.3 Coupled Model Ocean Vs OGCM 94
5.4 Atmosphere 99
5.4.1 Atmospheric Tropical Circulation 99
5.4.2 Monsoons 107
5.4.3 Midlatitudes 108
5.4.4 Heat Transport 111
5.5 Impact of coupling to a Dynamic Atmosphere 114
5.6 Implications for the Devonian 116
5.7 Model Uncertainties 126
5.7.1 Atmospheric Component 127
5.7.2 Boundary Conditions 128
5.7.3 Ocean Component 129
5.8 Summary 130

6 Conclusions and Future Work **131**
6.1 Conclusions 131
6.2 Future Work 137

References **140**

List of Figures

1.1 Key evolutionary and extinction events in the Late Silurian and Devonian period, including low latitude paleotemperature reconstructions and modelled atmospheric O_2 and CO_2. 3
1.2 Approximate palaeogeographic locations of known study sites of the Late Devonian Kellwasser Anoxia Event and F-F extinction horizons, and principal tetrapod body fossil and track locations. 5
1.3 Paleomap of the Late Devonian (379.9 Ma), Mollweide projection, sea level +120 m maximum flooding surface (Blakey, 2018). 7

2.1 Logical arrangement of the cube sphere grid topology with the 32×192 domain divided into six 32×32 tiles. 22
2.2 Late Devonian continental configuration based on Blakey (2018) (green). Ocean bathymetry in the model is indicated by the blue shading: paler colour indicates the continental slope, and the dotted grey line marks the point at which the slope reaches the flat deep-ocean floor. 24
2.3 Annual mean surface forcing fields, calculated from the De Vleeschouwer et al. (2014) Late Devonian (Frasnian) atmospheric simulation with slab ocean. 26
2.4 Spatially varying depth mean diapycnal diffusivity in the deep ocean calculated from Late Devonian tidal dissipation energy ($m^2\,s^{-1}$). 30
2.5 Late Devonian topography used in atmospheric simulations. 36
2.6 Late Devonian land surface types and biomes. 36

3.1 100-year average, zonal mean properties of density, temperature and salinity in the Late Devonian ocean for both the unventilated phase and ventilated phase. 42
3.2 100-year and upper 300m average currents during unventilated and ventilated phase shown against upper ocean velocity and average upper 300m temperature. 43
3.3 100-year mean zonally averaged residual overturning circulation. 4000 years, during the unventilated phase; 5000 years, during the ventilated phase. . . 44
3.4 100-year mean ocean surface mixed layer depth after 4000 years, during the unventilated phase; 5000 years, during the ventilated phase. 45
3.5 OGCM Zonal mean zonal velocity during unventilated and ventilated phase 47
3.6 OGCM Equatorial zonal velocity and temperature during the unventilated phase. 48
3.7 Meridional energy transport in the ocean: total heat transport, bolus heat transport, overturning heat transport and gyre heat transport during both the unventilated phase and ventilated phase. 51
3.8 Time series of mean potential density referenced to the surface; mean potential temperature and, mean salinity averaged in the region of first convection north west of Siberia. 55
3.9 Time series of salt transport, freshwater content, heat transport, heat content below 200 m, the density difference between surface and 800 m water depth, mass transport above 1000 m water depth and mixed layer depth north of 60 ° N where deep global convective mixing is initiated. . . 56
3.10 Schematic showing conditions in the North Panthalassa Ocean during unventilated and ventilated states and a schematic of the global MOC during the unventilated phase. 58
3.11 OGCM surface biogeochemistry during the unventilated and ventilated phase. 61
3.12 OGCM zonal mean DO during the unventilated and ventilated phase. . . 62

4.1 100 year and zonal mean of the global residual overturning circulation in the OGCMvert experiment. 69

4.2 Time series comparison of Northern Hemisphere parameters to diagnose unventilated and ventilated phases between OGCM,OGCMmix, and OGCMvert 70

4.3 100 year and zonal mean of the global residual overturning circulation when the model uses a spatially variable diapycnal diffusivity calculated from OTIS tidal dissipation estimate. 71

5.1 Annual and zonal mean atmospheric surface conditions between Vleeschouwer, ASGCM and CGCM. 76

5.2 Zonal mean properties of the CGCM ocean; comparison of the partly-ventilated state and the ventilated state. Showing zonal mean potential density, zonal mean temperature and zonal mean salinity. 81

5.3 Comparison of the 100 year mean partly-ventilated state and ventilated state upper 500 m velocity vectors with velocity and temperature colour shading. 82

5.4 100 year and zonal mean CGCM ocean residual overturning circulation during the partly-ventilated state and the ventilated state. 84

5.5 100 year mean CGCM mixed layer depth in the CGCM during unventilated and ventilated state. 84

5.6 100 year and zonal mean CGCM ocean residual overturning circulation in the Paleo Tethys and Rheic Oceans during partly-ventilated state and ventilated state. 85

5.7 100 year and zonal mean of atmospheric zonal wind and ocean zonal velocity during the ventilated state. 88

5.8 100 year mean of temperature along the equator in the atmosphere and ocean during the ventilated state. 89

5.9 100 year mean of equatorial atmospheric zonal wind and ocean zonal velocity during the ventilated state. 90

5.10 Time series of the atmosphere's role in the transition to ventilated ocean, showing atmospheric freshwater supply and atmospheric surface temperature in the north high latitudes. 91

5.11 CGCM time series of the salt transport, freshwater content, heat transport, heat content below 200 m, the density difference between surface and 800 m water depth, mass transport above 1000 m water depth and mixed layer depth north of 60 ° N where deep global convective mixing is initiated. . . 92
5.12 CGCM time series of mean potential density, temperature and salinity north of 55 ° N 93
5.13 Time series of coupled model atmospheric surface temperature and ocean Sea Surface Temperature (SST) mean globally, in the Northern Hemisphere high-latitudes, tropics, and Southern Hemisphere high latitudes. 95
5.14 Zonal mean CGCM minus OGCMduring the partly-ventilated/unventilated states for zonal mean temperature and zonal mean salinity. 97
5.15 Zonal mean CGCM minus OGCMduring the ventilated states for zonal mean temperature and zonal mean salinity. 98
5.16 DJF comparison of atmospheric Eularian mean Meridional Overturning Circulation (MOC). in the CGCM and ASGCM simulations. 100
5.17 JJA comparison of atmospheric Eularian mean MOC. in the CGCM and ASGCM simulations 101
5.18 100 year mean meridional overturning circulation in the atmosphere and ocean in the ventilated state of the CGCM. 102
5.19 Annual mean comparison of atmospheric Eularian mean MOC between the CGCM and ASGCM. 103
5.20 DJF comparison between CGCM, ASGCM and De Vleeschouwer et al. (2014) simulations of precipitation and zonal wind. 105
5.21 JJA comparison between CGCM, ASGCM and De Vleeschouwer et al. (2014) simulations of precipitation and zonal wind. 106
5.22 Locations of simulated Late Devonian monsoon systems. 107
5.23 Comparison of December-January-February (DJF) and June-July-August (JJA) of CGCM atmosphere precipitation and surface meridional wind. . 108

5.24 Monthly mean precipitation, 900 mbar wind vectors, and surface temperature for Late Devonian Monsoon systems. Precipitation and surface temperature in the East Gondwana Monsoon, region, South East Laurussia Monsoon region and in the West Laurussia Monsoon region. 109

5.25 CGCM absorbed solar radiation and outgoing longwave radiation compared to poleward energy transport calculated from top of the atmosphere energy budget and atmosphere minus ocean heat fluxes. 113

5.26 ASGCM absorbed solar radiation and outgoing longwave radiation compared to poleward energy transport calculated from top of the atmosphere energy budget and atmosphere minus ocean heat fluxes. 114

5.27 Modelled evaporation minus precipitation and SST comparison with approximate location of lithic indicators of palaeoclimate and primary tetrapod evolution sites. 117

5.28 Coupled ocean 100 year mean surface biogeochemistry during both partly-ventilated and ventilated state. Showing, Biological productivity, dissolved O_2, DIC and PO_4. 119

5.29 Coupled ocean 100 year, zonal mean dissolved O_2 during partly-ventilated and ventilated state 120

5.30 Coupled ocean 200 year, zonal mean dissolved O_2 during partly-ventilated and ventilated state in the Paleo Tethys and Rheic Oceans 122

5.31 Coupled ocean 200 year dissolved O_2 during the ventilated state at a depth of 290 m, this corresponds to the average depth of isotopic evidence of anoxia/euxinia, the approximate location of which are marked on the map. 124

5.32 Annual mean sea-ice thickness comparison between pCO_2 2180 ppm and 370 ppm 128

List of Tables

2.1 Vertical grid used in Massachusetts Institute of Technology General Circulation Model (MITgcm) ocean configuration. 24
2.2 Parameter values used for the physical component of ocean model. 27
2.3 Initial conditions for tracers of biogeochemistry package. 29
2.4 Vertical grid used in MITgcm atmosphere configuration. 32
2.5 Parameter values used for atmospheric model 35
2.6 Surface albedo and vegetation fractions assigned to different land surface types, based on De Vleeschouwer et al. (2014). 35
2.7 Parameter values used for the physical component of coupled model. . . . 37

Acronyms

AABW Antarctic Bottom Water

ACC Antarctic Circumpolar Current

ASGCM Atmospheric Slab Ocean General Circulation Model

AMOC Atlantic Meridional Overturning Circulation

CGCM Coupled Atmosphere-Ocean-Ice General Circulation Model

DIC Dissolved Inorganic Carbon

DJF December-January-February

DOP Dissolved Organic Phosphate

E-P Evaporation-Precipitation

EUC Equatorial Undercurrent

F–F Frasnian-Famennian

GCMs General Circulation Model's

HadSM3 Hadley Centre Slab Ocean Model

ITCZ Intertropical Convergence Zone

JJA June-July-August

LGM Last Glacial Maximum

LIP Large Igneous Province

MITgcm Massachusetts Institute of Technology General Circulation Model

MOC Meridional Overturning Circulation

NADW North Atlantic Deep Water

OAE Ocean Anoxic Event

OGCM Ocean General Circulation Model

OGCMmix Ocean General Circulation Model with spatially variable diapycnal diffusivity

OGCMvert Ocean General Circulation Model with vertically different diapycnal diffusivity

OTIS Oregon State University Tidal Inversion Software

PBL Planetary Boundary Layer

PDD Pripyat-Dnieper- Donets

POP particulate organic phosphorous

PZE Photic Zone Euxinia

RH Relative Humidity Threshold

SST Sea Surface Temperature

Chapter 1

Introduction

1.1 The Devonian Climate and Extinction

The Devonian (419.2 Ma to 358.9 Ma) is a period during which there were significant changes in the climate and biosphere. This key period in Earth's history is characterised by both major evolution events, and multiple extinction events, occurring at an extreme greenhouse climate transitioning towards a glacial climate in the end Devonian (Clack, 2012; Stigall, 2012; Chen et al., 2013; Bond and Grasby, 2017; De Vleeschouwer et al., 2017).

Prior to the Devonian, the continent showed little signs of life with no birds, insects, grasses or land animals. Nothing moved in the air except dust and few plant debris. Almost all life was in the marine realm. Yet, throughout the Devonian, significant change is observed in terrestrial and marine ecosystems. Primitive plant rooting structures evolved in the early Devonian, progressing to the first diverse forests at the end Devonian, along with the first forest fires and charcoals. Meandering and braided river systems became dominant due to increased channel support by rooted plants and trees, growing within the first soils (Davies and Gibling, 2010; Clack, 2012; Willis and McElwain, 2013). This widespread explosion of vegetation in terrestrial environments caused changes in silicate weathering profiles, as well as carbon sequestration in coal beds. These processes

may explain a significant drawdown in atmospheric carbon dioxide (CO_2) from ∼10 times the current levels of CO_2 in the Early Devonian falling close to pre-industrial modern CO_2 levels in the Early Carboniferous (Berner, 2006), terminating the Devonian period with glaciation (fig. 1.1).

Modelled paleo atmospheric composition is supported by soil carbonates and land-plant stomatal density calculations (Willis and McElwain, 2013). Decreasing CO_2 in the Devonian contributed to global climate cooling. The average temperature cooled near continuously between the Early Devonian to Late Mississippian. However, from the Late Givetian to Frasnian there is a period of warming by approximately 9 °C imposed on the long term Devonian cooling trend (fig. 1.1) (Joachimski et al., 2009). During the Frasnian, it is thought there was a low equator-pole temperature gradient, reef growth extending to paleo latitudes of 45° and humid conditions in the mid-high latitudes (Copper, 2002). Pulses of climate cooling of approximately 4 °C-7 °C and 3 °C-4 °C at the Frasnian-Famennian (F–F) boundary are linked with large deposition of the organic matter sediment beds known as Kellwasser horizons, causing atmospheric CO_2 drawdown (Joachimski et al., 2001; Balter et al., 2008; Bond and Grasby, 2017; Huang et al., 2018; Qie et al., 2019). Pronounced eustatic sea level fall is also recorded at the F–F boundary through the exposure of continental shelves. Glaciation in Gondwana due to climate cooling has been suggested as the cause of sea level fall, although geological evidence of glaciers is lacking (De Vleeschouwer et al., 2013; Song et al., 2017). Earliest known evidence of Gondwanan glaciation is Late Famennian, not during the Frasnian or early Famennian, and persisted for ∼300 ky in Bolivia, Brazil, South Africa, Peru and extending into the Appalachian Basin of Pennsylvania, Maryland and West Virginia at paleo latitudes of 30 ° S and 45 ° S.

Throughout the Late Devonian multiple extinction events took place. An extinction event is defined as widespread paleogeographical loss of biodiversity in both the marine and terrestrial environment (Whiteside and Grice, 2016). The Late Devonian mass extinction is recorded as a series of major extinction pulses at the Givetian-Frasnian (G-F) boundary (∼383 Ma), Frasnian-Famennian (F-F) boundary (∼372 Ma) and the Devonian-Carboniferous boundary (Hangenberg Event, ∼359 Ma) (Sallan and Coates,

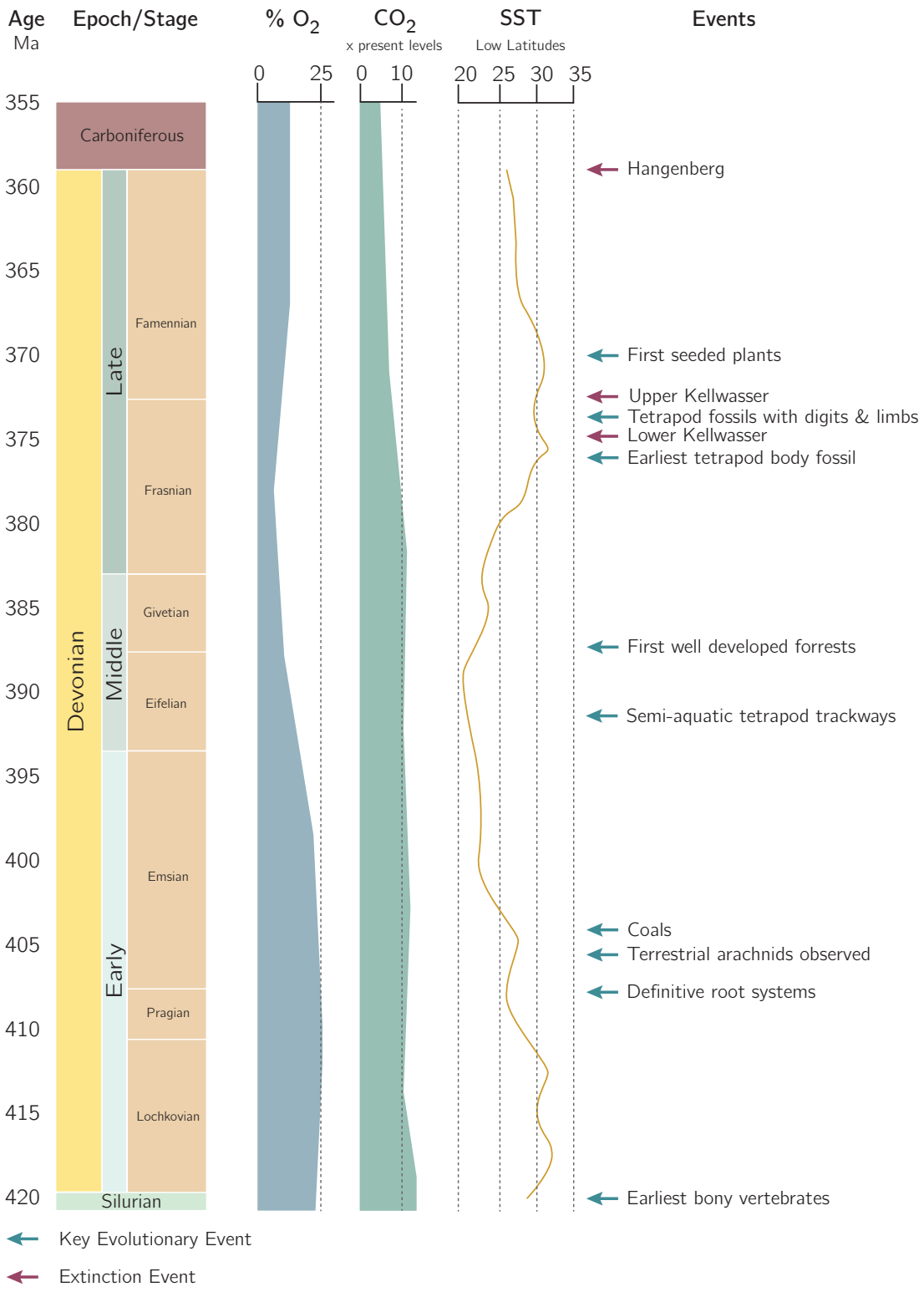

Figure 1.1: Key evolutionary and extinction events in the Late Silurian and Devonian period, including low latitude paleotemperature reconstructions and modelled atmospheric O_2 and CO_2. Adapted from Berner (2006); Clack (2012); Stigall (2012); Joachimski et al. (2009).

2010; Becker et al., 2012; Clack, 2012). The G-F event saw the extinction of benthic organisms such as echinoderms and bryozoans, while the F–F event eliminated coral reef ecosystems and the Hangenberg caused the extinction of many pelagic organisms including fish and cephalopods (Carmichael et al., 2019).

The F–F extinction ranks as one of the 'big five' Phanerozoic faunal biotic crises, with 80 % of benthic, planktonic and nektonic marine species affected and a smaller impact on terrestrial plants and animals. Biodiversity patterns highlight that low latitude regions experienced more significant loss than high latitudes, and the organisms which did survive experienced a loss of spread latitudinally. Shallow marine benthic organisms were affected more than deep water organisms. Paleontological evidence of the F–F extinction event is synchronous with black shale deposited in euxinic or anoxic environments (Buggisch, 1991; Copper, 1986). The event occurred in two main stages; the Lower Kellwaser (Late Frasnian) and Upper Kellwaser (Frasnian-Famennian boundary), known as LKW and UKW respectively, and represented in the sedimentary record as large deposits of black shales deposited under positive $\delta^{13}C$ excursions indicating anoxic oceans (fig. 1.1). Five distinct pulses of extinction took place within the LKW, followed by four extinction pulses in the UKW. The horizons are recorded globally indicating a major perturbation in the global carbon cycle (De Vleeschouwer et al., 2017; White et al., 2018), although the Kellwasser event varies around the globe in lithology, distribution and appearance. In Europe, eastern North America, South China, and North Africa epicontinental environments, the two distinct horizons of LKW and UKW are usually observed. However, the expression can be far more variable in shallower marine/intermediate depth sediments from South America, western North America, northwestern China, Siberia, Australia and southeast China (fig. 1.2).

Numerous hypotheses of what caused the F-F extinction exist, including bolide impacts, sea level fluctuations, eutrophication, and climate warming or cooling. However, the cause of this extinction event remains controversial (Stigall, 2012; Chen et al., 2013; Barash, 2016; Whiteside and Grice, 2016; Bond and Grasby, 2017; De Vleeschouwer et al., 2017; Liu and Luo, 2019). A common hypothesis for the Late Devonian extinction 'kill mechanism' is ocean anoxia and Photic Zone Euxinia (PZE). During an Ocean Anoxic Event (OAE) strong ocean stratification leads to a stagnant water column, widespread

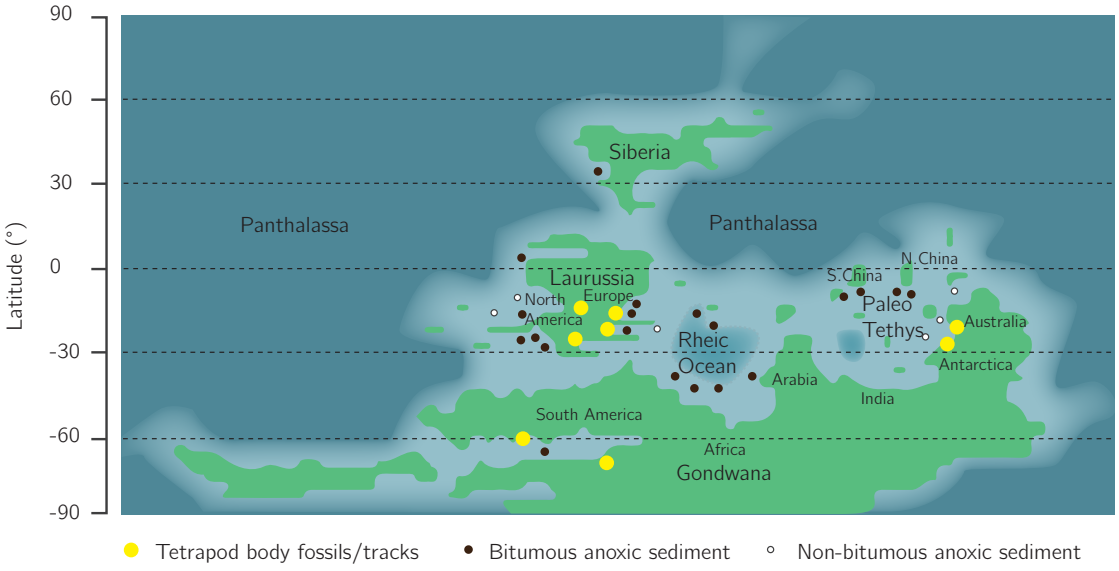

Figure 1.2: Approximate palaeogeographic locations of known study sites of the Late Devonian Kellwasser Anoxia Event and F-F extinction horizons, and principal tetrapod body fossil and track locations. Adapted from Lucas (2015); Carmichael et al. (2019).

anoxia and PZE. Euxinia is an oxygen depleted state enriched with toxic hydrogen sulphide in the water column which can mix into the photic zone causing PZE. A major cause of PZE is increasing algal productivity; since mineralisation of the organic matter consumes oxygen, there is a reduction of deep water oxygen and an increase in hydrogen sulphide (Naeher and Grice, 2015). Algeo et al. (1995); Algeo and Scheckler (1998) suggested the increased diversity of land plants with deep rooting systems in the Middle-Late Devonian caused more widespread soil development, ultimately leading to increased physical/chemical weathering, enhanced nutrient runoff and eutrofication in the oceans, resulting in greater primary production and ocean anoxia. Alternatively, upwelling of nutrient rich water can increase productivity, anoxia and PZE, or weak mixing and strong stratification can allow the PZE and anoxia to persist. Regions of PZE are ideal habitats for photosynthetic sulphur bacteria which are capable of anoxygenic photosynthesis. PZE and anoxia are reported in Late Devonian sediments and crude oils from various locations (fig. 1.2).

The method of how the anoxia is formed is still debated. The most severe ocean anoxic event was the F–F event, observed largely in the Kellwasser horizons. Wilde and Berry (1984) suggested upwelling of anoxic bottom waters into shallow regions as a cause of the Devonian extinctions. Subsequently, it was suggested that the migration of the oxygen minimum zone into shallow water regions resulted in upwelling of anoxic water, or upwelling of nutrient rich oxic bottom waters, causing eutrofication. Alternatively, Bond et al. (2004) suggested cycles of oxic ventilated ocean followed by periods of weak mixing leading to a stagnant water column and ocean anoxia. Detailed (cm-scale) analysis of sediments as well as fossil studies indicates cycles of oxic/dysoxic/anoxic/euxinic conditions during the F–F (Carmichael et al., 2019).

1.1.1 Devonian Continental Configuration

All the changes discussed in terrestrial and marine ecosystems along with perturbations in climate occurred against a backdrop of widespread tectonic activity. The Devonian continents were positioned predominantly within the Southern Hemisphere; Laurussia centred at the paleoequator, separated from Gondwana in the south by the Rheic Ocean (fig. 1.3). The Rheic Ocean was at its maximum width in the Middle Silurian. North-dipping subduction existed on the southern margin of Laurussia imposing a trench pull effect of Gondwana towards Laurussia and the gradual closure of the Rheic Ocean (Golonka, 2020). The closure was asymmetric, tapered to the west, forming a large geographical structure, similar to the present-day Bristol Channel. By the Early-Middle Devonian, the Rheic Ocean's width was reduced to 750 km at it's narrowest in the west and 1500 km in the east. Laurussia was drifting south with plate speed and rotation reaching $10\,\mathrm{cm\,year^{-1}}$ (Torsvik et al., 2012). The Laurussia supercontinent was assembled throughout the Caledonian Orogeny. This was a long process, taking about 150 million years beginning in the Cambrian and joining Laurentia (the majority of present-day North America) and northern Europe. The collision resulted in massive granite intrusions and the raising of a large mountain belt in Central Laurussia, known as the Appalachian Mountains of eastern North America. Vigorous erosion of these newly uplifted mountains yielded great volumes of sediment, which were deposited in vast lowlands and shallow seas nearby (Torsvik et al., 2012; Golonka, 2020).

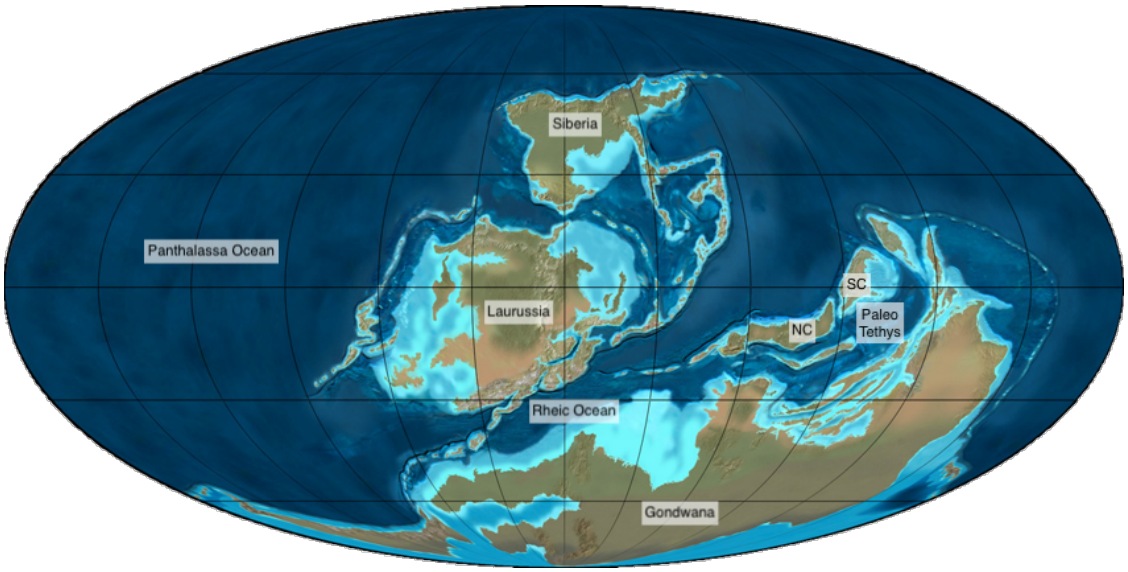

Figure 1.3: Paleomap of the Late Devonian (379.9 Ma), Mollweide projection, sea level +120 m maximum flooding surface (Blakey, 2018). *Abbreviated continental units:* NC, North China; SC, South China.

The Panthalassa Ocean was vast, but despite covering such a large area in the Devonian, little is known about this area, which was mainly interior ocean, due to its subsequent destruction. Subduction zones were present along nearly all boundaries of the Panthalassa (Domeier and Torsvik, 2014; Torsvik and Cocks, 2004).

The main extensional tectonics in the Devonian was the spreading of the Paleo Tethys Ocean. Rifting began in the Late Silurian between Gondwana and regions which now make up southern Europe and South China further to the east. As the Paleo Tethys opened, its western end merged with the Rheic Ocean, although the Rheic Ocean became increasingly smaller (Golonka, 2020).

In the Early Devonian Siberia was located in the Northern Hemisphere low latitudes. As the Devonian progressed, Siberia slowly drifted northwards while rotating clockwise. The paleolatitude of Siberia throughout the Devonian is interpolated from two paleomagnetic records from Middle Silurian to Late Devonian. However, the Late Devonian position is centred just north of 30 °N. Late Devonian climate perturbations correlate with Large Igneous Province (LIP) volcanism on the Siberian Platform known as the Viluy Traps. Volcanism began in the Frasnian and continued into the Early Carboniferous, extruding a 7 km thick layer of magma. Additionally, on the Russian Platform the Pripyat-Dnieper-

Donets (PDD) rift system contributed at least $1.5 \times 10^6\,\mathrm{km}^3$ of magma, although this is slightly younger than the F–F boundary extinction (Bond and Grasby, 2017). LIP volcanism causes climate warming through outgassing of greenhouse gases CO_2 and SO_2. Cooling can then follow LIP volcanism through weathering of the LIP basalts causing CO_2 drawdown. The PDD rift system was located close to the Late Devonian equator which is shown to lead to rapid weathering of the LIP basalts under the humid conditions in this region, acting to decrease atmospheric CO_2 (Wilson and Lyashkevich, 1996; Macdonald et al., 2019; Percival et al., 2019).

1.1.2 Evolution in the Devonian

In addition to widespread terrestrial plant evolution, multiple phases of extinction and perturbations in the climate, the Devonian is known as the age of the fish. Jawless, cartilage-supported fish evolved to fish with jaws, bony fish and large predator fish, in addition to lungfish, by the end of the Devonian. Towards the Middle to Late Devonian the first land animals evolved, known as tetrapods (Clack, 2012) (fig. 1.1). Stem tetrapod fossils are recorded in South China, and early tetrapod fossils are identified in eastern Laurussia; it is thought that at some point the stem tetrapods were swept by ocean currents along the equator to the location of tetrapod first appearance. Geographical evidence based on the fossil record shows that early tetrapods evolved in south east Laurussia (Blieck et al., 2007). Tropical climates dominated this region, where rainfall was high but confined to monsoonal periods (Clack, 2012). Until recently all Devonian age tetrapod fossil localities lay within 30° of the paleoequator. However, Gess and Ahlberg (2018) identified well preserved tetrapod deposits in the south polar region at a paleolatitude of 70 ° S. The fossils are Famennian in age, suggesting that Late Devonian tetrapods were not restricted to tropical climates but were global in distribution. The flora identified at this polar location suggests the climate was not truly polar, but the conditions these tetrapods may have experienced is poorly constrained, and the proximity to the pole implies several months of complete winter darkness (Lakin et al., 2016; Gess and Ahlberg, 2018).

The environment in which fish transitioned to tetrapod is still highly debated. Early hypotheses concentrated on a fish-tetrapod transition within freshwater swamps, lakes and fluvial environments. It is now largely agreed that the transition occurred within a marine environment, although current interpretations of tetrapod body fossil or trackway-bearing sediments range from shallow marine, marginal marine, intertidal to lagoonal environments (Blieck et al., 2007; Clack, 2012). Within these settings varying amounts of freshwater input, water energy, and tidal activity are inferred. A marine environment for tetrapod evolution is also favoured due to the widespread global occurrence of tetrapod body fossils within the Late Devonian. These have been found at several localities thought to be remote from each other in the Devonian, on separate continents (Zhu et al., 2002).

Recent theories on the transition of fish to a terrestrial environment consider a combination of evolutionary forces. Anoxic water may have affected the evolution of air gulping: air-breathing fish increase the incidence of air gulping or the amount of body exposed when living in anoxic conditions. Alternatively, increased competition for food or space plays a role in modern fish leaving the water, in addition to predation or aggression, though a common hypothesis is due to feeding on terrestrial or semi-terrestrial food sources (Clack, 2012; Stossel et al., 2016). One recent idea is that tetrapods were pressured by predatory fish or arthropods to seek more marginal habitats, where large Devonian predator fish could not follow into shallow vegetation-choked water. The earliest tetrapod trace fossil is known as the Eifelian trackways in the Zachelmie succession, Poland. The trackways are interpreted as an intertidal environment where fish would become stranded in ephemeral saline lakes/tidal pools, which were periodically refreshed with marine water, and did not have a major freshwater source from rivers (Niedźwiedzki et al., 2010; Clack, 2012; Balbus, 2014). Tetrapods may have evolved limbs, air gulping capabilities and terrestrial locomotion to exploit the food sources within stranded ephemeral lakes/tidal pools. These environments can become uninhabitable through evaporation/draining or the humid climate causing dysoxia/anoxia (Balbus, 2014). Low oxygen levels in waters today occur for a variety of reasons, including high daytime temperatures in shallow tropical freshwaters, low activity of photosynthetic organisms at night in tide pools, oxidising of decaying vegetable matter by bacteria, or upwelling of deep anoxic water.

The asymmetric closure of the Rheic Ocean formed a large geographical structure, similar in shape to the Bristol Channel. Balbus (2014) highlighted this large tapered geographical structure as a potential region of enhanced tidal dissipation during the Early/Middle Devonian, which may have evolved to a region of weak tidal dissipation in the Late Devonian. Tidal dissipation rates have changed significantly in the past due to both continental configuration, and variations in the rate of recession of the moon (Green et al., 2017). Thus, Balbus (2014) suggested a combination of continental configuration and enhanced recession rate may have caused stronger tides during the Middle Devonian when tetrapods were first moving onto land. High tides would potentially flood inland, filling ephemeral lakes or forming tidal pools. Subsequently, the lake/pool could become isolated from freshwater or marine refreshment for large periods, during which time the lake may become uninhabitable and provide an evolutionary pressure on tetrapods to find more habitable environments (Balbus, 2014; Qvarnström et al., 2018). During the Late Devonian, weak tidal dissipation could be linked with weak ocean mixing, and potentially ocean anoxia. However, it is not clear to what extent the Devonian climate affected tetrapods' habitability, and the impact of continental configuration and bathymetry on tidal mixing, and subsequently ocean circulation. It is important to consider the global large-scale climate pattern to gain insight into the broader environment tetrapods were evolving within, and the conditions they met when venturing onto land.

1.1.3 Equatorial Ocean Dynamics

The equatorial region of the Late Devonian ocean is of particular importance and interest. Large reefs existed close to the equator in Canada and China (Copper, 2002); the F–F extinction eliminated these reef regions. Ocean anoxia is inferred in these equatorial regions.

Ocean currents flowing within $\sim 2^\circ$ of the equator. In the present-day, westward surface currents which are restricted to the equator cause water to build upon the western boundaries of the Atlantic and Pacific Oceans, and hence cause a pressure gradient along the equator. There must be some return flow and so this excess water returns as an eastward current below the surface current, known as the Equatorial Undercurrent (EUC). Warm water builds up on the western boundaries of ocean basins, and colder

deep water upwells to the surface on the eastern boundaries. The zonal pressure gradient force, related to the zonal sea level slope, is maintained by the easterly trade winds and the westward surface current and constitutes the dominant acceleration term in the momentum budget of the EUC. The balance between westward surface wind stress and eastward zonal pressure gradient force determines the strength and the vertical structure of the EUC (Philander, 1973; McPhaden and Taft, 1988).

In the modern-day Pacific the EUC typically flows between 2 °N and 2 °S at depths from 30 m to 300 m, and at a maximum speed of $1\,\mathrm{m\,s^{-1}}$ (Johnson et al., 2002). In the Atlantic, the EUC flows between 30 m to 120 m water depth and reaches a maximum speed of $\sim 0.8\,\mathrm{m\,s^{-1}}$ (Brandt et al., 2014).

The EUC plays a crucial role in climate and biogeochemical cycles, delivering cold, nutrient and CO_2 rich water to the eastern regions of the Pacific and Atlantic Oceans. In the Pacific, this cold tongue region is the largest oceanic source of atmospheric CO_2 (Liu et al., 2019). The warm pool in the western regions of ocean basins causes deep atmospheric convection. Changes in the intensity of the EUC have important feedbacks on atmospheric circulation and equatorial ecosystems (Drenkard and Karnauskas, 2014).

Strong inter-annual variations in the Pacific associated with El Nino/Southern Oscillation cause fluctuations in the strength of the EUC. During an El Nino phase the EUC weakens or even becomes absent.

1.2 Energy and General Circulation in the Ocean

The ocean circulation plays a crucial role in redistributing heat, carbon and tracers around the Earth. In the simplest sense ocean circulation is driven by mechanical wind and tidal forcing and buoyancy forcing. At the surface, ocean currents can be explained largely by the balance between the Coriolis acceleration and pressure gradient (geostrophic component); and the balance between Coriolis acceleration and wind stress (Ekman component). Mechanical wind energy input to the present-day ocean is thought to be in the range of 7 TW to 36 TW (Wunsch and Ferrari, 2004). Most of this remains in the surface layer, with a small fraction contributing to the large scale circulation. Due

to the Coriolis force, the wind stress gives rise to a current to the right of the surface wind in the Northern Hemisphere; and to the left in the Southern Hemisphere, this is the Ekman layer. Divergence and convergence of the flow in the Ekman layer generates vertical velocities and sets the general circulation of the ocean (Wunsch, 2017).

The ocean is responsible for transporting huge amounts of heat from the tropics to polar regions. External forcing due to heat fluxes (heating and cooling) and freshwater fluxes (evaporation, precipitation and land precipitation runoff) at the ocean surface leads to changes in the density of seawater (Talley et al., 2011). Abyssal meridional overturning circulation is fed by water that is dense enough to sink to the abyss. Water is supplied to the deep ocean through buoyancy loss, but upwelling of deep water is linked with vertical mixing, which requires external mechanical energy; without this, the thermohaline circulation would not be sustained (Wunsch and Ferrari, 2004; Huang, 2010).

In the present-day, most of this sinking takes place in high latitude marginal seas such as the Labrador and Greenland Seas. Widespread small-scale mixing in the bottom boundary layer provides energy to upwell this North Atlantic Deep Water (NADW) to 2000 m. Much of this water continues flowing southwards at 2000 m until it is upwelled to the surface adiabatically through intense surface winds (Ferrari et al., 2016).

The ocean is a key factor in determining Earth's climate through poleward heat transport. Both surface winds, which drive mass transport in the ocean gyres, and air-sea fluxes setting temperature distribution, contribute to ocean heat transport. Several studies have attempted to decompose the vertical structure of ocean heat transport (Talley, 2003; Boccaletti, 2005). Ferrari and Ferreira (2011) demonstrated that deep ocean heat transport in the present-day ocean is supported through the strength and direction of surface winds, and convection processes in the high latitudes impose only a secondary forcing on heat transport. Ferrari and Ferreira (2011) also highlighted that this sensitivity to winds is not only linked to Southern Ocean winds, but that heat transport is also sensitive to mid and low latitude winds, concluding that the bulk heat transport in the Pacific and Indian oceans is linked with tropical and subtropical wind-driven circulation.

1.2.1 Mixing in the Ocean

One of the major determinants in the global meridional overturning circulation is diapycnal mixing, which therefore has important climatological influences (Wunsch, 2017). Mixing across density surfaces occurs due to turbulence in the ocean and is crucial in explaining the large scale ocean state. Changes in mixing due to tidal dissipation alter the global overturning circulation; an increase in tidal dissipation rates would lead to greater abyssal mixing, which would strengthen the meridional overturning circulation (MOC), and subsequently enhance ocean heat transport (Munk, 1966; Laurent and Garrett, 2002; Wunsch and Ferrari, 2004).

Water that is dense enough to sink to the deep ocean must return to the surface. Munk (1966) proposed dense bottom waters are mixed to the surface through breaking internal waves, which mix water across density surfaces. Internal waves are generated by both winds ($\sim$0.6 TW) and tidal flows over topography ($\sim$1 TW) (Wunsch and Ferrari, 2004). Internal or baroclinic tides are generated by the interaction of barotropic tidal currents with the seafloor in stratified waters. Displacement of isopycnals causes the formation of internal waves. Observations of breaking internal waves along major ridges and sea mountains in the present-day highlight that $\sim$70 % of the waves break close to the ocean bottom, while the remaining 30 % propagate away from the site of formation and break on the continental slopes (Waterhouse et al., 2014).

Until recently the consensus was that small-scale mixing generated by breaking internal waves provides the energy required to upwell the present-day NADW and the Antarctic Bottom Water (AABW) up to a depth of approximately 2000 m. It was thought that these internal waves break within a few hundred meters of abyssal ridges, mountains, and rises, which are most common below 2000 m (Munk, 1966; Waterhouse et al., 2014). However, Ferrari et al. (2016) have recently suggested the vertical transport of water due to mixing depends on the distance above the seafloor. The observed increase in mixing with depth drives diapycnal sinking of deep waters toward the abyss in the ocean interior,

and the diapycnal upwelling of waters is confined to thin, turbulent boundary layers along the sloping ocean boundaries. The boundary layer diapycnal upwelling must therefore be so intense as to overcome the interior diapycnal sinking and allow waters to rise toward the surface in the net.

Mixing in the ocean is not spatially uniform, but occurs in regions of especially rough topography in the deep ocean. It is thought that the spatial distribution of mixing is an important factor in maintaining the large-scale global ocean circulation (Munk and Wunsch, 1998; Wunsch and Ferrari, 2004; Egbert and Ray, 2001). The level of stratification in the ocean is also thought to be linked with the strength of tides. Several studies have recently simulated tides during the Last Glacial Maximum (LGM) and Eocene, then applied the tides simulated to ocean general circulation models to determine the effects of tidal mixing on the large-scale ocean circulation. The results highlight that a change in input of tidal energy leads to significant alterations of the global overturning circulation. The authors emphasise that changes in tidal dissipation should be accounted for in paleoclimate simulation setup, as this could lead to large differences in ocean mixing and the global MOC (Green et al., 2009; Schmittner and Egbert, 2014; Wilmes and Green, 2014).

Late Devonian tidal dissipation rates have been modelled by the University of Bangor. These estimates are utilised in this study to consider how a spatially variable diapycnal diffusivity calculated from tidal dissipation rates can alter global ocean circulation. The uncertainties in modelling Devonian tidal dissipation are also being considered by Steve Balbus and Tomos David at the University of Oxford. Additionally, it is possible to gain insights into ocean mixing from the geological record, although this data is limited to continental shelves and deep seas close to the coastlines.

1.2.2 Circum-navigating Currents

There are multiple opportunities for a current to circumnavigate the globe in the Late Devonian. First, the Late Devonian continental configuration consists of no meridional boundaries north of Siberia, and second Hüneke (2006) highlighted the possibility for a circum-equatorial current flowing between Siberia and Laurussia through analysis of

seafloor sediments to understand flow directions and ocean currents. The first is similar to the present-day Southern Ocean which has no meridional boundaries at the latitudes of Drake Passage, and as a result, the Antarctic Circumpolar Current (ACC) encircles Antarctica. The ACC is an eastward circumpolar current driven by strong westerly southern ocean winds. The westerly wind stress drives an equatorward Ekman transport. The ACC has the largest volume transport of any present-day ocean current and Tansley and Marshall (2001); Marshall et al. (2013) showed the ACC can have substantial circumpolar transport even when subject to weak forcing.

When the meridional circulation in the Southern Ocean is viewed in the zonal mean the surface equatorward Ekman transport appears to downwell to 3000 m depth just north of the ACC. This then appears to flow southward and upwell south of the ACC; this circulation is known as the Deacon Cell. The Deacon cell, however, does not indicate that actual water parcels are downwelling in this one single location but is an artefact of the zonal averaging with water parcels instead following non-zonal streamlines on density surfaces which are tilted in the zonal direction. When the MOC is viewed in density coordinates, the Southern Ocean receives NADW with little diapycnal flow into the thermocline, and some of this transforms into AABW through surface cooling. The AABW is then converted back to NADW in the deep interior, and for this deep interior mixing is crucial. So the Southern Ocean upper overturning is driven by winds, while the deeper is driven by small scale mixing (Döös and Webb, 1994; Döös et al., 2008; Marshall and Speer, 2012).

The ACC occupies a narrower latitudinal band than the zonally unbounded latitudes in the Late Devonian north hemisphere. Therefore, it is difficult to make dynamical comparisons, and instead it is useful to consider the aquaplanet simulations such as Smith et al. (2006) and Marshall (2007). Both Smith et al. (2006) and Marshall (2007) found that the lack of boundaries meant the MOC consisted of deep Ekman cells, concluding the meridional flow was dominantly driven by zonal wind stress and bottom friction. These studies both used the Gent and McWilliams (1990) eddy parameterisations.

1.3 Thesis Aims and Outline

Considering the dramatic changes throughout the Devonian, little is known about the climate, and the coupled relationship between the climate and the evolution of land plants, land animals, and fish. The primary aim of this DPhil project is to understand further the Devonian climate, and the effects of continental configuration and plant evolution on ocean circulation, and climate. Developments in ocean modelling and coupled atmosphere-ocean modelling, coupled with a greater understanding of the Devonian geological record, allows computational modelling of the Devonian climate with the Devonian continental configuration and bathymetry. This will enable understanding of the coupling between climate and evolution.

Current and previous efforts modelling the deep time ocean circulation have focused primarily on the Permian, Jurassic, and Cretaceous Periods (Donnadieu et al., 2006; Brunetti et al., 2015; Brunetti and Vérard, 2017; Weber and Thomas, 2017). Brugger et al. (2019) recently investigated the climates sensitivity to changes in continental configuration, vegetation cover, carbon dioxide concentrations, solar constant, and orbital forcing parameters, throughout the Devonian using a coarse resolution CLIMBER-3α Earth System. Brugger et al. (2019) results showed a general climate cooling trend across the Early, Middle and Late Devonian inline with CO_2 concentrations. However, the authors of this study highlighted concerns in the model's course resolution (ocean: 3.75°; atmosphere: 22.5° longitude and 7.5° in latitude), as well as the lack of a biogeochemical component. The study also suggested further investigation into the Late Devonian F–F warming trend observed in the geological record, which was not simulated with the CLIMBER-3α model. There have also been attempts to understand the Devonian ocean circulation through isotope analysis to reconstruct the general ocean circulation in a region north of Gondwana (Dopieralska, 2009; Saltzman, 2003). Hüneke (2006) inferred Frasnian global ocean circulation based on physical oceanography theory to support trilobite and ostracod fossil evidence. More recently, Crasquin and Horne (2018) considered the possible ocean circulation patterns in the Early and Late Devonian based on the

De Vleeschouwer et al. (2014) atmospheric model results, presenting potential locations for deep water formation and upwelling. These qualitative attempts at considering Late Devonian ocean circulation highlight the need for a more rigorous quantitative understanding of the ocean circulation during this critical period in Earth history.

De Vleeschouwer et al. (2014) simulated the atmospheric circulation of the Frasnian using an atmospheric model coupled to a slab ocean to investigate the impact of changes in orbital parameters (at a fixed CO_2 concentration) on the Devonian climate. This model did not have a dynamic ocean. De Vleeschouwer et al. (2014) found the amplitude of warming recorded in the isotope record to be greater than that simulated using an atmospheric slab ocean climate. The results of the De Vleeschouwer et al. (2014) paper are discussed in detail throughout this thesis, and are used as a tool for modelling the ocean only circulation, as well as a comparison when running similar model experiments of the Late Devonian atmospheric circulation. However, the De Vleeschouwer et al. (2014) study highlights uncertainties in using an atmospheric slab ocean model with no dynamic ocean to understand past climates. The authors suggest future work should consider experiments with a dynamic ocean, since the major events in the Late Devonian are thought to stem, or at a minimum, have links to changes in ocean anoxia.

The first step towards understanding the Late Devonian is to utilise the De Vleeschouwer et al. (2014) atmospheric modelling efforts to simulate the Late Devonian ocean circulation. The MITgcm is used to put some constraints on the ocean circulation in the Late Devonian, establish the degree of ocean ventilation, and assess whether ocean anoxia could have developed given the climate and continental configuration.

The primary aim of this DPhil project is to understand the Devonian climate and the role of continental configuration and ocean circulation. With this in mind, there are three key objectives:

- Determine the ocean circulation in the Late Devonian and the extent of ocean anoxia.

- Understand the effects of spatially varying diapycnal mixing due to tidal dissipation on Late Devonian Ocean Circulation, in particular on ocean ventilation.

- Review the relationship between climate and evolution in the Late Devonian using coupled atmosphere-ocean model simulations.

This thesis is arranged in four key chapters. Chapter 2 describes the model used to simulate the various components of the Devonian climate in detail.

In chapter 3, the mean state of a Late Devonian ocean forced with De Vleeschouwer et al. (2014) atmospheric data is described. Details of how the simulated Late Devonian ocean circulation oscillates between two quasi-stable ocean states; an unventilated phase where the ocean is stratified and a ventilated phase with high latitude deep convective mixing are presented. Although there is considerable uncertainty, both states appear plausible within Late Devonian forcing constraints, and it is indeed possible that the ocean did oscillate between two stable states. The oscillatory mechanism shows similarities to that proposed to have operated in the Nordic Seas during the last glacial period, which gave rise to periodic Dansgaard-Oeschger (D-O) events. Implications of the ocean model results are discussed in the context of the Devonian and comparisons with the paleo-record outlined.

Chapter 4 presents multiple experiments computed with a spatially variable diapycnal diffusivity and makes comparisons to chapter 3. It is shown that the ocean circulation does change slightly. Similarly, in chapter 3 the Late Devonian ocean circulation oscillates between two quasi-stable ocean states; an unventilated phase and a ventilated phase, but the timescale of oscillation between phases is different due to changes in the rate of erosion of the ocean stratification by diffusion.

Chapter 5 considers the Late Devonian oceanic and atmospheric circulation using the MITgcm fully coupled atmosphere-ocean-sea-ice model. Comparisons are made with the De Vleeschouwer et al. (2014) atmosphere and with a separate MITgcm atmospheric slab ocean model to determine the importance of coupling with a dynamic ocean and sea-ice package. The coupled ocean and atmosphere results are described; as in chapter 3, the ocean exhibits multiple ocean states; a partly-ventilated ocean and a ventilated ocean. The coupled climate model results are compared to Late Devonian geological data, such as reef extent, paleotemperature reconstructions and lithic palaeoclimate indicators.

Chapter 6 draws the main conclusions of the thesis, highlighting the significance of using a coupled atmosphere-ocean-sea-ice model to simulate deep time palaeoclimates and discussing the implications of the results in terms of Late Devonian evolution and extinction.

Chapter 2

MITgcm Setup

The purpose of this chapter is to outline configuration details of the various General Circulation Model's (GCMs) used to investigate Late Devonian climate and its implications for ocean anoxia, extinction and evolution. The model domain, boundary conditions and forcing are described, as well as additional biological tracers used to provide additional diagnostics of changing ocean circulation and the carbon cycle.

Modelling experiments are performed using the MITgcm (Marshall et al., 1997a,b). This model was chosen since it is open source, can be modified for use in past geological time periods, and can be used to study the ocean, atmosphere and coupled atmosphere-ocean. MITgcm is easily configurable in terms of ocean bathymetry and forcing, and has been used in a wide range of idealised and palaeoclimate studies modelling the recent Pleistocene climate, as well as deep time periods such as the Jurassic, Permian and Ordovician and also aqua-planet simulations (Marshall, 2007; Brunetti et al., 2015; Brunetti and Vérard, 2017; Pohl et al., 2017) (also see `mitgcm.org`).

MITgcm has the ability to render atmosphere and ocean models from one dynamical core at both large and small scale by exploiting 'isomorphisms' of the vertical 'r' coordinate. The vertical coordinate 'r' is interpreted as pressure (Pascals) if modelling the atmosphere, and height (metres) if modelling the ocean.

Additionally, MITgcm includes optional extra coded 'packages' to help organise and layer various building blocks. Packages can be included in the simulation and assembled to perform a specific experiment. The top layer packages are generally specialised to specific simulation types. To consider the Devonian climate additional packages are utilised to deal with biogeochemical processes, ocean tracers, ocean interior and boundary layer processes, atmospheric processes, sea-ice and coupled simulations.

The chapter will describe the common attributes between all the models used, before outlining specific details for the ocean only model, atmospheric slab ocean model and the coupled atmosphere-ocean-ice model.

2.1 Resolution

The models are discretised on a 'cubed sphere' horizontal grid at C32, meaning each face of the cube consists of a 32 x 32 matrix of cells. The resolution at the equator or along the Greenwich meridian is similar to a 128×64 equally spaced longitude-latitude grid (2.8° resolution) but requires 25% less grid points. A cubed sphere grid avoids problems with converging meridians that leads to ever-decreasing zonal grid spacing as one approaches the poles. These small grid sizes impose severe limits on the time step demanded by explicit time-stepping schemes (Adcroft et al., 2004). Figure 2.1 illustrates how the C32 grid is arranged into six faces and the coordinate system used to match edges. The coloured edges highlighted in fig. 2.1 match the equivalent colour edge e.g. orange edge labelled *f4s* would match the orange edge *f5n*.

2.2 MITgcm Ocean Model

The first stage in working towards a coupled atmosphere-ocean model is to run an ocean only model. The oceanic component of MITgcm is a state-of-the-art OGCM rooted in the incompressible, Boussinesq form of the Navier-Stokes equations (Marshall et al., 1997a,b). In this study the hydrostatic, implicit free-surface, partial step topography formulation of the model is used to simulate the global ocean domain. The MITgcm was designed to study both large and small scale processes. This is achieved mainly by its non-hydrostatic capability and finite volume formulation for small scale (20 m - ∼10 km) simulations. Here

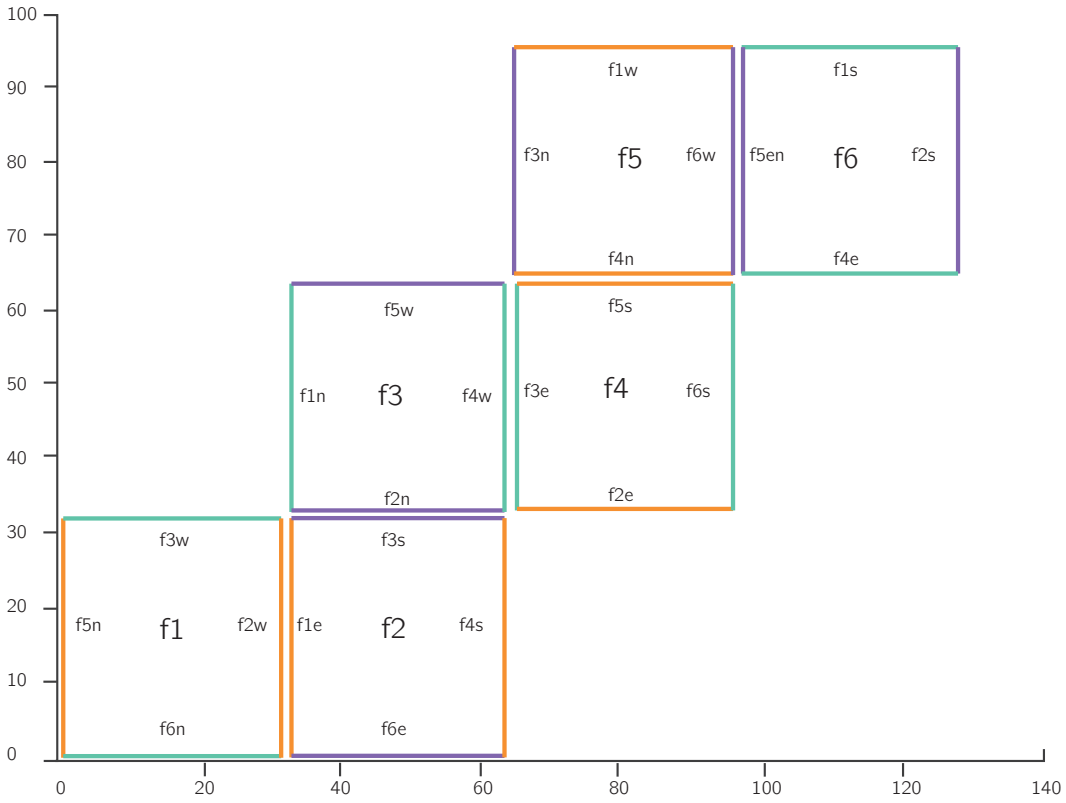

Figure 2.1: Logical arrangement of the cube sphere grid topology with the 32×192 domain divided into six 32×32 tiles. The coordinate systems match across the interior edges, while the exterior edges need either a $+\pi/2$ or $\pi/2$ rotation of coordinates.

however, the modelled ocean is assumed to be in hydrostatic equilibrium. The large scales of interest in this study mean that the vertical pressure gradient and gravity dominate, and the horizontal scale (L) of motion exceeds the vertical scale (D). The hydrostatic assumption breaks down when D and L are comparable, for processes on scales that are not properly resolved in this study.

The Devonian OGCM is integrated for 10 000 years, reaching a statistical equilibrium after approximately 3000 years, and subsequently oscillates between two ocean states. The configuration for this simulation is subsequently described in detail.

2.2.1 Continent Outline and Bathymetry

Late Devonian continent outlines were prescribed based on a quantified version of the Late Devonian Blakey (2018) global paleogeographic reconstruction illustrated in fig. 2.2, where dark blue corresponds to the deep ocean (5000 m) and green is land. The ocean depth then increases in 1000 m increments for each grid cell away from the coastline until a maximum depth of 5000 m is reached. The seafloor is then uniform depth, with the exception of a ridge, positioned north of Siberia at a depth of 3800 m. This ridge runs north-south across the pole and terminates on the far side of the Earth at a similar latitude to Siberia. The ridge in this region is considered important to allow a bottom pressure gradient to form, such that momentum input by the zonal surface winds can be transferred to the solid Earth. Although it is not known whether a ridge existed here in the Late Devonian, it is certain the seafloor was not a uniform depth.

The Ferrari et al. (2016) study highlights the importance of mixing on continental slopes. Thus it was decided the inclusion of a simple continental slope was important, but including unknown seafloor topography would introduce more uncertainties in understanding the results.

The ocean has 15 vertical levels spread over the flat-bottomed, 4 km deep ocean, increasing in thickness from 50 m at the surface to 690 m at depth (table 2.1).

Figure 2.2: Late Devonian continental configuration based on Blakey (2018) (green). Ocean bathymetry in the model is indicated by the blue shading: paler colour indicates the continental slope, and the dotted grey line marks the point at which the slope reaches the flat deep-ocean floor.

Level	Thickness (m)	Depth Centre (m)	Initial Temperature °C
1	50	-25	20
2	70	-85	18.9
3	100	-170	17.8
4	140	-290	16.7
5	190	-455	15.7
6	240	-670	14.6
7	290	-935	13.5
8	340	-1250	12.5
9	390	-1615	11.4
10	440	-2030	10.3
11	490	-2495	9.2
12	540	-3010	8.2
13	590	-3576	7.1
14	640	-4190	6.0
15	690	-4855	5.0

Table 2.1: Vertical grid used in MITgcm ocean configuration.

2.2.2 Atmospheric Surface Forcing

The ocean is forced with monthly mean atmospheric temperature, wind stress, and evaporation minus precipitation minus runoff (E-P-R) taken from the De Vleeschouwer et al. (2014) Late Devonian (Frasnian) Hadley Centre Slab Ocean Model (HadSM3) results. Precipitation falling over land is uniformly distributed into the ocean within the same latitudinal band. Figure 2.3 shows the annual mean atmospheric surface temperature, zonal wind stress, meridional wind stress and E-P-R forcing. Large equator-pole temperature gradients are a common problem when using GCMs, in particular atmospheric slab ocean models, since the ocean is not able to redistribute heat, as well as uncertainties in the cloud effect on radiative forcing. Figure 2.3A illustrates the pattern of E-P-R; precipitation is greatest at the equator and over the mid-latitude ocean, with excess evaporation in the sub-tropics. There is an asymmetry in E-P-R between hemispheres, with more evaporation in the Northern Hemisphere tropics and excess precipitation in the Southern Hemisphere tropics. The wind stress forcing (figs. 2.3B and 2.3C) comprises weak westerly jets in the mid-latitudes and a strong equatorial easterly jet. Annual mean meridional wind stress is southwards across the equator, and in both the Rheic and Paleo Tethys Ocean there is a dipole in meridional wind stress with southward stress on the western boundary and northward on the eastern boundary of the basin.

The following equations describe how the De Vleeschouwer et al. (2014) fields are used to force the model surface layer (the uppermost grid point):

$$F_u = \frac{\tau_x}{\rho_0 \Delta z_s}, \tag{2.1}$$

$$F_v = \frac{\tau_y}{\rho_0 \Delta z_s}, \tag{2.2}$$

$$F_\theta = -\lambda_\theta(\theta - \theta*), \tag{2.3}$$

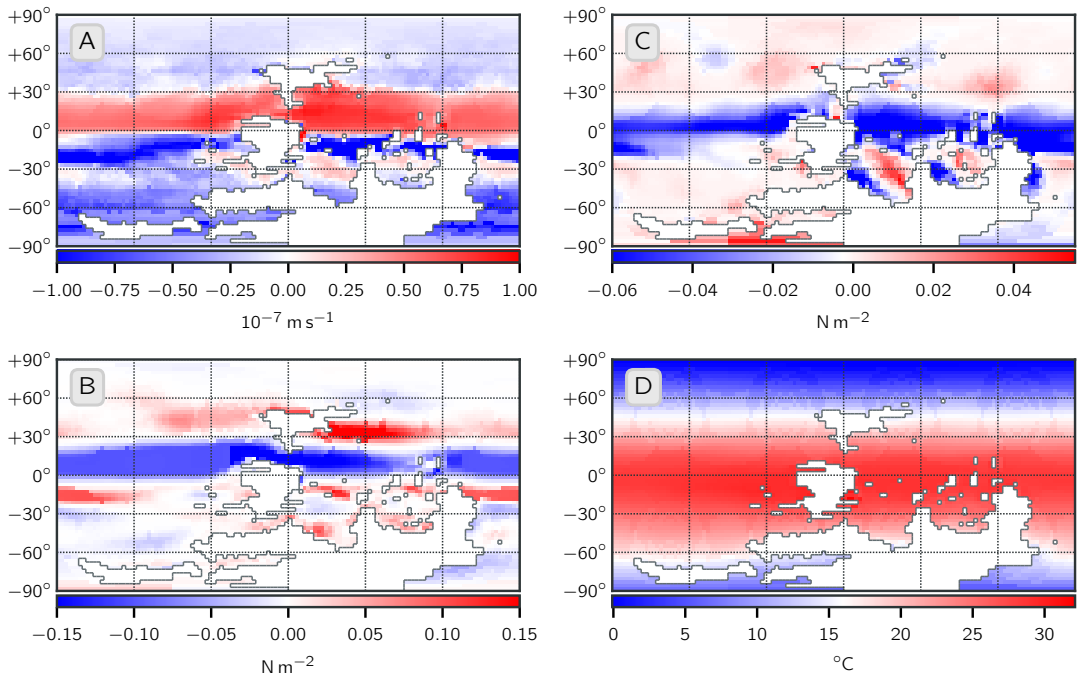

Figure 2.3: Annual mean surface forcing fields, calculated from the De Vleeschouwer et al. (2014) Late Devonian (Frasnian) atmospheric simulation with slab ocean. (A) E-P-R; (B) zonal surface wind stress; (C) meridional surface wind stress; (D) atmospheric surface temperature.

Parameter Name	Units	Value
Acceleration due to gravity	$\mathrm{m\,s^{-1}}$	9.81
Earth Rotation Period	s	79200
Momentum time step	s	1000
Tracer timestep	s	10000
Reference Density	$\mathrm{kg\,m^{-3}}$	1035
Reference Salinity	psu	35
Diapycnal Diffusivity	$\mathrm{m^2\,s^{-1}}$	$3e^{-5}$
Vertical Eddy Viscosity	$\mathrm{m^2\,s^{-1}}$	$1e^{-3}$
Horizontal Eddy Viscosity	$\mathrm{m^2\,s^{-1}}$	$3e^{5}$
Implicit vertical diffusivity for convection	$\mathrm{m^2\,s^{-1}}$	10
Gent and McWilliams (1990) Isopycnal diffusivity	$\mathrm{m^2\,s^{-1}}$	$1e^{3}$
Advection scheme	-	number 33

Table 2.2: Parameter values used for the physical component of ocean model.

$$F_S = \frac{S_0}{\Delta z_s}(E - P - R), \tag{2.4}$$

where F_u, F_v F_θ, F_S are the zonal momentum, meridional momentum, potential temperature, and salinity forcing respectively. Δz_s is the upper ocean grid layer thickness in metres. A reference density, ρ_0 ($999.8\,\mathrm{kg\,m^{-3}}$), and reference salinity S_0 (35), convert the externally supplied forcing values, wind stress τ_x and τ_y ($\mathrm{N\,m^{-2}}$), temperature, θ (°C), and $E - P - R$ ($\mathrm{m\,s^{-1}}$) into tendencies of F_u, F_v, F_θ, F_S.

To prevent model drift, there is a relaxation in the upper layer toward monthly climatological atmospheric surface temperature ($\theta*$), over a time scale of 2 months.

2.2.3 Initial Conditions

The ocean is initialised with a global salinity of 35 psu, and temperature decreasing linearly with each level from 20 °C at the surface to 5 °C in the abyss. Table 2.2 shows the standard physical model parameters and the values employed in the ocean model.

2.2.4 Mixing Parameterisations

Sub-grid scale physical processes such as mesoscale eddies are not explicitly resolved and need to be represented in relation to the large scale flow. Steep isopycnals in the ocean are unstable due to baroclinic instability. Baroclinic instability transforms gravitational potential energy in the mean state into kinetic and potential energy of mesoscale eddies, and the slope of the isopycnals is reduced. An eddy parameterisation scheme must be incorporated to mimic the conversion of mean potential and kinetic energy to eddy potential energy and produce a realistic modelled state with a sensible distribution of tracers.

These unresolved processes associated with mixing and advection in the ocean are parameterised following the Redi (1982) parameterisation of neutral density surface diffusion and the Gent and McWilliams (1990) eddy parameterisation. The Gent and McWilliams (1990) parameterisation is widely accepted and has been applied in non-eddy resolving numerical simulations with success. The aim is to parameterise baroclinic instability as isopycnal layer thickness diffusion; this diffusion can then be expressed as the transport or advective effect of geostrophic eddies through a bolus velocity term, v^* (Gent et al., 1995).

2.2.5 Biogeochemistry

The marine biogeochemistry package explicitly solves for oxygen concentration and primary productivity in the ocean. The package considers the cycling of carbon, phosphorous and oxygen in the ocean. The tracers used include Dissolved Inorganic Carbon (DIC), alkalinity, PO_4, Dissolved Organic Phosphate (DOP) and O_2. Table 2.3 outlines the globally uniform initial values of biogeochemical tracers. The export of biological matter is computed as a function of available light and PO_4. The model velocity and diffusivities are used to redistribute tracers in the ocean. MITgcm does not take into account the changes to tracer concentrations due to surface freshwater fluxes. These changes are negligible for most tracers, with the exception of CO2, so a 'virtual' flux is considered (Dutkiewicz et al., 2005). The air-sea exchange of CO2 is parameterised with a uniform gas transfer

Tracer	Units	Initial value
O_2	mol O $/m^3$	0.0959212
PO_4	mol P $/m^3$	0.00219434
Alkalinity	mol eq $/m^3$	2.36004
DIC	mol C $/m^3$	2.20837
DOP	mol P $/m^3$	$5.60655e-6$

Table 2.3: Initial conditions for tracers of biogeochemistry package. All values are initialised globally across all vertical layers.

coefficient. The flux of CO2 into/out of the ocean is passed directly into a well mixed atmospheric box, whose total mass is such that the observed ratio between atmospheric mass and ocean surface area is maintained. The atmospheric box is not radiatively active, and as such the restoring condition for surface temperature is independent of pCO2.

An idealised parameterisation of net primary productivity, limited by the availability of photosynthetically active radiation (PAR) and phosphate (PO_4), is applied as follows:

$$PP = \alpha \frac{PAR}{PAR + K_{PAR}} \frac{PO_4}{PO_4 + K_{PO_4}} \tag{2.5}$$

where $\alpha = 2 \times 10^{-3}\,\mathrm{mol/m^3/year}$ is the maximum community production, and the half saturation constants are $K_{PAR} = 30\,\mathrm{W\,m^{-1}}$ and $K_{PO_4} = 5 \times 10^{-4}\,\mathrm{mol\ m^3}$. It is assumed two-thirds of the net production will enter the dissolved organic pool at an e-folding timescale for remineralisation of 6 months. The remaining one-third of net organic production is exported to depth as particulate organic phosphorous (POP), where it is then remineralised according to the empirical power law of Martin et al. (1987).

The residence time of phosphorus in the ocean is 10 ky to 40 ky, and is much longer than the oceanic turnover timescale. The global average oceanic concentration of phosphorous is therefore fixed, riverine and atmospheric sources are not represented, and sedimentation is not allowed.

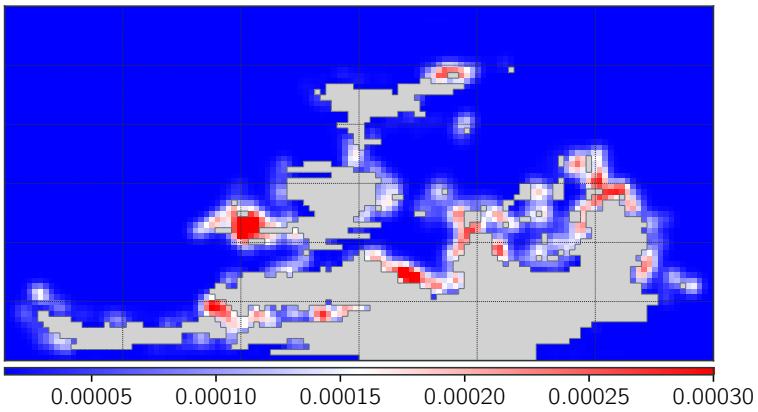

Figure 2.4: Spatially varying depth mean diapycnal diffusivity in the deep ocean calculated from Late Devonian tidal dissipation energy ($m^2\,s^{-1}$).

Phosphate in the ocean is consumed during photosynthesis, fuelling marine primary productivity in the photic zone, and is exported to the disphotic zone as particulate or dissolved organic matter, ultimately to be advected by the global ocean circulation, returning to the surface in upwelling zones.

Phosphate is the limiting nutrient included in the OGCM setup. It was chosen not to include iron in the present study. Although iron is an important constraint on primary productivity, present-day fluxes are difficult to quantify and so simulating Devonian iron fluxes would imply major assumptions on land surface composition and topology.

2.2.6 Tidal Mixing

Given the importance of the Late Devonian Ocean Circulation for both evolution and extinction, it is important to consider the effects of tidal mixing on the ocean circulation. The vertically integrated turbulent energy dissipation rate ϵ is provided by Mattias Green (University of Bangor). The tidal simulations are based on Wilmes and Green (2014) and use Oregon State University Tidal Inversion Software (OTIS), which solves the linearised shallow water equations on a horizontal grid. The only forcing in that model is an astronomic tide-generating force, and energy is dissipated through a quadratic bed-friction term and a linear tidal conversion scheme representing the energy losses to internal tides.

To allow vertical distribution of the tidal mixing a vertical decay function is used,

$$F(z) = \frac{e^{-(H+z)\backslash\zeta}}{\zeta(1 - e^{-H\backslash\zeta})} \tag{2.6}$$

where z is the depth decreasing from zero at the surface, H is the bottom depth, and $\zeta = 500\,\mathrm{m}$ is the e-folding height.

A tidal mixing parameterisation is then used based on Schmittner et al. (2015), and the spatially varying diapycnal diffusivity is computed offline from turbulent energy dissipation rate ϵ, using the structure function F:

$$k_v(x, y, z) = k_{bg} + \frac{\Gamma\epsilon(x, y)F(x, y, z)}{N^2} \tag{2.7}$$

where $k_{bg} = 1.5 \times 10^{-5}\,\mathrm{m^2\,s^{-1}}$ is a global background constant diffusivity, N is the buoyancy frequency, and $\Gamma = 0.2$ is a mixing efficiency. The total energy from mixing is kept constant between the OGCM simulation and the Ocean General Circulation Model with spatially variable diapycnal diffusivity (OGCMmix) simulation. This is done by having a lower value for the global background constant diffusivity in the latter experiment compared to the defined diapycnal diffusivity in the uniform mixing simulation.

2.2.7 Model Performance

The model setup presented here for the ocean simulation was tested rigorously. Additional simulations considered different advection schemes, GMRredi parameter and implicit vertical diffusivity for convection values, etc. Experiments with varying seafloor bathymetry, as well as different north hemisphere ridge heights were also run to validate the setup presented here. Using this setup, a control run of the present day continental configuration and a similar seafloor bathymetry pattern (incrementing 1000m per grid cell away from the coastline) showed the results were comparable to other model simulations of a similar vertical/horizontal resolution, and consistent with observations of the present day ocean circulation (Talley, 2003; Lumpkin and Speer, 2007; Lauderdale et al., 2013).

Level	Thickness (Pa)	Height Centre (Pa)	Initial Potential Temperature (K)
1	10000	95 000	289.6
2	25000	77 500	298.1
3	30000	50 000	314.5
4	20000	25 000	335.8
5	15000	7500	437.4

Table 2.4: Vertical grid used in MITgcm atmosphere configuration.

2.3 MITgcm Atmospheric Model

The second step in understanding the Late Devonian climate is to mimic the De Vleeschouwer et al. (2014) atmospheric slab ocean model using the MITgcm. This allows comparison between atmospheric models, and subsequently when the MITgcm atmosphere is coupled to a dynamic ocean, comparison with the MITgcm atmospheric model results can be made to determine the potential importance of simulating deep time palaeoclimates with a coupled atmosphere-ocean-sea-ice model. However, De Vleeschouwer et al. (2014) imposed an ocean heat flux within their slab ocean to simulate a low equator-pole temperature gradient. This is not possible in the MITgcm; however, not using the De Vleeschouwer et al. (2014) approach and neglecting ocean heat transport will allow us to gain a better understanding of the importance of a dynamic ocean in simulating the climate.

The atmospheric physics package developed by Molteni (2003) is well suited to exploratory climate simulation. The atmospheric component can be used with a non-dynamic ocean, a simple mixed layer ocean, or coupled to a fully dynamic ocean and ice package. The atmosphere is of 'intermediate' complexity, consisting of five vertical levels (table 2.4), and applies the Simplified Parameterisation, Primitive Equation Dynamics (SPEEDY) physics package, comprising a four-band radiation scheme, parameterisation of moist convection, boundary layer scheme, and resolved baroclinic eddies.

The atmospheric with slab ocean model is integrated for 80 years, of which the last 10 years are retained to compute for both monthly/seasonal averages and a 10 year average. Each component of SPEEDY is discussed briefly here, in addition to the boundary conditions and model configuration.

2.3.1 Convection

When conditional instability is present, mainly when saturation moist static energy decreases with height between the Planetary Boundary Layer (PBL) and the upper troposphere, a simplified mass-flux scheme is activated. This also applies when humidity in the PBL exceeds a certain threshold. The cloud-base mass flux (at the top of the PBL) means the PBL humidity is relaxed towards the threshold value (0.9). Detrainment occurs only at the cloud-top level (determined by the conditional instability criterion), while entrainment occurs in the lower half of the troposphere. The air in the updrafts is assumed to be saturated.

2.3.2 Large Scale Condensation

If relative humidity exceeds a threshold, specific humidity is relaxed towards that threshold value, and latent heat content in the atmosphere is converted to dry static energy.

2.3.3 Cloud Cover

Cloud cover within an air column is calculated diagnostically from maximum relative humidity within all tropospheric layers excluding the PBL.

2.3.4 Shortwave Radiation

The shortwave radiation scheme allows shortwave radiation to be reflected by clouds at the top of the troposphere and at the surface; the cloud albedo is proportional to the total cloud cover. The shortwave transmissivity is a function of layer mass, specific humidity and cloud cover.

2.3.5 Longwave radiation

A four-band longwave radiation scheme is used; for the atmospheric 'window' and for the absorption by water vapour and carbon dioxide. At each layer, transmissivities in each of the four bands is a function of layer mass and humidity. Clouds represent a decrease in transmissivity of the 'window' band, as a function of cloud cover.

2.3.6 Surface fluxes of momentum and energy

Surface fluxes are specified by bulk aerodynamic formulae with varying exchange coefficients between land and the ocean. Coefficients for sensible and latent heat fluxes are dependent on the vertical gradient of potential temperature between the surface and the lowest model level.

2.3.7 Vertical diffusion

Vertical diffusion is a redistribution of dry static energy and moisture and is only applied between the two lowest model layers. This calculates shallow convection in regions of conditional instability; diffusion of water vapour in stable conditions, acting to lower the tropopause; and diffusion of dry static energy if the lapse rate approaches the dry-adiabatic limit.

2.3.8 Ice Package

A three-layer thermodynamic sea-ice model is implemented, based on Winton (2000). The model considers two equally thick ice layers; while the upper layer has a variable specific heat resulting from brine pockets, the lower layer has a fixed heat capacity. Above the ice is a zero heat capacity snow layer. Changes in snow and ice layer thicknesses are calculated from heat fluxes at the top and bottom surfaces. Grid cells of the ocean model follow a parameterisation to allow fractions of the cell to have ice in both the atmospheric slab ocean model and coupled atmosphere-ocean-sea-ice model.

2.3.9 Boundary Conditions

A simple two-layer land model is also included (Hansen et al., 1983), with a top layer depth of 0.1 m, and second layer depth of 4 m, allowing the exchange of heat and moisture between layers. The initial aim of running the MITgcm atmospheric model with a slab ocean model is to compare with the De Vleeschouwer et al. (2014) study, which used the Hadley Centre Slab Ocean Model (HadSM3). De Vleeschouwer et al. (2014) imposed an ocean heat flux calculated from SST, which had a parabolic decline from a maximum

Parameter Name	Units	Value
Acceleration due to gravity	$\mathrm{m\,s^{-1}}$	9.81
Earth Rotation Period	s	79200
Momentum time step	s	200
Tracer timestep	s	200
Solar Constant	$\mathrm{W\,m^{-2}}$	1324
Drag coefficient over land	-	0.0018
Drag coefficient over sea	-	0.0008
CO_2	ppm	2200
Albedo of wet snow	-	0.45
Albedo of cold snow	-	0.80
Albedo of ice max	-	0.60
Albedo of ice min	-	0.25
Obliquity	°	23.45
Eccentricity	°	0

Table 2.5: Parameter values used for atmospheric model

Parameter	Tropical	Arid	Mid-Latitude Severe	Mid-Latitude	Ocean
Vegetation Fraction	0.95	0.25	0.8	0.9	NA
Surface albedo	0.15	0.3	0.2	0.2	0.3

Table 2.6: Surface albedo and vegetation fractions assigned to different land surface types, based on De Vleeschouwer et al. (2014).

32 °C at the equator to 0 °C at the poles. In the MITgcm model, however, we prescribe an initial SST in the same pattern as De Vleeschouwer et al. (2014); declining from 32 °C at the equator to 0 °C at the poles. But, the model then calculates the ocean heat, freshwater and salt fluxes from changes in ocean temperature at each iteration.

Continental outlines are consistent across both the atmosphere and ocean models, and the same cube sphere C32 grid is used. Figure 2.5 shows the Late Devonian topography; the Laurussia orographic barrier has the highest elevation since Torsvik et al. (2012) determined fast convergence surrounding this continent. The model is run without vegetation feedbacks. Figure 2.6 illustrates the geographic representation of land surface types applied. For each land surface type, a surface albedo and vegetation fraction is set (corresponding values in table 2.6). Initial soil moisture, sea-ice fraction, snow depth, and land temperature are zero. The Late Devonian solar constant is $1324\,\mathrm{W\,m^{-1}}$ (Gough, 1981), and pCO_2 is 2180 ppm (Berner, 2006). The orbital forcings are defined in table 2.5, these are the present day values of obliquity and eccentricity based on Hartmann (2015).

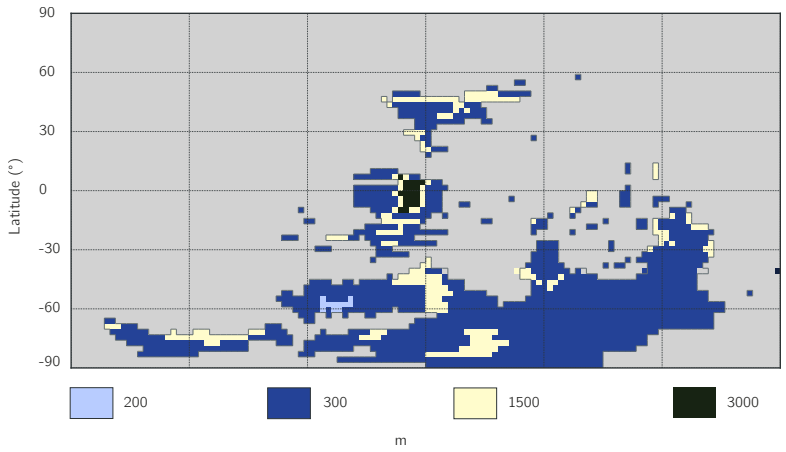

Figure 2.5: Late Devonian topography used in atmospheric simulations.

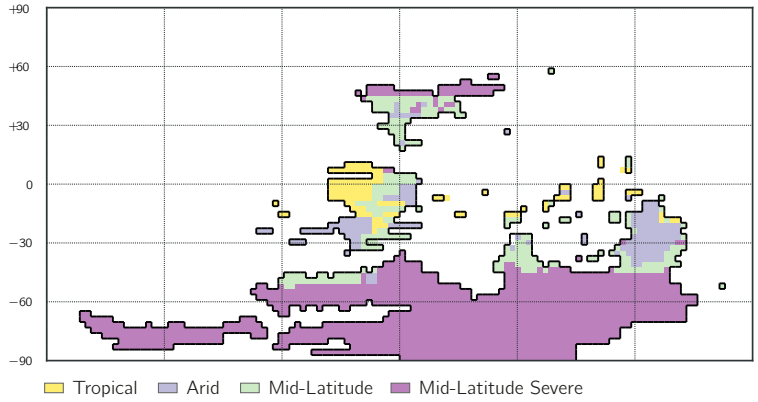

Figure 2.6: Late Devonian land surface types and biomes.

Parameter Name	Units	Value
Momentum time step atmosphere	s	900
Tracer time step atmosphere	s	900
Momentum time step ocean	s	3600
Tracer time step ocean	s	3600
Coupler exchange timescale	s	3600

Table 2.7: Parameter values used for the physical component of coupled model.

The model setup presented was tested against various additional simulations to consider the impact of changes in vegetation parameter values/locations, pCO_2, and the position and height of mountains, as well as testing different initial conditions of SST pattern, soil moisture and land temperature to determine the effects on the resultant climate. This investigation showed the vegetation parameter to have little impact on the climate, but the position of large mountains does alter the atmospheric circulation pattern. Though, as discussed the positions of major mountains used in this model are widely accepted. The model setup presented here was verified with the present day continental configuration and topography. The present day atmospheric circulation was comparable to what would be expected for an atmospheric slab ocean model of this resolution and complexity.

2.4 Coupled Atmosphere-Ocean-Ice Model

The oceanic and atmospheric components are largely as described above. Each component uses the same C32 horizontal model grid, greatly simplifying their coupling. The vertical grid layering and initial temperature in the ocean and atmosphere are as described in tables 2.1 and 2.4. However, instead of providing monthly atmospheric forcing fields for the ocean, fluxes of momentum, heat and freshwater are exchanged between the ocean and atmosphere every hour. Parameter values used for the oceanic and atmospheric components of the coupled model are largely the same as in their individual simulations with the exception of time-stepping (tables 2.2 and 2.5). Altered parameter values required for coupling are listed in table 2.7. The ice model used is the same as that described in section 2.3.

No explicit river model is included: the amount of water that exceeds the field capacity of the soil in a given grid point is transferred following the slope of topography to the nearest ocean grid cell following a prescribed mapping.

The coupled model is launched from a state of rest and has been integrated for 20 000 years. The whole system is integrated forward on a parallel computer, six processors being employed for the atmosphere, six for the ocean and one to handle coupling.

An additional simulation of the Late Devonian coupled climate is also presented with a reduced CO_2 forcing of 375 ppm. Control experiments of the coupled atmosphere-ocean-sea-ice model setup were simulated for the present day continental configuration, the results were as expected and comparable to the observed climate. Although, the results are not shown, the model setup discussed is reproduced from studies of the present day climate using MITgcm (Lauderdale et al., 2013; Ferreira and Marshall, 2015), which have also been applied to idealised climates (Marshall and Plumb, 2007; Ferreira and Marshall, 2015), and palaeoclimates (Brunetti and Vérard, 2017; Pohl et al., 2017).

2.5 Summary

In this chapter, we have provided an introduction to the MITgcm model setup that will be used in the following chapters of this thesis. In chapter 3, the Late Devonian ocean circulation, simulated with the MITgcm ocean-only setup is described. The ocean-only experiment is then modified to include spatially variable diapycnal diffusivity consistent with OTIS tidal energy dissipation in chapter 4. This enables exploration of how changes in the model's diapycnal diffusivity affects the large-scale ocean circulation. In chapter 5, the results of an MITgcm atmospheric slab ocean model are presented and then compared to experiments with a coupled atmosphere-ocean-sea-ice model. The importance of using a coupled climate model to gain insight into palaeoclimates is of particular interest in this study, and so comparison with the geological record is essential. The potential implications for further understanding of the Late Devonian climate, extinction, and evolution are then presented.

Chapter 3

Ocean General Circulation Model

In this chapter, the results of the ocean only general circulation model referred to as the OGCM, will be presented and discussed in relation to Devonian extinction and evolution events. The focus will be on the experiments with uniform diapycnal diffusivity.

The model's Late Devonian ocean circulation alternates between two distinct states. It comes into equilibrium in an unventilated state, where the deep ocean is strongly stratified and isolated from the surface. The model remains in this state for a few thousand years. Approximately 4700 years after the start of the simulation, a ventilated phase is initiated, with strong convective mixing in the Northern Hemisphere allowing exchange with the deep ocean. Conditions then remain relatively constant until 6000 years into the run, after which the ocean gradually returns to an unventilated state. This cycle repeats 9200 years into the model simulation.

We first discuss the mean state and ocean circulation in each of the two quasi-equilibrium states, before considering the characteristics of the transitions between them.

3.1 Unventilated phase

Once the model reaches equilibrium, the ocean is strongly stratified, and there is a clear asymmetry between hemispheres in the zonal mean. Figure 3.1 (A-C) shows the zonal average potential temperature, salinity and density. During this unventilated phase, there is a warm lens in the subtropics, with temperatures >15 °C extending to depths of 1000 m. This warm pool is asymmetric between hemispheres, as in the present-day Atlantic Ocean, with warm water extending deeper in the Northern Hemisphere than in the Southern Hemisphere, and thins markedly at the equator. However, this thermocline region is substantially warmer in the Late Devonian than in the present-day ocean, with a temperature of approximately 12°C in the Northern Hemisphere subtropics at 1300 m, in comparison with temperatures of 7 °C and 4 °C at similar depths in the present-day Atlantic and Pacific, respectively.

The zonal mean salinity structure is dominated by a saline tongue which appears to emanate from the surface between 30 ° N to 45 ° N, and then extends southward at a depth of 500 to 3000 m and eventually fills the deep ocean. In the present-day North Atlantic there is also a saline-tongue feature from the surface penetrating to depths of 2000 m and forming a salinity maximum between 1000 m to 2000 m, although that saline tongue is largely the signature of saline water outflowing from the Mediterranean Sea at 36 ° N, as well as of North Atlantic Deep Water sinking at high northern latitudes and flowing south in the Atlantic Meridional Overturning Circulation (AMOC) (Baringer and Price, 1997; Huang, 2010).

There are strong meridional gradients in temperature and salinity within the upper few hundred metres of the ocean. In the high latitudes, surface waters are cold and relatively fresh with warmer, more saline subtropical intermediate water extending beneath. The fresh surface layer results in strong stratification, which buffers mixing with the underlying warm water. This high latitude surface water is colder and extends deeper in the Northern Hemisphere than the Southern Hemisphere, resulting in a stronger vertical temperature gradient in the north. The subsurface southward transport of salt into the high latitudes of the Southern Hemisphere makes the region of warm intermediate water below the halocline saltier and denser than its Northern Hemisphere equivalent.

The polar regions of the unventilated Devonian Ocean and the present-day Arctic Ocean show some similarities. Both have a cold freshwater cap, with a sharp halocline beneath. Below the halocline, temperature increases and subsequently decreases, along with salinity, to the deep ocean. In the present-day Arctic Ocean this surface structure pre-conditions the region for sea-ice formation (Talley et al., 2011), but sea-ice is not formed in the Late Devonian Ocean simulation since surface temperatures only reach a minimum of 0 °C.

The lowest density waters occur in the Southern Hemisphere at high latitudes, due to fresh surface waters. Deep isopycnals are not ventilated to the surface in either hemisphere. The deep ocean is strongly stratified in density.

At the surface, wind stress in the tropics drives a westward current centred just north of the equator which is partially diverted northwards, flowing between Siberia and Laurussia and generating a circum-equatorial current (Figure 3.2). This current also interacts with the western boundaries, flowing southward along the western boundary of south Panthalassa (eastern Gondwana), the Paleo Tethys and the Rheic Ocean, and northward along the western boundary of North Panthalassa (eastern Siberia). This aids transport of water away from the equator. Both the Rheic and Paleo Tethys are semi-restricted net evaporative basins where the only source of refreshment is inflow of the circum-equatorial current, at depths shallower than the gateways on their northern boundaries.

Throughout the unventilated phase, northward currents along both meridional boundaries of Siberia transport warm water northward (Figure 3.2). Figure 3.8 shows that subsurface heat content north of Siberia gradually increases because this northward transport of subsurface warm water leads to a gradual accumulation of heat in the subsurface which is unable to mix to the surface due to the stratified fresh surface layer above.

The residual overturning circulation shown in Figure 3.3A is the sum of the Eulerian meridional overturning streamfunction $\psi(\phi, z)$ and the eddy bolus transport $\psi * (\phi, z)$, defined as follows:

$$\psi = -\int_{z_{bottom}}^{z} \int_{\lambda_E}^{\lambda_W} v \, d\theta \, dz' \tag{3.1}$$

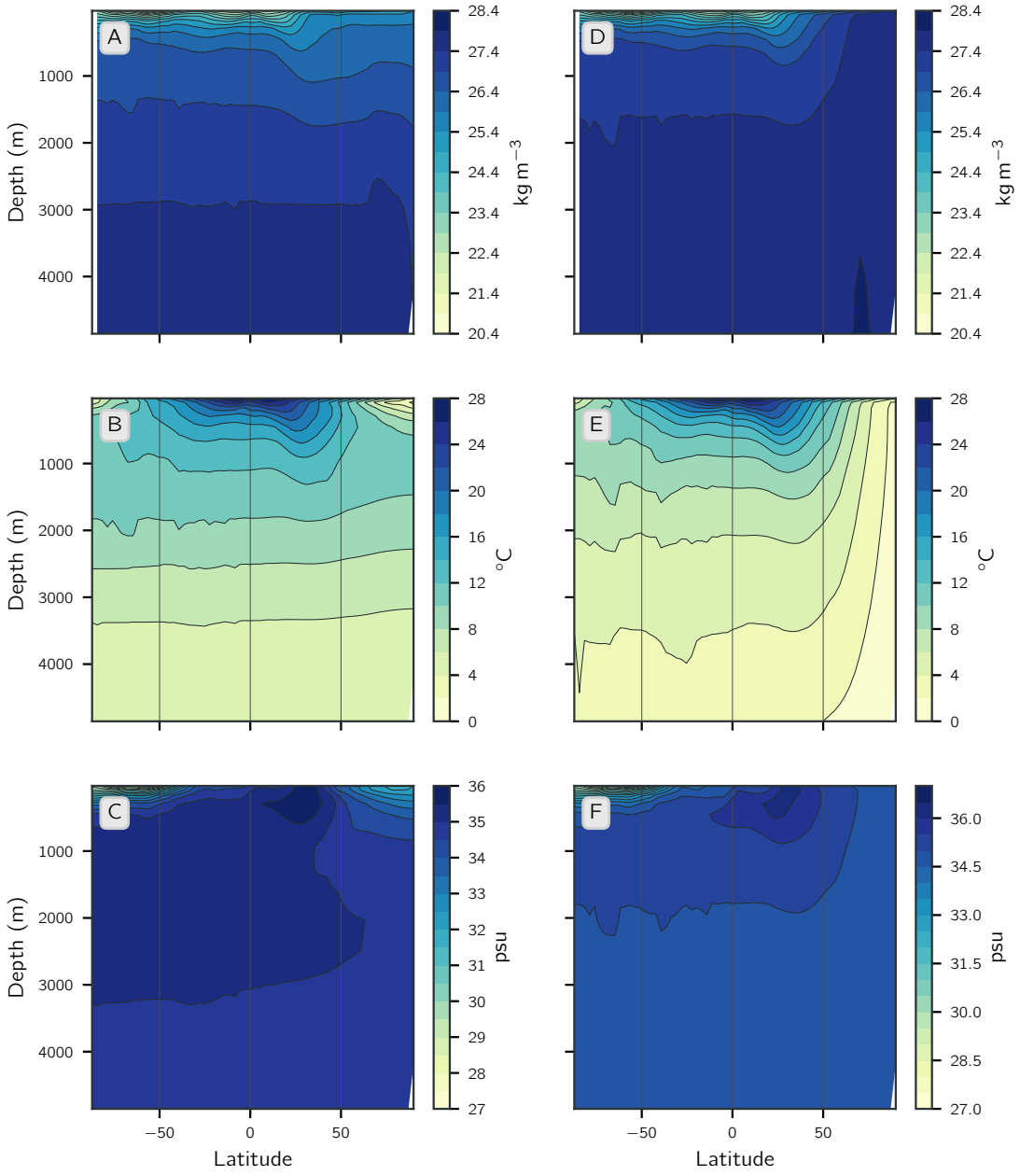

Figure 3.1: 100-year average, zonal mean properties of the Frasnian ocean for both the unventilated phase (left) and ventilated phase (right). (A & D) potential density; (B & E) potential temperature; (C & F) salinity.

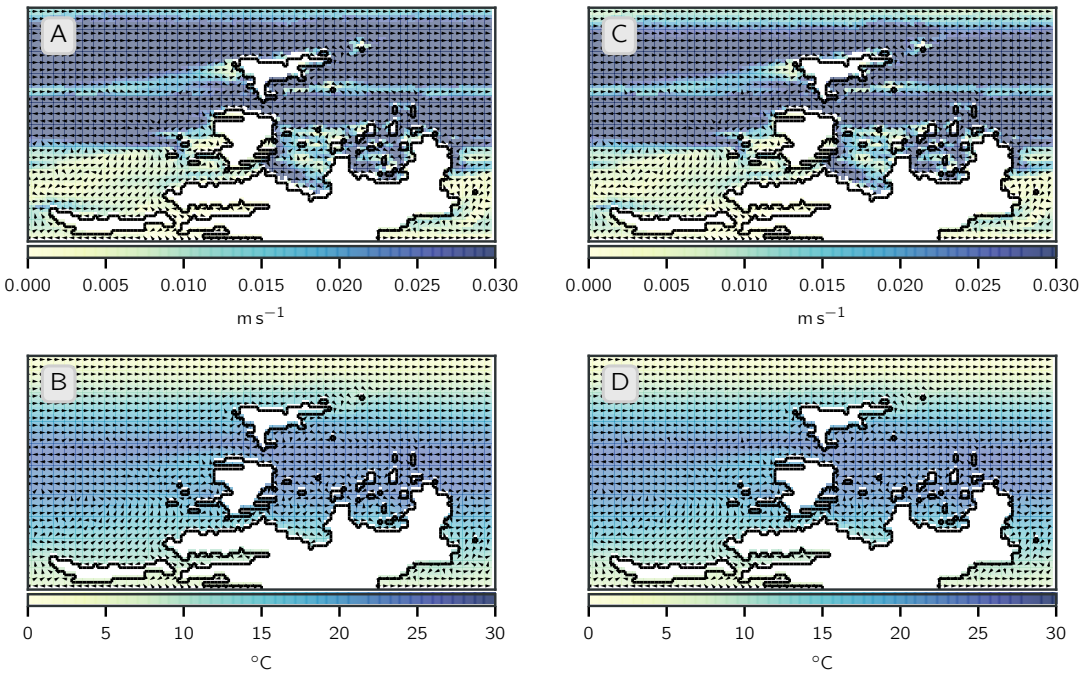

Figure 3.2: 100-year and upper 300m average currents. (A & B) After 4000 years, during unventilated phase; (B & C) After 5000 years, during ventilated phase. Arrows indicate direction and colours indicate upper 300 m speed (A & C) and average upper 300m temperature (B & D).

$$\psi* = -\int_{z_{bottom}}^{z} \int_{\lambda_E}^{\lambda_W} v^* \, d\theta \, dz' \tag{3.2}$$

$$\psi_{res} = \psi + \psi* \tag{3.3}$$

where v is the meridional velocity, v^* is the meridional bolus velocity, calculated by the MITgcm GMREDI package, θ is the longitude, z is depth, and ϕ is the latitude. Both ψ and $\psi*$ are integrated up from the seafloor and from eastern (λ_E) to western (λ_W) ocean boundaries.

The residual overturning circulation is dominated by two counter-rotating meridional cells on either side of the equator and extending throughout the sub-tropics. Strong westward wind stress in the region surrounding the equator drives poleward surface Ekman transport in both hemispheres, resulting in Ekman upwelling on the equator. In the

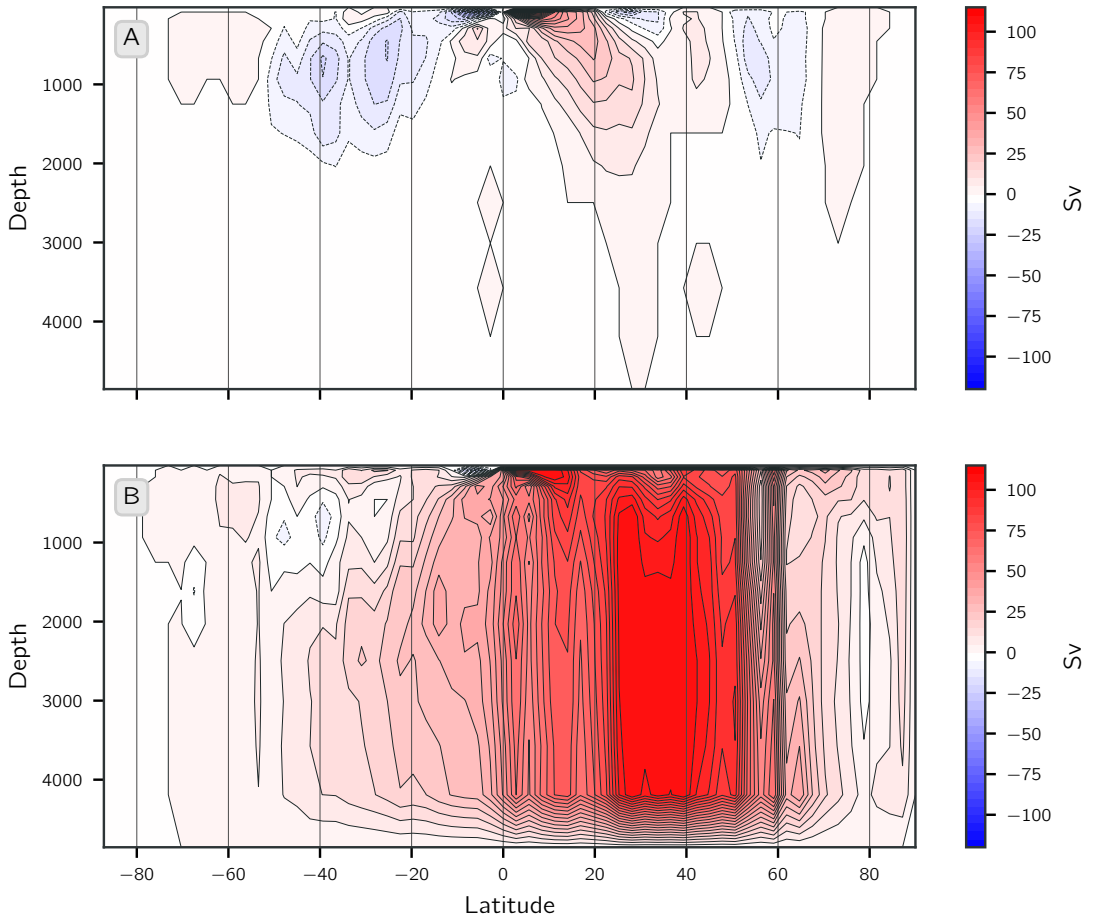

Figure 3.3: 100-year mean zonally averaged residual overturning circulation. (A) 4000 years, during the unventilated phase; (B) 5000 years, during the ventilated phase.

Northern Hemisphere, the surface water flows poleward, density increases due to net evaporation, coupled with Ekman convergence, leading to warm saline water sinking at about 30 °N. Sinking at this latitude is prominent around Siberia, particularly in the western Panthalassa. This region experiences the strongest convective mixing simulated and the mixed layer depth reaches up to 300 m (Figure 3.4). Sinking of this water mass is restricted to the upper 1500 m, and deep circulation is weak, indicating that the convective mixing does not penetrate into the deep ocean.

The zonal-mean Southern Hemisphere subtropical overturning cell is a combination of weak circulations in each of the Rheic, Paleo Tethys and Panthalassa Oceans. Within all basins Ekman processes transport the surface waters poleward away from the equator, and they subsequently increase in density and sink. Within the Paleo Tethys and Rheic

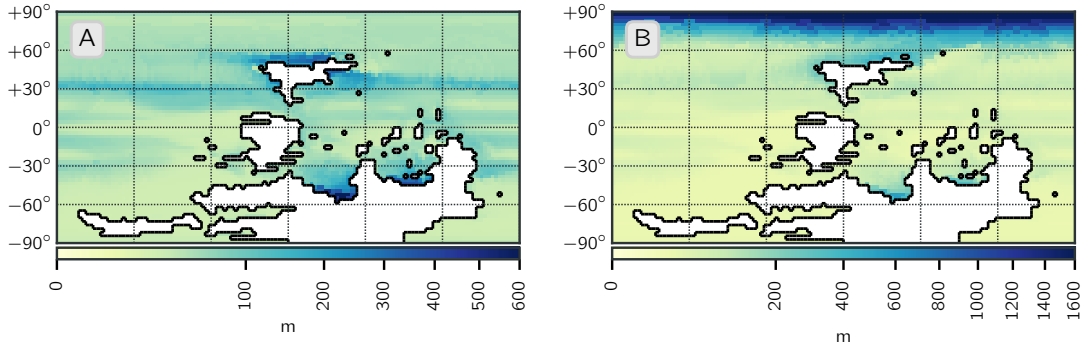

Figure 3.4: 100-year mean ocean surface mixed layer depth after (A) 4000 years, during the unventilated phase; (B) 5000 years, during the ventilated phase.

Oceans, dense saline surface waters sink along the southern boundaries at 40 ° S to 50 ° S to depths of 1000 m to 1500 m. This is apparent in fig. 3.3, which shows a weak overturning cell within the latitude range of the Rheic and Paleo Tethys. In the Panthalassa Ocean, poleward surface waters flow predominantly as a western boundary current, sinking at 30 ° S due to converging Ekman transport (figs. 3.2 and 3.4). When the present-day global overturning circulation is viewed in the zonal mean, as in fig. 3.3, there are also two distinct counter-rotating meridional cells in the upper ocean. However, the present-day circulation also comprises a deep inter-hemispheric overturning cell associated with buoyancy loss in the Northern Hemisphere high latitude regions and adiabatic upwelling in the Southern Ocean around Antarctica (Lumpkin and Speer, 2007; Richardson, 2008).

In the mid-latitude Northern Hemisphere, a shallow overturning circulation is driven mechanically by wind forcing. Ekman transport drives downwelling at 30 ° N, forming a shallow depth northward flow which is brought to the surface at 50 ° N.

In the Northern Hemisphere higher latitudes there are no meridional boundaries northward of 50 ° N. In this region there are two weak counter-rotating cells circulations. The continuous eastward wind stress north of Siberia drives southward Ekman transport. This forms a weak overturning cell, with downwelling on the northern boundary of Siberia (Figure 3.3).

The circumpolar currents of the northern Panthalassa Ocean are similar to those in the present-day Southern Ocean, which also has no meridional boundaries, and as a result hosts the ACC which encircles Antarctica driven by strong westerly winds (Gill, 1982; Döös and Webb, 1994).

The Rheic and Paleo Tethys mid-latitude ocean circulation is similar to the north Panthalassa ocean. The upper ocean is well mixed due to haline-driven overturning, and below this well mixed surface layer the deep oceans are strongly stratified with a lack of convective mixing.

The tropics dominate the ocean circulation during the unventilated phase. Similar to the present-day, the upper tropical oceans of the Late Devonian are strongly stratified in potential density and temperature; this is due to solar heating, and E-P.

Zonal mean zonal ocean currents (fig. 3.5) show a strong westward surface current close to the equator. This continuous westward current causes a build up of fluid on the western boundaries of the Panthalassa and Rheic Oceans, resulting in an east-west pressure gradient. Since the Coriolis force is negligible at the equator, this flow returns eastward, below the surface current, known as the Equatorial Undercurrent (EUC) (fig. 3.5) (Philander, 1980; Gill, 1982). The surface westward current, driven by strong easterly trade winds, extends to depths of 100 m on the equator. This is deeper than the present-day surface current. Below this surface current the is EUC, a relatively weak eastward current ($0.08\,\mathrm{m\,s^{-1}}$), at greater depths than the present-day EUC, between 150 m to 900 m. The surface wind stress is driving these currents and explains the pattern observed in the zonal mean potential temperature. The east-west pressure gradient brings the thermocline up to the surface, causing coastal upwelling on the western boundary of Laurussia and China, making the surface temperature in the west of the ocean basin warmer, and colder in the east (fig. 3.6). The sloping caused by the east-west pressure gradient in the Panthalassa Ocean is clearly shown in fig. 3.6. The EUC slopes upwards from ∼800 m at 100 °E to 200 m at 75 °W where the water then upwells to the surface on the eastern boundary of Panthalassa at 50 °W.

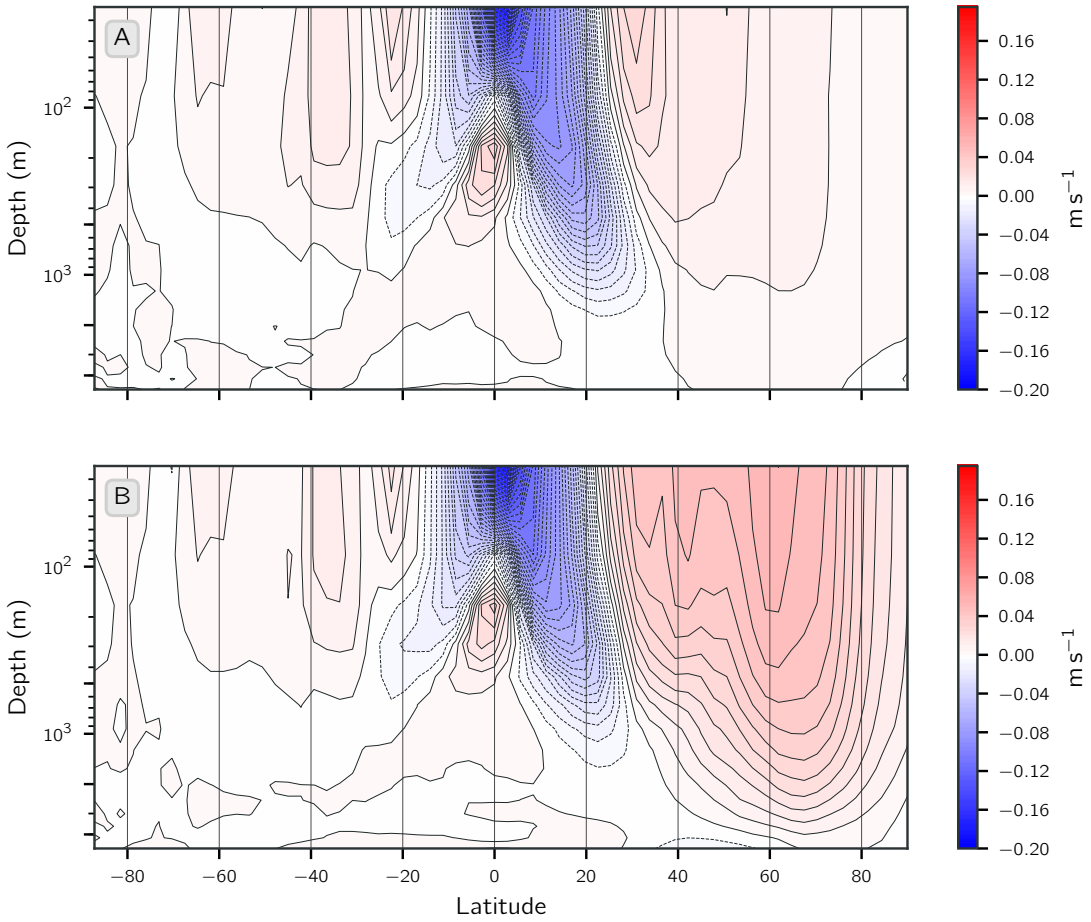

Figure 3.5: 100 year and zonal mean zonal velocity during (A) unventilated phase; (B) ventilated phase.

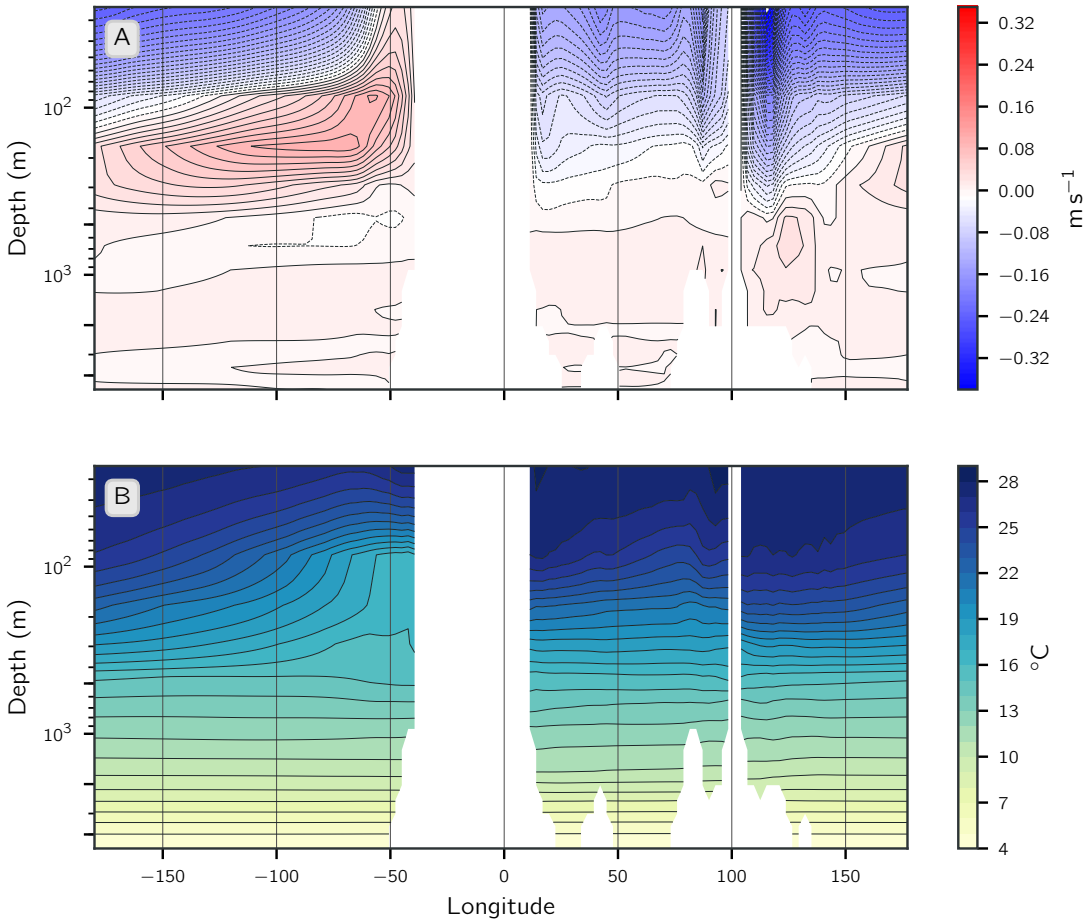

Figure 3.6: Equatorial zonal velocity (A) and temperature (B) during the unventilated phase.

In the present-day Pacific Ocean the effects of this east-west tilting of the thermocline are greater than in the Atlantic since the Pacific is broader than the Atlantic (Katz, 1977; Meyers, 1979; Gill, 1982; McWilliams and Danabasoglu, 2002). The Panthalassa Ocean is once again broader than the present-day Pacific, causing the EUC to flow deeper than the present-day Pacific EUC. However, fig. 3.2 shows the depth-integrated surface currents, and the flow is partially diverted northward, which allows flow between Laurussia and Siberia, resulting in a circum-equatorial current. This explains the weaker EUC seen in the Devonian Ocean simulation in comparison to the present-day.

Outside the tropics and subtropics, the weak westerly wind stress drives the weak surface eastward currents, also visualised in fig. 3.2. The strength decreases in both hemispheres poleward. Ekman pumping causes upwelling of cooler water in the tropics and downwelling of warm surface waters between 20° to 60° in each hemisphere.

The total meridional ocean heat transport

$$H_{total} = \rho_0 c_p \int_{\lambda_E}^{\lambda_W} \int_{-H}^{0} H \, d\theta \, dz \tag{3.4}$$

is the sum of any overturning component, gyre heat transport and eddy heat transport (Meijers et al., 2007):

$$H = \langle V \rangle \langle T \rangle + \langle V \rangle T^{'} + V^{'} \langle T \rangle + V^{'} T^{'} + V^{*} T, \tag{3.5}$$

where ρ_0 is a reference density, c_p is the specific heat capacity, $\langle\rangle$ refers to the zonal mean, $^{'}$ is the departure from that mean, and V^{*} is the meridional eddy bolus velocity.

Ekman upwelling and downwelling results in sloping isopycnals and the storage of potential energy at large scales. The GMREDI package parameterises the release of this energy via baroclinic instability, whilst conserving density and volume, thus acting to flatten the isopycnals and oppose the steepening resulting from the winds. Eddy bolus heat transport therefore generally opposes any Eulerian mean heat transport, acting to reduce the total heat transport slightly (fig. 3.7).

Heat transport during the unventilated phase is very weak polewards of 45° in both hemispheres. The Northern Hemisphere tropics and sub-tropics are active transporters of heat northwards, with peak transport of 2 PW in the region of 20 ° N. Peak ocean heat transport at equivalent latitudes in the Southern Hemisphere is less than 1 PW poleward. This tropical and sub-tropical transport of heat is associated with poleward Ekman transport, transporting warm water away from the equator. The mid-latitudes and high latitudes are inefficient transporters of heat in both hemispheres, although the Southern Hemisphere heat transport is marginally weaker.

The general pattern of meridional heat transport in the unventilated phase is similar to the present-day, although two key differences are worth emphasising. Peak transport today is also observed in the sub-tropics at approximately 25°, but is much weaker with maxima of 1.2 PW and 1.3 PW in the northern and Southern Hemispheres, respectively. Pacific and Indian ocean heat transport is linked to the strength of the tropical and subtropical wind-driven circulation (Ferrari and Ferreira, 2011). The Late Devonian tropical/subtropical winds drive an intense westward circum-equatorial current and strong poleward surface Ekman transport in both hemispheres; the strength of these winds is key to transporting heat polewards and regulating the climate.

A second key difference between the present-day and Late Devonian unventilated ocean is the much weaker mid-high latitude heat transport in the Late Devonian. Once again this is linked to weak wind stresses at these latitudes and the lack of a deep overturning circulation.

The meridional ocean heat transport has a significant impact on the Earth's climate, transporting heat out of the tropics toward the poles. A lack of heat transport towards the high-latitudes, if not compensated by the atmospheric heat transport or local radiative effects such as cloud-induced warming, would increase the meridional pole-equator temperature gradient, and cool the polar regions. Modelling of Earth's more recent warm climates such as the Eocene and Cretaceous also suggests weak ocean heat transport in the mid-high latitudes (Bice et al., 2000; Huber and Sloan, 2001). Coupled climate modelling of these warm periods has shown that the atmospheric meridional heat transport does not increase to compensate for reduced poleward heat transport; instead increased moisture

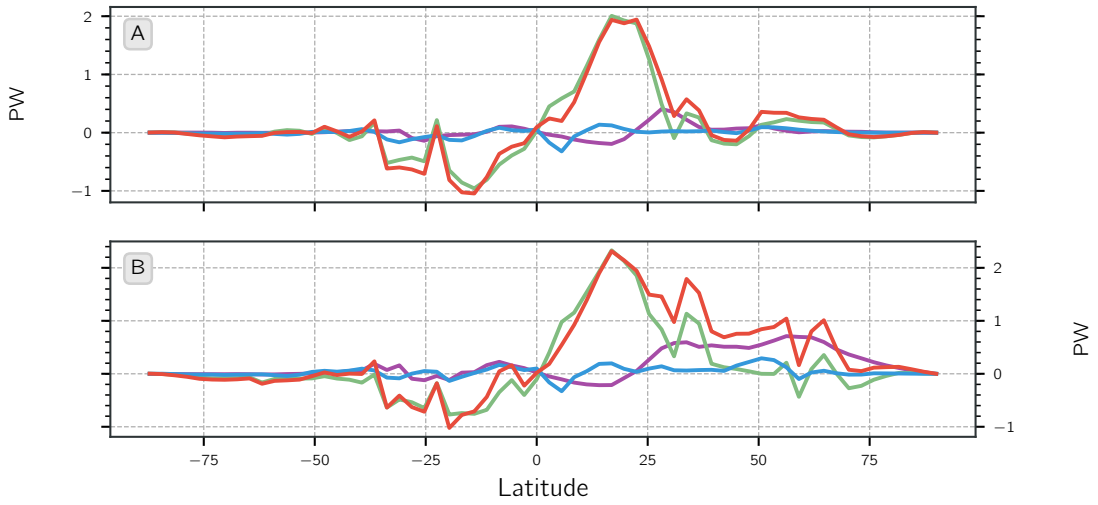

Figure 3.7: Meridional energy transport in the ocean: total heat transport (*red*), bolus heat transport (*purple*), overturning heat transport (*green*), gyre heat transport (*blue*). (A) After 4000 years, during the unventilated phase; (B) After 5000 years, during the ventilated phase.

and latent heat transport induces wetter cloudier conditions. Increased cloud coverage reduces the planetary albedo, and incoming solar radiation is reflected to space, acting to warm the high latitude regions (Weaver, 2003; Donnadieu et al., 2006; Kump and Pollard, 2008; Barreiro et al., 2011; Poulsen and Zhou, 2013).

3.2 Ventilated phase

During the ventilated phase, the fresh surface layer in the Northern Hemisphere high latitudes is absent, and the polar region is well-mixed over the whole water column. The surface temperature in this region decreases by approximately 0.8 °C, while the global mean ocean temperature above 500 m is 1.5 °C lower than during the unventilated phase.

Figure 3.1 shows the significant change between ventilated and unventilated phases in zonal mean ocean structure. Most noticeably there is a collapse of Northern Hemisphere polar stratification in the ventilated phase. Isopycnals outcrop from the deep ocean, and temperature and salinity are well mixed over the entire ocean north of 60 ° N. The zonal mean structure outside the Northern Hemisphere appears similar to the unventilated phase in the zonal mean, although there are some distinct differences. The cold surface

water in the Southern Hemisphere high latitudes is warmer and does not extend as deep, while the subsurface temperature maximum there is cooler. The thermocline is shallower in the subtropics, and the sub-tropical north hemisphere saline tongue does not extend as deep, although the salinity at the surface and intermediate depths is increased.

Surface currents in the Southern Hemisphere are almost identical between the two phases (figs. 3.2 and 3.5). In the Northern Hemisphere, the circum-equatorial current is reduced in strength westward of the Siberia-Laurussia gateway in the ventilated phase, although the circumpolar current increases in strength, as does the western boundary current on the east side of Siberia, transporting warm, saline water to the circumpolar current. Due to the absence of a fresh surface layer, this warm water flowing northward remains in contact with the atmosphere.

The global meridional overturning circulation is dominated by one full depth overturning cell (fig. 3.3B). Strength of the overturning increases significantly with peak transport of 100 Sv in the Northern Hemisphere tropics/subtropics. Buoyancy loss takes place in a number of regions in the mid- and high-latitude Northern Hemisphere. First, the collapse of stratification in the ventilated phase causes deep convective mixing north of Siberia, allowing dense water formation. This flows equatorward at depth in a Panthalassa overturning circulation. Figure 3.4B shows a significant increase in the mixed layer depth in the north pole region. There is a second region of deep water formation at 50 ° N on the western and eastern boundaries of Siberia. Here the warm, salty surface waters flowing northward lose their heat causing an increase in density, and converging currents drive downwelling which allows penetration to the deep ocean (fig. 3.2B), contributing to the deep Panthalassa overturning circulation.

Deep ocean water masses sinking in the northern Panthalassa Ocean are brought to the surface when the equatorward flow interacts with the sloping northern boundary of China, Laurussia and Gondwana. The extent of the sloping coastline is highlighted in fig. 2.2. The upwelling is further enhanced at the equator due to Ekman upwelling.

There is an increase in Northern Hemisphere bolus heat transport during the ventilated phase, associated with the steep isopycnals resulting from the deep water formation. The heat transport by the overturning circulation shows a peak at 35 °N and a trough at 60 °N, representing a redistribution of heat. In the Southern Hemisphere, peak poleward heat transport is reduced to 0.8 PW in the sub-tropics.

The global overturning circulation in the Late Devonian Ocean ventilated phase is more similar to the present-day, with a buoyancy driven deep overturning circulation (Richardson, 2008). Conditions in the Northern Hemisphere high latitudes, where buoyancy loss takes place, are broadly comparable to those in the present-day Nordic Seas. North of Svalbard, the present-day Nordic Seas are relatively ice-free and, in the absence of sea-ice, warm water flowing northward from the Atlantic remains at the surface, in contact with the atmosphere. The water column is weakly stratified, and heat is efficiently transported northward through the ocean and released to the atmosphere. Consequently, the subsurface Nordic Seas are cold, and fresh water deposited in the surface layer is easily mixed downwards by winds and convection (Meincke, 1997; Hansen and Østerhus, 2000; Eldevik et al., 2014).

3.3 Transition to Ventilated Phase

The transition between unventilated and ventilated phases involves a reorganisation of the water column structure north of 55 °N. The gradual accumulation of a subsurface reservoir of heat acts to reduce the vertical density gradient and erode the stratification. This is clearly shown in figs. 3.8 and 3.9; during the unventilated phase freshwater content in this region increases (fig. 3.9B), since the freshwater deposited by the atmosphere is not transported out at a sufficient rate. Subsurface heat content also increases (fig. 3.9D). As the heat content increases in this warm subsurface reservoir, the density reduces, acting to weaken the vertical density difference between the fresh surface layer and warm subsurface (fig. 3.9E). A reduction in the vertical density gradient allows for the initiation of convection. The warm reservoir of water in the subsurface is then rapidly mixed to the surface and polar convective mixing is initiated, dramatically increasing the mixed layer depth (fig. 3.9G). The transition is marked by a rapid increase in polar convective mixing, downwelling cold, dense water from the surface in polar regions, and consequently

increasing upper ocean northward mass transport (fig. 3.9F). As more warm surface water is transported northward in the initial phases of the transition, a sharp spike in heat transported into the region is recorded (fig. 3.9C). Warm incoming northward water is now in contact with the atmosphere, losing heat and buoyancy, and reinforcing the convective mixing.

Abrupt climate change events have been observed in the more recent geological record. Dansgaard-Oeschger (D-O) cycles occurred every 1-2 kyr during the last glacial period (Dansgaard et al., 1993), and are characterised by abrupt warming of 10 °C over Greenland from a cold stadial to a warm interstadial state, followed by a more gradual two-stage cooling (Dokken et al., 2013). The mechanism of transition between D-O stadial and interstadial states was similar to the Late Devonian transition between the unventilated and ventilated phases, with a reorganisation of the vertical thermohaline structure at high northern latitudes.

During D-O stadials the surface of the Nordic Seas was cold and fresh, and there was sea-ice, which was completely absent at high northern latitudes in the Late Devonian. Below the halocline there was a northward flux of warm Atlantic Water, creating a warm subsurface reservoir as in the Late Devonian. This warm Atlantic Water was isolated from the surface by the halocline and sea-ice. Unable to lose its heat to the atmosphere, the incoming warm Atlantic water in the D-O stadial phase is thought to have gradually weakened the stratification to the point of collapse, at which time the heat from the subsurface would have been rapidly mixed to the surface and lost to the atmosphere. During the D-O interstadial phase the Nordic Seas therefore had no sea-ice or fresh surface layer. The water column was weakly stratified and incoming warm Atlantic water was in contact with the atmosphere, resulting in dense water formation and a local overturning circulation (Dokken et al., 2013; Petersen et al., 2013).

The transition between stadial and interstadial conditions was abrupt, with a distinct overshoot in Atlantic Meridional Overturning Circulation (AMOC) (Rasmussen and Thomsen, 2004; Dokken et al., 2013; Petersen et al., 2013; Sadatzki et al., 2019; Sessford et al., 2019); the overturning transport was strong for a short time period, and then decreased to a point which nevertheless remained stronger than in the stadial phase. This is very similar to the evolution of the local overturning circulation during the Late

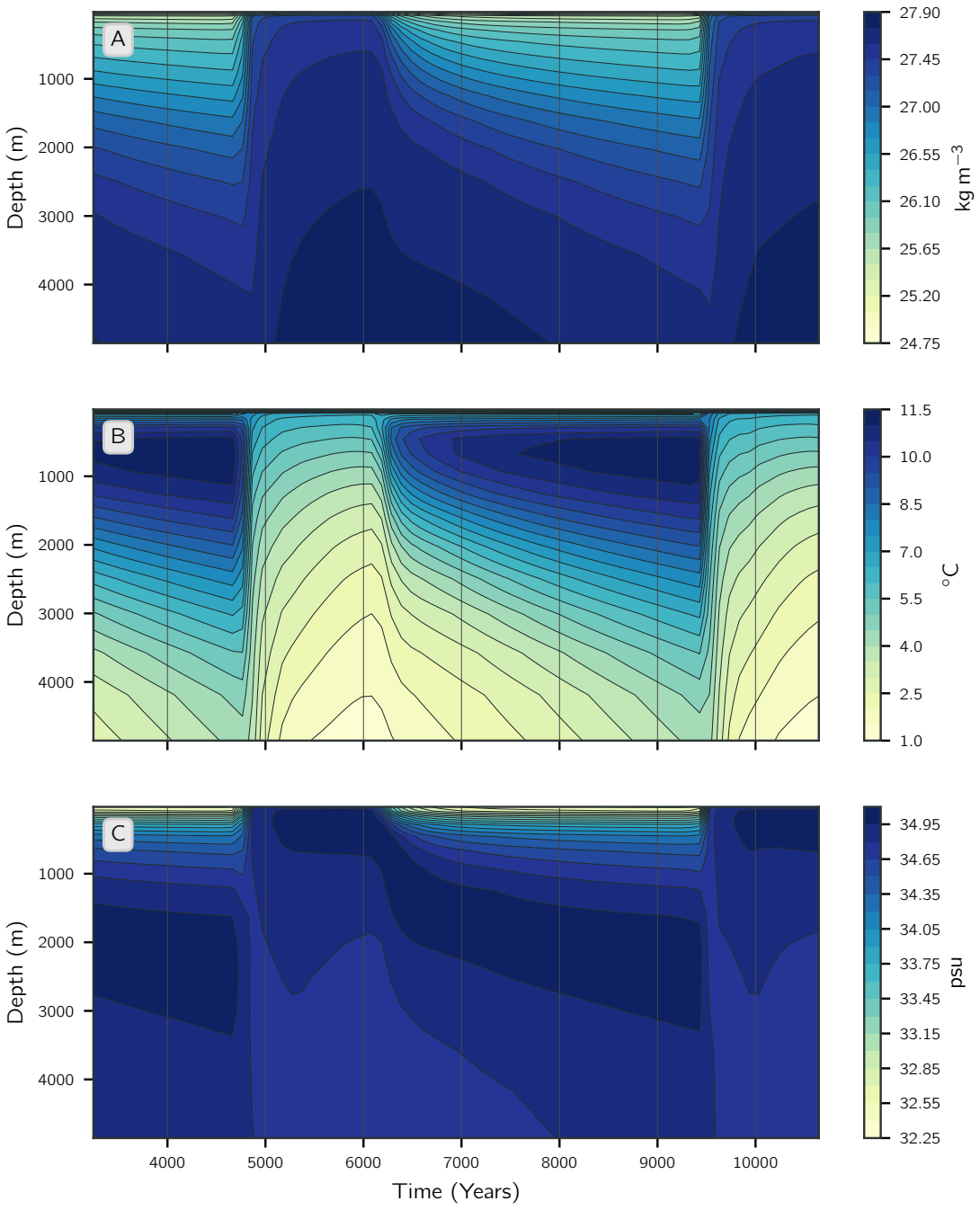

Figure 3.8: Time series of (A) mean potential density referenced to the surface; (B) mean potential temperature; (C) mean salinity north of Siberia.

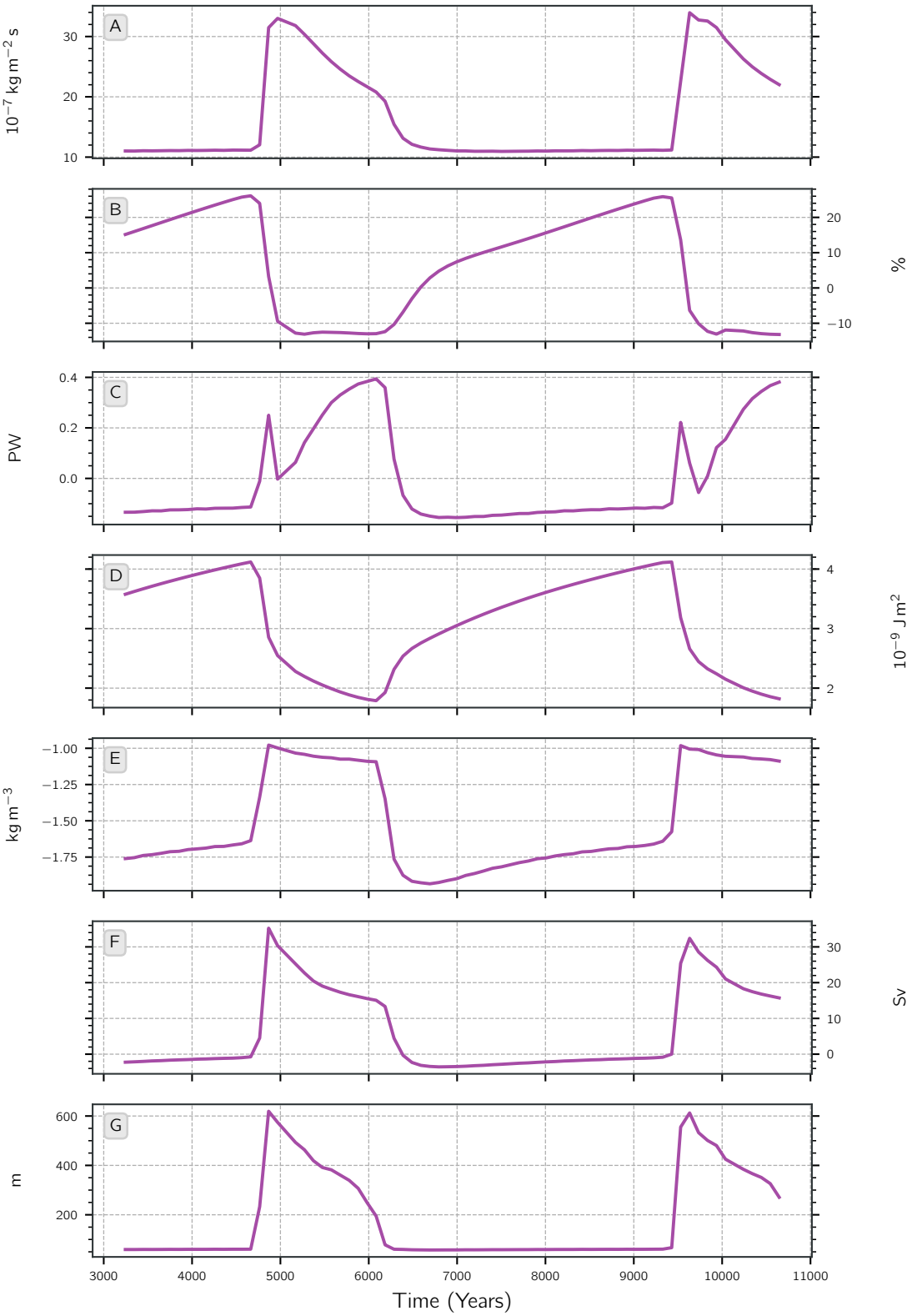

Figure 3.9: Time series of (A) salt transport across the section 60 ° N; (B) freshwater content north of Siberia; (C) heat transport across the section 60 ° N; (D) heat content below 200 m north of 60 ° N; (E) density difference north of 60 ° N between the surface and 800 m water depth; (F) mass transport above 1000 m water depth across the section 60 ° N; (G) mean mixed layer depth north of 60 ° N.

Devonian unventilated to ventilated transition (fig. 3.9F). Until recently, it was thought that meltwater input from land-based ice sheets was involved in the D-O oscillatory mechanism. However, Peltier and Vettoretti (2014) suggest the AMOC overshoot is due to enhanced northward transport of salt, contributing to the densification of Atlantic surface waters, and hence conclude that the Dansgaard-Oeschger oscillation is a salt oscillation, not associated with any additional meltwater input. Similar mechanisms for transitioning out of an unventilated ocean state are also known to occur during Heinrich events (Marcott et al., 2011; Freeman et al., 2015) and during polynya formation in the Weddell Sea (Dufour et al., 2017).

3.4 Transition to Unventilated phase

In the Devonian ocean model simulations, the ventilated phase persists for approximately 1000 years. During this time salinity, freshwater content, and density difference between the surface and 800 m are stable in the high latitudes of the Northern Hemisphere; however, temperature, along with salt transport, heat content, mixed layer depth and mass transport all decrease (figs. 3.8 and 3.9). The wind stress and surface heat loss imposed are not strong enough to maintain the high-latitude vertical mixing in the presence of strong atmospheric freshwater input. As local overturning reduces, the amount of salt being transported northwards is reduced. This also contributes to a reduction in convective mixing, which eventually reaches a point where it can no longer prevent the high-latitude stratification characteristic of the unventilated phase from being re-established.

There are strong parallels with the present-day Arctic Ocean. Zhang and Steele (2007) showed that reduced diapycnal mixing in the present-day Arctic Ocean leads to stronger stratification, giving rise to warmer and saltier subsurface waters, whereas excessively strong mixing weakens the stratification, preventing heat from accumulating in the sub-surface.

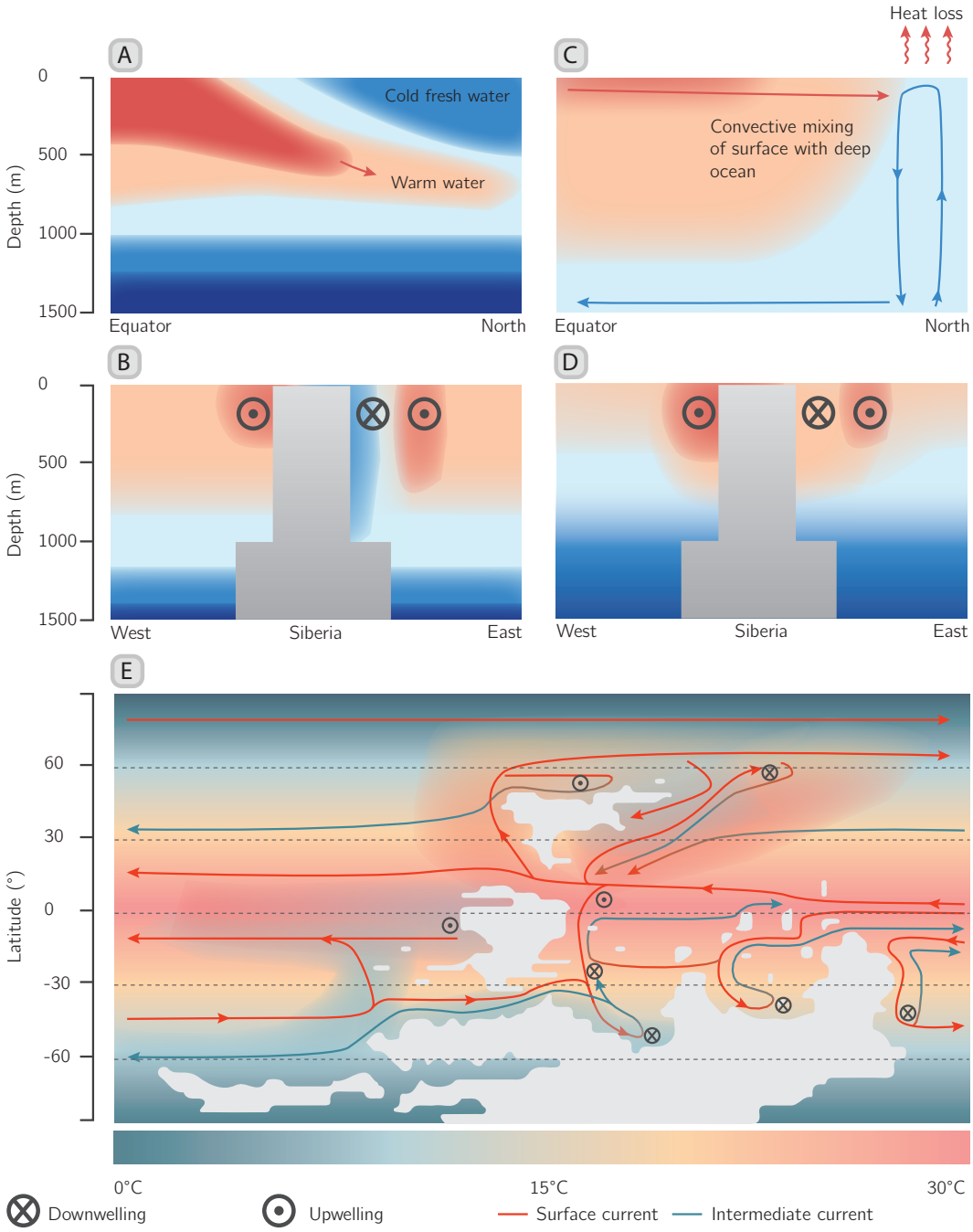

Figure 3.10: Schematic showing conditions in the North Panthalassa Ocean during unventilated (left) and ventilated (right) states. (A) & C) show north-south sections from the equator to the pole to the west of Siberia. (C & D) show east-west sections along the latitude 50 ° N. (E) shows a schematic of the global MOC during the unventilated phase. The surface circulation is marked by red arrows. Where near-surface waters become denser or where Ekman transport causes downwelling intermediate currents are formed in the unventilated phase (blue arrows). During the unventilated phase the circulation is restricted to the upper 2000 m. In the ventilated phase buoyancy loss in the Northern Hemisphere polar region pushes all intermediate currents deeper, forming a global deep overturning circulation. Background colours indicate surface temperature, which is similar between phases, although during the ventilated phase the global mean surface temperature is colder by 1.5 °C.

Considering the results of the ocean model and insights from D-O cycles we propose the following dynamics which could plausibly have led to oscillatory behaviour in the Late Devonian ocean: (1) a fresh surface layer at high northern latitudes restricts incoming warm subsurface water from coming into contact with the atmosphere, causing both gradual warming of the subsurface reservoir and weakening of stratification; (2) transition towards a ventilated phase caused by a reduced vertical density gradient as the heat content increases in the subsurface and the stratification weakens to the point of collapse; (3) a ventilated phase where deep water is formed in the high latitudes of the Northern Hemisphere, resulting in a deep global overturning circulation; (4) gradual return to an unventilated phase caused by gradual decrease in convective mixing and re-accumulation of a fresh surface layer, and (5) return to a well stratified ocean with cold fresh surface and warm sub surface.

3.5 Discussion: Frasnian-Famennian Extinction

The Late Devonian Frasnian-Famennian is characterised by two extinction phases (lower and upper Kellwaser horizons), during which 80 % of marine faunal species were lost, and did not recover until the end of the Devonian (Bambach et al., 2004; Stigall, 2012). Shallow water tropical species were most widely affected by the mass extinction (Chen et al., 2013). It is widely agreed that regions of the shallow and deep Rheic, Paleo Tethys and Panthalassa Oceans experienced ocean anoxia (Algeo et al., 1995). During OAEs, strong ocean stratification leads to a stagnant water column, widespread anoxia and euxinia. Euxinic waters can mix into the photic zone causing PZE. A key cause of PZE is increasing algal productivity (Naeher and Grice, 2015).

Uranium, sulphur and carbon isotopes in carbonates are used as proxies to understand redox conditions, sulphur cycles and carbon burial rates. Isotope research has highlighted regions of the Late Devonian ocean that were at least anoxic. These include: (1) the Paleo Tethys, in particular the northern region of the basin (Chen et al., 2013; Song et al., 2017), (2) the Rheic ocean, predominantly the western equatorial region; (3) regions of Panthalassa such as eastern equatorial Panthalassa (De Vleeschouwer et al., 2017).

The prevailing consensus is that the anoxia was caused by sea level rise, which is associated with multiple 'kill' methods including flooding of marine habitats, upwelling of deep anoxic/euxinic water, and increased erosion (Chen et al., 2013). Alternatively, it has been suggested that the anoxia occurred 'top-down', i.e. it resulted from terrestrial nutrient runoff which formed an anoxic surface layer through eutrofication. The ocean circulation model results presented here suggest that either hypothesis is possible.

Results of the Late Devonian OGCM suggest the ocean may have switched between two states: (1) an unventilated, strongly stratified state, in which the deep ocean could potentially have become anoxic; and (2) a ventilated state with a strong, deep overturning circulation which could have mixed any anoxic deep water to the surface. Although the unventilated phase is a plausible ocean state, it is unlikely that the ocean would have been able to remain in this state indefinitely; background vertical mixing would eventually weaken the stratification and allow for convective mixing and deep water renewal. Whether the ocean would subsequently return to an unventilated state is difficult to constrain; alternatively, the ocean could settle into a less vigorous, ventilated state. Further simulations of the Late Devonian ocean, with a representation of spatial variations in diapycnal mixing, and of coupling with the atmosphere, are required to make further progress on this question, and we take some first steps in this direction in later chapters.

Figure 3.11 shows the surface biogeochemistry results for both the unventilated and ventilated states of the Late Devonian OGCM. Phosphate (PO_4) is the main driver of the primary productivity pattern. The surface concentration of PO_4 is highest in the tropics and subtropics, particularly the eastern boundary of Panthalassa, the eastern Rheic Ocean and southern Paleo Tethys, and increases in the ventilated phase. High PO_4 boosts primary productivity, and subsequently increases eutrophication and potentially ocean anoxia when this organic matter is exported to depth. The biogeochemistry package does not include nutrient flux from land, and so the PO_4 is primarily determined through zones of increased vertical velocity. PO_4, is greater in the ventilated phase; this is expected since the overturning circulation is stronger during the ventilated phase.

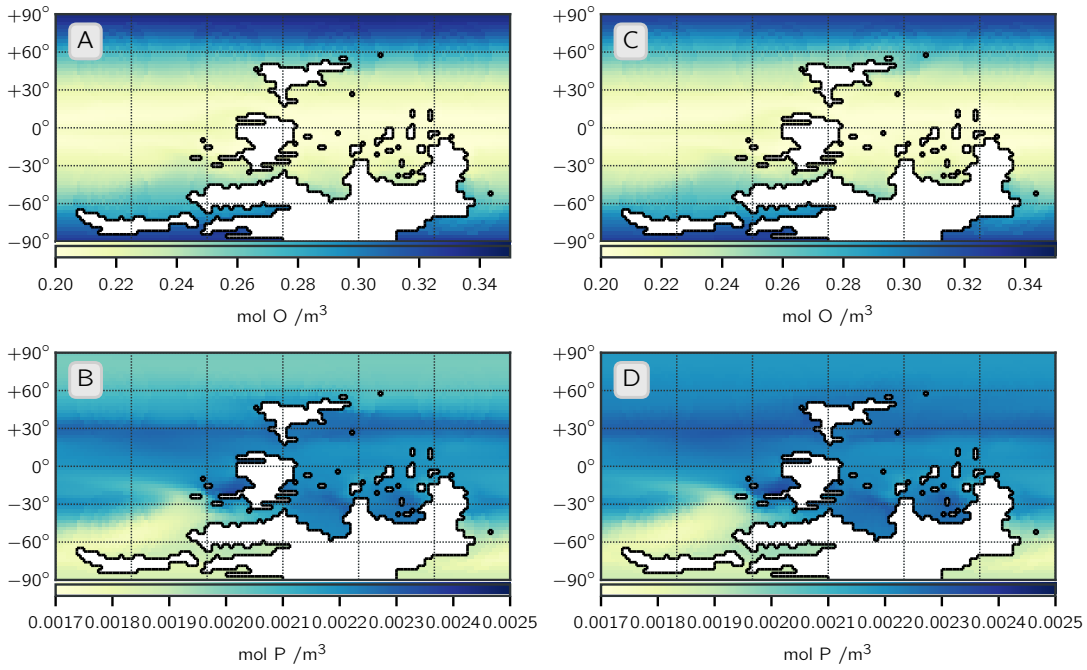

Figure 3.11: 100 year average surface biogeochemistry during the unventilated (left) and ventilated (right) phase; (A & C) O_2; (B & D) PO_4.

Dissolved oxygen (DO) is initialised in the biogeochemistry model at 0.095 mol O/m^3 globally, and during ocean spin-up the deep ocean is ventilated, filling the deep ocean with oxygen rich water. Warmer ocean water holds less oxygen and so the pattern of DO is similar to zonal mean temperature (fig. 3.1). Once the ocean has spun-up to the unventilated state the deep ocean has relatively high oxygen concentration. The deep ocean gradually deoxygenates over the unventilated phase, although the simulated levels are still relatively high (fig. 3.12A). A key result of the simulated DO is the gradual decline in the deep ocean, and then a subsequent rapid increase in DO in the ventilated phase, filling the deep ocean with high DO Northern Hemisphere surface polar water (fig. 3.12B).

During the unventilated phase, the model ocean overturns to depths of 1000 m in both the Rheic and Paleo Tethys Oceans, associated with water mass transformation and the sinking of warm saline water, yet is relatively stagnant at deeper depths. The southern Panthalassa Ocean is also strongly stratified with fresh, cold surface waters and a deep saline ocean. The strong stratification is resistant to wind and convective mixing, and the residence time of water in the deep ocean is long. Meyer and Kump (2008) suggested that this resistance to vertical mixing, coupled with efficient nutrient trapping, is a dominant

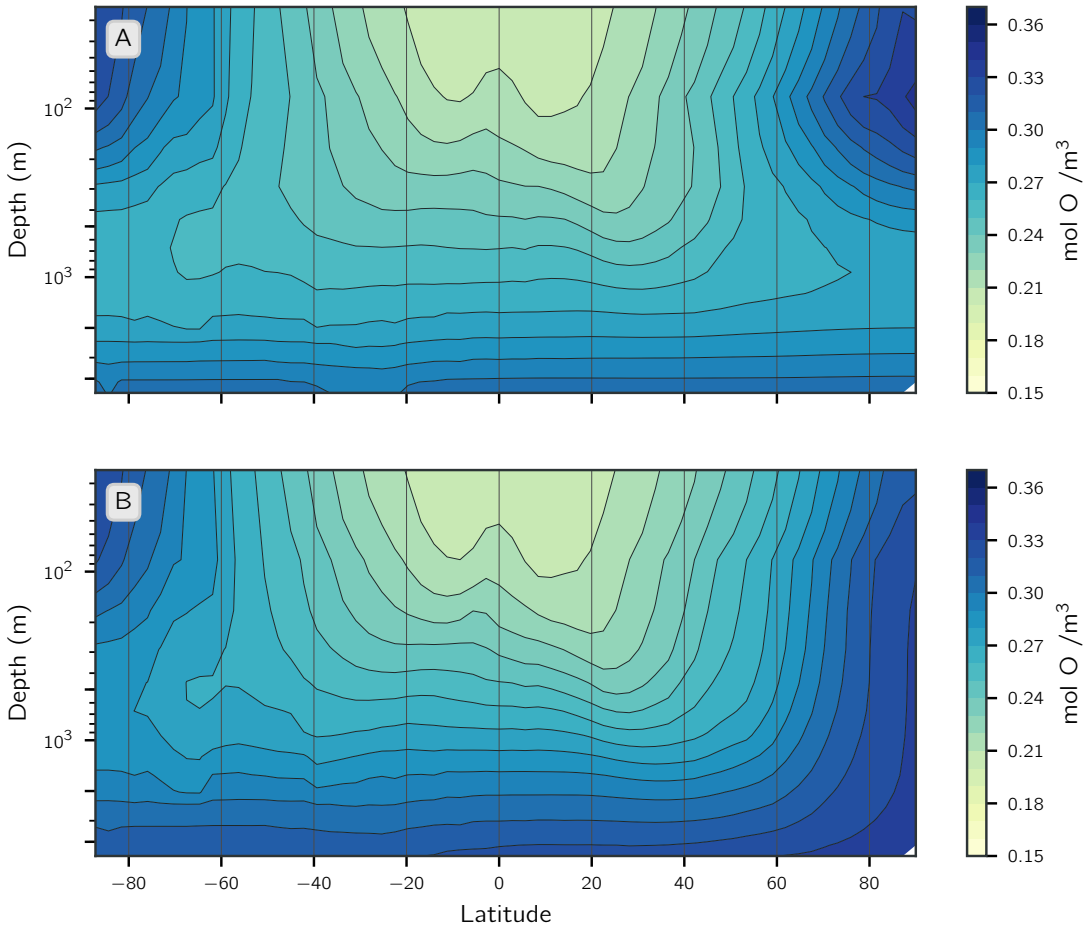

Figure 3.12: 100 year average zonal mean DO during the (A) unventilated, and (B) ventilated phase.

control in waters becoming anoxic/euxinic, This may therefore have enabled regions of the semi-restricted Panthalassa, Rheic and Paleo Tethys to become anoxic. Shallow water regions in restricted basins with enhanced nutrient runoff such as the Rheic and Paleo Tethys Ocean could also become oxygen depleted, and result in ideal conditions for PZE. During the ventilated phase anoxic deep water would be mixed to the surface, and over the cause of the ventilated phase the deep ocean and shallow regions would be well ventilated and oxygenated.

Isotope data records episodic shallow and deep water deoxidation throughout the Late Devonian (Bond et al., 2004; Carmichael et al., 2014). This is consistent with the simulated oscillatory pattern presented, showing deep ocean convective mixing events followed by unventilated stagnant periods.

The Devonian is a critical period in Earth's history for the evolution of tetrapods. Stem tetrapod fish fossils are observed in the Paleo Tethys in the Early Devonian, and it is conjectured that surface ocean currents swept these early tetrapods towards the western boundary of the Rheic in the Middle-Late Devonian, where the fish-tetrapod transition is observed in the geological record (Clack, 2012). This is consistent with the simulated surface ocean currents in fig. 3.2. Stem tetrapods and early tetrapods would have been exposed to warm saline surface conditions in these regions.

Poor poleward heat transport as simulated here would cause gradual cooling of polar regions. The Frasnian climate is described as a greenhouse climate, with evidence of glaciers recorded in the sedimentary record only in high altitude Gondwana (Eyles, 2008). The De Vleeschouwer et al. (2014) atmospheric results also support the formation of only high altitude glaciers. Current literature also suggests the Devonian oceans were devoid of sea-ice. The early Famennian is then marked by glaciation, which is well-established by the late Famennian, extending across the polar regions of Gondwana, with evidence of glacial marine environments (Isaacson et al., 2008). The earliest evidence of Northern Hemisphere polar sea-ice is recorded in the Early Carboniferous. Therefore, the simulated ocean heat transport, which is weak to the high latitudes, supports the transitioning climate from a greenhouse to icehouse, but only if this lack of ocean heat transport is not compensated by atmospheric heat transport or radiative adjustments.

3.6 Model Limitations

Modelling deep time ocean circulation involves simplifications and uncertainties. The Late Devonian spans 16 million years, during which time the continents and land were evolving. The results presented here represent only a snapshot, and there is considerable uncertainty in forcing and ocean bathymetry. The continent configuration is based on Blakey (2018) reconstructions, although there are alternative continental reconstructions which differ slightly. In this study, a continental slope is included by increasing the depth by 1000 m per grid cell away from the continent until a maximum depth of 5000 m is reached. The deep ocean is flat with the exception of a ridge in the Northern Hemisphere where there are no meridional boundaries. This is considered the most conservative estimation of bottom bathymetry since the location and depth of any ridges and other seafloor features are unknown, but crucially allows for an abyssal zonal pressure gradient in the Northern Hemisphere.

Orbital forcing is prescribed at present-day values, which may be a limitation, although the De Vleeschouwer et al. (2014) study, which considered the atmospheric circulation for a number of orbital forcing values, found that obliquity of 23.5° (close to the present-day value) best matched the geological record.

An ocean only model forced with monthly mean atmospheric temperature, wind stress, and evaporation-precipitation will always be limited by its atmospheric forcing, and ultimately simulations of the Late Devonian ocean should be made with a coupled atmosphere-ocean-sea-ice model. The coupled approach allows possible feedbacks between the atmosphere and ocean, reducing the uncertainty due to the forcing fields applied.

3.7 Summary

In this chapter, the Late Devonian ocean circulation has been simulated to investigate its relevance to Late Devonian mass extinction events and ocean anoxia. Under a warm climate and Late Devonian continental configuration the ocean oscillates between two states: (1) an unventilated state where the deep ocean is relatively isolated due to a fresh surface layer at northern high latitudes which restricts deep water formation; and (2) a

ventilated state with a strong and deep global ocean overturning driven by high latitude buoyancy loss. An oscillatory cycle between periods with a well-ventilated and periods with a poorly ventilated ocean is supported by periodicity in oxygen content of sediments in the geological record in regions of the Late Devonian ocean.

Both states presented are plausible for the Late Devonian ocean, and it is possible there was an oscillation between states. However, the unventilated phase would not be stable over long time periods. The ocean would eventually need to be ventilated to maintain stratification in the presence of erosion by tidally driven vertical diffusion. However, whether the ocean would subsequently return to an unventilated state, and the timescales of the oscillation are difficult to constrain.

Chapter 4

Ocean Circulation with variable mixing

Results of the OGCM with uniform diapycnal diffusivity suggest the Late Devonian ocean potentially oscillated between two states: (1) an unventilated ocean where there was no deep convection and overturning was dominated by the tropics and dense water formed through saline waters sinking at 30 ° N; (2) and a ventilated state, in which deep convective mixing occurred in the Northern Hemisphere, but Southern Hemisphere overturning circulation remained weak. One of the major determinants in the global meridional overturning circulation is diapycnal mixing, which therefore has important climatological influences (Wunsch, 2017). Here, diapycnal mixing is represented by a vertical diffusion coefficient for temperature and salinity, and in chapter 3 both were set to $3 \times 10^{-5}\,\mathrm{m^2\,s^{-1}}$, and were uniform spatially.

Zhang et al. (2001) modelled the ocean circulation in the Permian to understand whether the ocean may have been anoxic, and to review plausible localities of ocean anoxia. The study considered two scenarios; both forced with weak (relative to the present-day) zonally averaged profiles of wind stress, surface temperature with a weak equator-pole surface temperature gradient, and Evaporation-Precipitation (E-P), with a warm climate (5 x CO_2) and a 1 % reduction in the solar luminosity. Scenario 1 considered a diapycnal diffusivity of $5 \times 10^{-5}\,\mathrm{m^2\,s^{-1}}$, and scenario 2 prescribed a reduced diapycnal diffusivity

of $3 \times 10^{-5}\,\mathrm{m^2\,s^{-1}}$. This change in diapycnal diffusivity was significant enough to change the mode of overturning circulation. Scenario 1 was described as the 'thermal mode ocean circulation' and circulation was driven by Southern Hemisphere high latitude sinking, resulting in large southward heat transport and a significantly warmer Southern Hemisphere, with deep water temperatures of 5 °C.

Reducing the diapycnal diffusivity in scenario 2 resulted in a 'haline mode' ocean circulation, with sinking in the subtropics due to dense saline water formation. Overturning circulation in this state was weak, and subsequently, less heat was transported poleward. Zhang et al. (2001) concluded ocean anoxia would only be sustained in the 'haline mode' with reduced diapycnal diffusivity. The results presented in the Late Devonian OGCM show similarities to this scenario, with dense saline water formation in the Northern Hemisphere sub-tropics and weak poleward heat transport. The Permian ocean model suggests that whether an ocean is anoxic strongly depends on the prescribed diapycnal diffusivity, which is linked with both winds and tides.

In this chapter, we test the effect of a spatially variable diapycnal diffusivity on global Late Devonian ocean circulation. Estimates of present-day diapycnal mixing vary both laterally and vertically. Present-day global estimates suggest an average diapycnal diffusivity of $10^{-4}\,\mathrm{m^2\,s^{-1}}$ is needed in the deep ocean (below 1000 m depth) to maintain present-day stratification and water mass transformation rates; a value of $10^{-5}\,\mathrm{m^2\,s^{-1}}$ is then required above 1000 m in the main thermocline (Munk, 1966; Munk and Wunsch, 1998). Implementing this pattern of diapycnal diffusivity in the OGCM, whilst keeping all other model parameters constant is the first step towards understanding how changes in diapycnal diffusivity may change the large scale ocean circulation. The results do not show changes in the global overturning circulation in the Devonian ocean unventilated or ventilated states. However, the timescale of oscillation between the two ocean states is different, and the Northern Hemisphere strong stratification persists for 8000 years before the deep convection is initiated (fig. 4.2).

Secondly, we consider the large scale ocean circulation under spatially variable diapycnal diffusivity calculated from maps of Late Devonian tidal dissipation energy, which have been produced by a modelling team at the University of Bangor as discussed in chapter 2. It's important to note that the OTIS tidal model did not include variable deep ocean

bathymetry and so only considers the effect on tidal mixing of continental shelf regions. A tidal mixing parameterisation (Schmittner and Egbert, 2014) is used to compute spatially varying diapycnal diffusivity from the turbulent energy dissipation. The total energy from mixing is kept constant between simulations by modifying the global background diffusivity constant. The depth-mean diapycnal diffusivity used in the ocean model with spatially variable diapycnal diffusivity (OGCMmix) is illustrated in fig. 2.4.

4.1 OGCMvert

In this experiment the diapycnal diffusivity is no longer uniform with depth but instead takes two different values based on depth; the deep ocean (below 1000 m) the diapycnal diffusivity is set to $1 \times 10^{-4}\,\mathrm{m\,s^{-2}}$, and the upper ocean (above 1000 m) the diapycnal diffusivity is set to $1 \times 10^{-5}\,\mathrm{m\,s^{-2}}$. In this experiment the global residual overturning circulation changes little when compared to the OGCM experiment. A shallow circulation dominated by the subtropics is simulated in the unventilated state (fig. 4.1A), with similar overturning strengths to the OGCM in shown in fig. 3.3 A. In the ventilated state the residual MOC is also similar to the OGCM, although the strength of overturning is slightly stronger in the deep ocean (fig. 4.1B).

The upper ocean value of diapycnal diffusivity in the OGCMvert simulation is lower than the spatially uniform diapycnal diffusivity experiment presented in chapter 3, which was set to $3 \times 10^{-5}\,\mathrm{m\,s^{-2}}$. This reduction slows the vertical erosion of the stratification in the northern high latitudes, and so the transition from an unventilated to ventilated state takes place at 8000 years instead of 4700 years in the OGCM experiment.

4.2 OGCMmix

Figure 4.3 shows the residual overturning circulation when modelling the ocean with spatially variable diapycnal diffusivity computed from tidal dissipation energy (OGCM-mix) as described in eq. (2.7). The Northern Hemisphere tropical/subtropical circulation extends deeper in both states, and upwells in the Southern Hemisphere between 20 ° S to

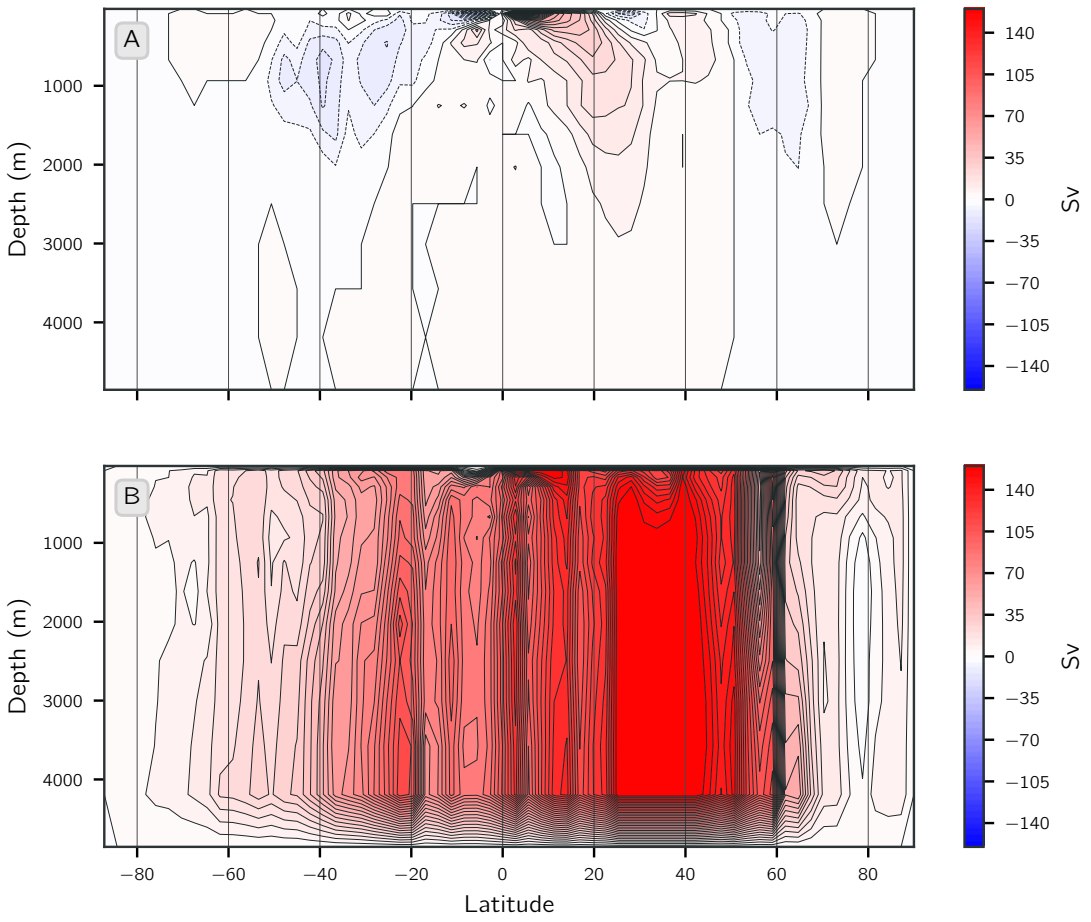

Figure 4.1: 100 year and zonal mean of the global residual overturning circulation in the OGCMvert experiment. (A) unventilated phase; (B) ventilated phase.

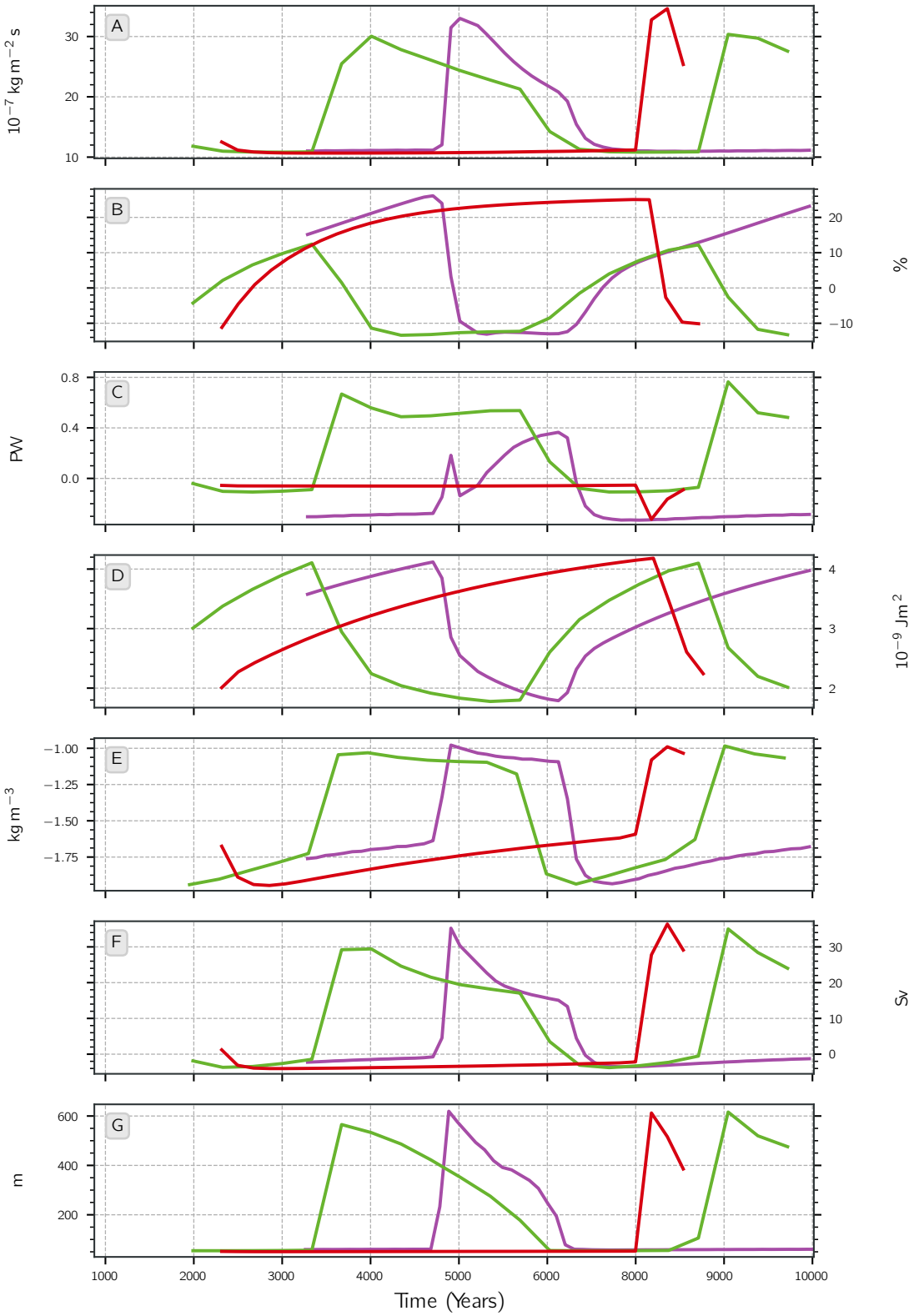

Figure 4.2: Time series comparison across 60 °N for OGCM (purple), OGCMmix (green), and OGCMvert (red). (A) salt transport; (B) freshwater content north of Siberia; (C) heat transport; (D) heat content below 200 m; (E) density difference between surface and 800 m; (F) mass transport above 1000 m water depth; (G) mixed layer depth.

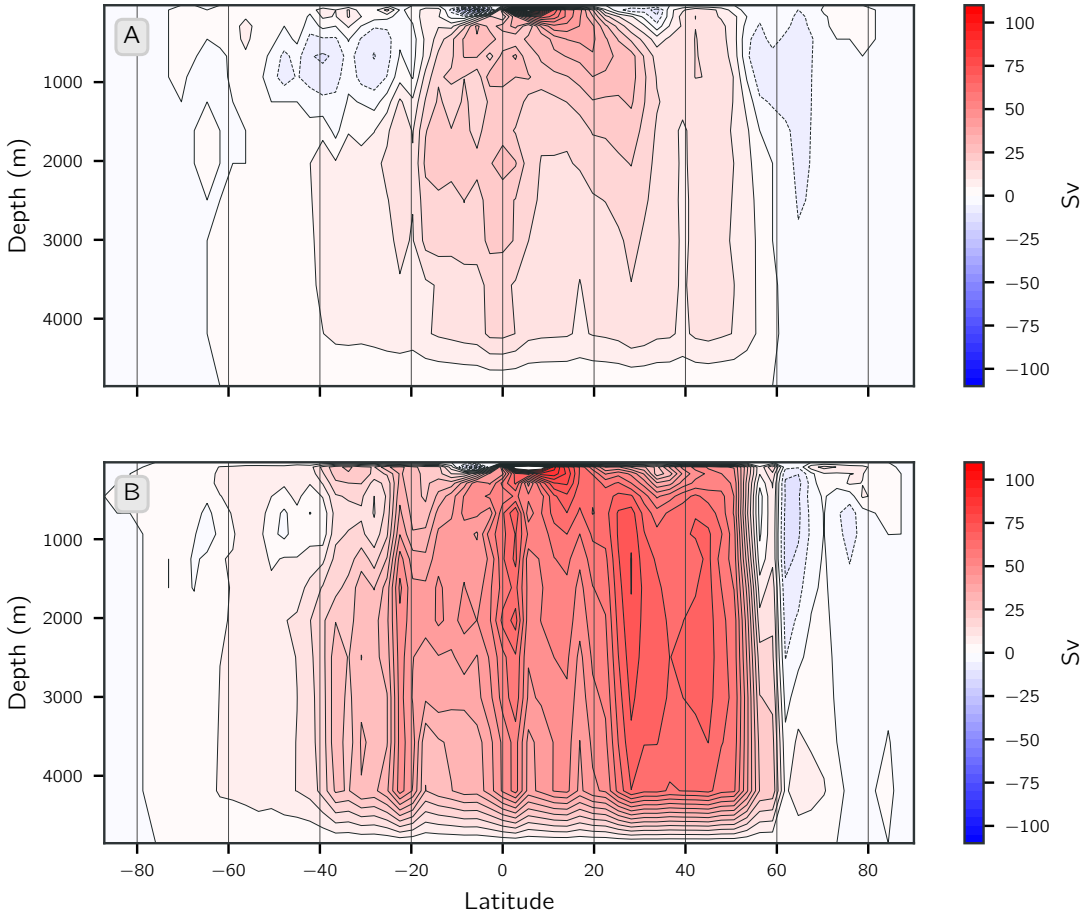

Figure 4.3: 100 year and zonal mean of the global residual overturning circulation when the model uses a spatially variable diapycnal diffusivity calculated from OTIS tidal dissipation estimates. (A) unventilated phase; (B) ventilated phase.

40 ° S (Figure 4.3A). Outside the Northern Hemisphere tropics/subtropics, the circulation is largely unchanged during the unventilated state. Diapycnal diffusivity calculated from tidal energy dissipation in the Late Devonian is highest in the tropics/subtropics (fig. 2.4, explaining the increased overturning circulation in this region of the deep ocean.

During the ventilated state the deep overturning in the high latitudes north of Siberia is now absent. The weakened mixing in the higher latitudes also means the global deep overturning circulation in the ventilated phase is weaker, reduced from ∼100 Sv in the OGCM to ∼60 Sv (fig. 4.3B). Thus, including spatially variable diapycnal diffusivity with a structure based on tidal energy loss acts to reduce high latitude mixing and global overturning circulation, with the exception of a deeper tropical/subtropical circulation during the unventilated state.

The transition between unventilated and ventilated states is similar to that described in the original OGCM simulation. However, the timescales of oscillation are different in the OGCMmix experiment since diapycnal mixing erodes the stratification at a different rate. The ocean transitions from an unventilated state to a ventilated ocean after 3300 years. Once the ocean is ventilated, it remains in this state for 2000 years, until it begins to transition back towards an unventilated ocean (fig. 4.2). Freshwater content in the Northern Hemisphere high latitudes in lower, and poleward heat transport greater than in the original OGCM experiment. However, the erosion of stratification at northern polar latitudes takes place when the density difference between the surface and 800 m is the same in both simulations. At this time, the vertical density gradient is eroded to the point of collapse and the deep ocean convects. Convective mixing is less substantial in the OGCMmix experiment, with lower mixed layer depth throughout the ventilated state and an absence of the initial 'overshoot' in heat transport and mass transport.

The general reduction in overturning circulation is primarily due to keeping total energy input to the ocean fixed when changing diapycnal diffusivity. In the OGCMmix simulation there are hotspots of enhanced mixing linked with tidal energy dissipation, and outside these hotspots mixing is weaker due to a lower background diapycnal diffusivity. The barotropic OTIS model simulation did not include variable deep ocean bathymetry, and so only considered variations in tidal mixing associated with continental shelf regions. There are no continents in the high northern latitudes, and so diapycnal diffusivity is set to the background diffusivity there, which is low since total energy available is kept constant between the OGCM and OGCMmix experiment. Therefore, the ocean circulation can be sensitive to the background diffusivity away from the continental slope where diapycnal diffusivity is greatest. Palaeotidal simulations in more recent time slices have included

a realistic seafloor bathymetry, leading to increased tidal dissipation rates surrounding seafloor topography (Schmittner and Egbert, 2014; Wilmes and Green, 2014; Wilmes et al., 2019). Ultimately, a realistic Late Devonian seafloor bathymetry needs to be included; otherwise, the interior ocean mixing away from coastlines is not realistic due to very low background diapycnal diffusivity. Subject to this caveat, a key takeaway from these preliminary experiments varying ocean diapycnal diffusivity is that the Late Devonian global overturning circulation does not change, and the oscillation between an unventilated/ventilated state still exists, although the timescale for oscillation is different.

4.3 Summary

This work illustrates how changing diapycnal diffusivity and tides impacts global ocean circulation. Two different experiments were presented with different methods to implement spatially variable diapycnal diffusivity. First, we considered the simple approach of a vertically varying diapycnal diffusivity, with differing values above and below 1000 m. This showed little change in the global overturning circulation when compared with the uniform diapycnal diffusivity experiment presented in chapter 3 and in fact oscillated between an unventilated and ventilated state as in the OGCM. We then considered the more complex approach of implementing a spatially variable diapycnal diffusivity computed from OTIS tidal energy dissipation. Total energy input was kept constant between the OGCM and OGCMmix simulations, and since the OTIS barotropic tidal simulation only included continental slope bathymetry mixing is strongest in shelf regions, and so the internal ocean is set to a very low background diapycnal diffusivity (to keep total energy input constant between simulations). The OGCMmix simulation shows again an unventilated and a ventilated state, but the circulation is constrained to the tropics and midlatitudes where tidal energy dissipation is strongest. Both simulations with spatially varying diapycnal diffusivity show that changes in diapycnal mixing erode Northern Hemisphere high latitude stratification in the unventilated state on different timescales, changing the timescale of the oscillation between states.

Chapter 5

Coupled Ocean-Atmosphere-Sea-Ice

The ocean provides important feedbacks to the atmosphere and vice versa; these ocean-atmosphere interactions are excluded in the experiments discussed so far. Results of a Late Devonian coupled atmosphere-ocean-sea-ice simulation integrated for 20 000 years are presented in this chapter. As highlighted in chapter 2, the ocean component is identical, except for its surface forcing.

First, the surface atmospheric conditions are discussed, comparing the CGCM atmosphere with the De Vleeschouwer et al. (2014) results, which force the OGCM, and with an MITgcm atmospheric circulation model with a slab ocean (ASGCM).

The ASGCM is an MITgcm equivalent of the De Vleeschouwer et al. (2014) simulation. The only difference is that the De Vleeschouwer et al. (2014) imposed an oceanic heat flux based on a parabolic decline of temperature from 32 °C at the equator to 0 °C at the poles (this is designed to simulate a low meridional temperature gradient). In the ASGCM experiment, the same surface temperature pattern is simply prescribed as an initial condition, for reasons that will become clear.

After comparing the atmospheres of the three simulations, the ocean component of the CGCM is presented. The coupled model's Late Devonian ocean begins in a partly-ventilated state. This state persists for 8500 years and after this point the ocean transitions to a ventilated state. Atmospheric surface conditions do not change significantly

between partly-ventilated and ventilated ocean states, and the general pattern of global atmospheric circulation is largely the same between states. The atmospheric surface conditions and atmospheric circulation are therefore presented for the ventilated state, since this is the model's final state and diagnostics suggest the ocean would stay in this state if the simulation were continued. Finally, implications for Late Devonian extinction and evolution are discussed.

5.1 Atmospheric Surface Conditions in the ASGCM, CGCM and De Vleeschouwer simulations

The key differences between the OGCM and CGCM ocean states arise due to differences in conditions at the air-sea interface. The CGCM ocean is coupled to an intermediate complexity atmosphere, allowing feedback between the ocean and atmosphere every hour, which reduces uncertainty in the atmospheric forcing of the ocean.

Annually-averaged zonal mean atmospheric surface conditions during the ventilated state show similarities between the ASGCM and CGCM (fig. 5.1).

The ASGCM surface temperature shows large equator-pole temperature gradients. Southern Hemisphere winter atmospheric surface temperatures reach a minimum of $-9\,^{\circ}\mathrm{C}$: in comparison, the CGCM minimum is $0\,^{\circ}\mathrm{C}$. The tropical and subtropical regions of the CGCM and ASGCM show a clear signature of the Hadley circulation, shifting seasonally and forming an annual mean temperature plateau. The ASGCM plateau is constrained between $20\,^{\circ}\,\mathrm{N}$ and $20\,^{\circ}\,\mathrm{S}$, whereas the CGCM extends further polewards from $25\,^{\circ}\,\mathrm{N}$ to $25\,^{\circ}\,\mathrm{S}$. The greater Southern Hemisphere temperatures in the CGCM are due to a dynamic ocean transporting heat along meridional continental boundaries.

Sea-ice does not form in the CGCM; however, seasonal sea-ice can form in the ASGCM in both hemispheres. The sea-ice extends from the pole to $80\,^{\circ}\,\mathrm{N}$ and $70\,^{\circ}\,\mathrm{S}$.

The De Vleeschouwer et al. (2014) annual mean atmospheric surface temperature pattern is different to both MITgcm atmospheres. The dominant feature of the De Vleeschouwer et al. (2014) model is a weaker equator-pole temperature gradient than in the ASGCM and CGCM; this is because the the De Vleeschouwer et al. (2014) study imposed an

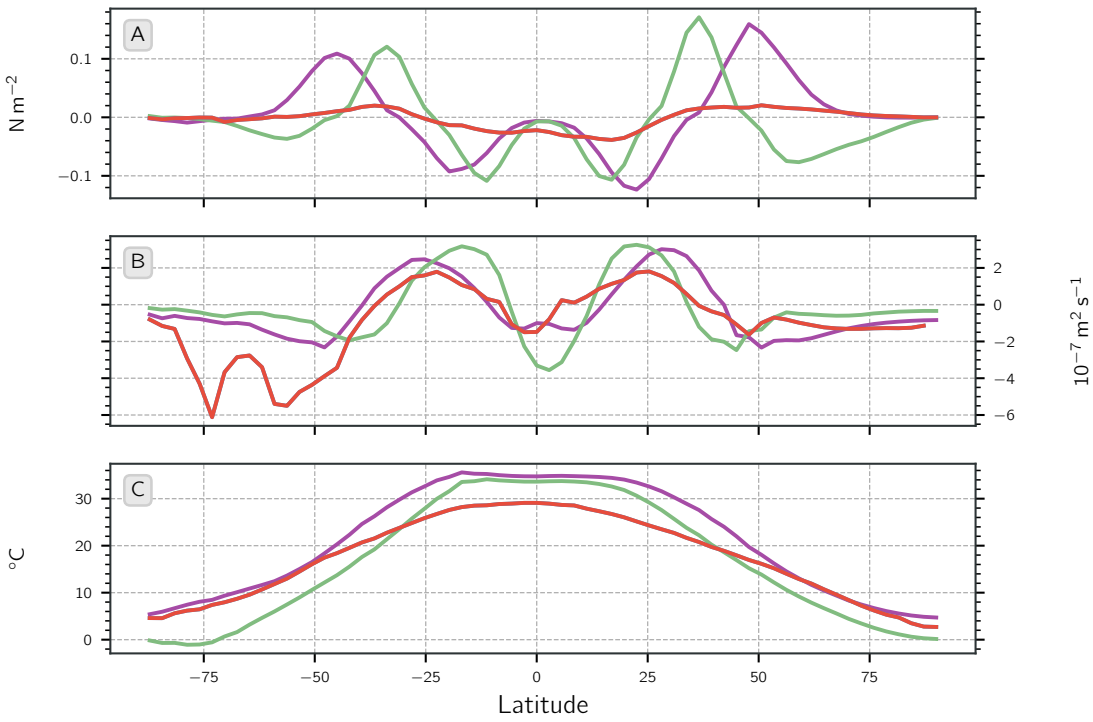

Figure 5.1: Annual and zonal mean atmospheric surface conditions in (*red*), De Vleeschouwer et al. (2014) study used to force the OGCM in chapter 3, (*purple*), the CGCM, and (*green*), ASGCM. (A) zonal wind stress; (B) E-P; (C) atmospheric surface temperature.

artificial ocean heat flux designed to produce a low equator-pole temperature gradient (the ASGCM and OGCM simulations do not use fluxes to force the climate to stay within an 'expected' gradient). The surface temperature in the De Vleeschouwer et al. (2014) study is lower across all latitudes when compared to the CGCM atmosphere. The ASGCM tropics/subtropics are warmer than the De Vleeschouwer et al. (2014) results; with significantly colder poles. The plateau feature does not exist in Vleeschouwer's results, instead the temperature peaks at the equator and decreases polewards. The temperature gradient is shallower in the Southern Hemisphere tropics suggesting the Hadley circulation is stronger in the Southern Hemisphere compared to the Northern Hemisphere.

E-P patterns of all models are similar, although the ASGCM sees greater evaporation in the Southern Hemisphere tropics, enhanced precipitation just north of the equator, and reduced precipitation in the Southern Hemisphere polar region. The De Vleeschouwer et al. (2014) E-P has significantly more precipitation in the Southern Hemisphere high latitudes, although in general the E-P distribution is similar to the CGCM.

The most significant difference between atmospheric surface conditions is between the winds in the De Vleeschouwer et al. (2014) model and the MITgcm simulations. The zonal surface wind stress is substantially weaker and follows a markedly different meridional distribution in the De Vleeschouwer et al. (2014) model, consistent with the weaker equator to pole temperature gradient. As discussed in Chapters 2 and 3, the De Vleeschouwer et al. (2014) zonal wind is weak, dominated by equatorial westward wind, exerting a wind stress of $\sim 0.03\,\mathrm{N\,m^{-1}}$ between 25° north and south in the annual mean. In the mid-high latitudes weak eastward wind stress peaks at 35° in each hemisphere, reducing in strength polewards. It is possible that part of the weak wind stress in the De Vleeschouwer et al. (2014) study is associated with the weaker meridional temperature gradients, but also perhaps due to the model inadequately resolving the midlatitude synoptic eddies that create the momentum convergence leading to strong surface westerlies. In contrast, both the ASGCM and CGCM simulate wind stress patterns similar to the present-day, with westerlies exerting an eastward zonal stress poleward of 30°, and trade winds imposing strong ($\sim 0.1\,\mathrm{N\,m^{-1}}$) westward wind stress either side of the equator in the subtropics. In the equatorial region, the westward wind stress is weak. Known as the Intertropical

Convergence Zone (ITCZ), this region is observed between ∼5° either side of the equator in the present-day. Weak winds of the ITCZ are caused by converging eastward wind stress either side of the equator, coupled with intense solar heating, which forces the air upwards and there is a lack of horizontal wind movement.

Although the CGCM and ASGCM wind stress patterns are similar, the latter model has stronger winds, shifted towards the equator. This is consistent with the fact that the ASGCM atmosphere needs to transport more heat in the absence of a dynamic ocean. Midlatitude westerlies are associated with momentum flux convergence in the storm tracks, which follow the meridional temperature gradient. Thus, the equatorward shift in the winds is linked with an increased temperature gradient in the subtropics in the ASGCM experiment. Increased strength of the winds and shifting towards the equator is linked to the greater equator-pole temperature gradient. Another key difference is the existence of polar easterlies exerting a westward wind stress in both hemispheres in the ASGCM. Minor Southern Hemisphere polar easterlies exist in the CGCM, and there are no polar easterlies in the Northern Hemisphere.

5.2 Ocean

The coupled system is simulated for a total of 20 000 years. After a spin-up time of 2500 years the model equilibrates to a state with a zonal mean structure that is similar to the Late Devonian OGCM unventilated state in that the deep ocean is stratified and isolated from the surface (fig. 5.2). However, in the CGCM the ocean is ventilated to an intermediate depth (fig. 5.2); equivalent isopycnals outcrop in the CGCM at high latitudes but not in the OGCM, and residual overturning circulation, although weak, extends to the deep ocean (fig. 5.5). Therefore, this less-stratified initial CGCM state is termed a 'partly-ventilated' state. This partly-ventilated state is sustained for approximately 8800 years, at which point the ocean transitions to a 'ventilated' state in which the ocean temperature is well mixed at high northern latitudes and deep isopycnals outcrop at the surface. Unlike the OGCM simulation, the coupled ocean does not oscillate between unventilated and ventilated ocean states but instead remains ventilated with more minor oscillations in the intensity of Northern Hemisphere polar convective mixing.

Here, first the mean state and ocean circulation in each of the CGCM quasi-equilibrium states is discussed, before considering the characteristics of the transition between them, and the minor oscillatory behaviour in the ventilated state.

5.2.1 Partly-ventilated State

The zonal mean structure of the coupled ocean partly-ventilated state is similar to the OGCM simulation. There is a warm lens in the subtropics extending to depths of 1300 m and reaching temperatures >20 °C (fig. 5.2B).

The zonal mean salinity in fig. 5.2C shows a double saline tongue structure which appears to emanate from the surface between 30° to 45° in each hemisphere. The Southern Hemisphere tongue extends deeper and spreads southwards below the surface layer.

There are strong meridional gradients in temperature and salinity within the upper hundred metres of the ocean. High latitude surface waters are cold and relatively fresh with warmer, more saline subtropical intermediate water beneath (fig. 5.2). The fresh surface layer buffers mixing with the underlying warm water. This high latitude surface water is fresher in the Southern Hemisphere than the north, and the subsurface southward extension of the subtropical saline tongue results in warm intermediate water below the halocline that is saltier than the Northern Hemisphere equivalent, leading to a stronger vertical density gradient in the south. Due to the high latitude fresh surface waters, the lowest density waters are in the Southern Hemisphere high latitudes. Deep isopycnals are not ventilated to the surface in either hemisphere, and the deep ocean is strongly stratified in density.

The intense zonal winds in the tropics force a westward current at the surface centred just north of the equator. The current circumnavigates between 0 ° N and 30 ° N (fig. 5.3A). The peak flow does not reach the eastern boundary of Laurussia, meaning flow diverted into the Rheic Ocean is weak and contributes to a weak Rheic western boundary current. As the circumequatorial current flows between Siberia and Laurussia the current is partially diverted along the eastern boundary of Siberia, generating an intense north Panthalassa western boundary current. The western boundary current then detaches from the north east Siberia coastline; and a strong eastward current forms. As this current

reaches western Siberia it is diverted primarily north of Siberia making an eastward circumpolar current flowing between 50 ° N and 75 ° N. In the Northern Hemisphere polar regions there is also a very weak westward circumpolar current completely isolated from the coastline.

In the Southern Hemisphere, surface currents are dominated by a Panthalassa western boundary current flowing southwards and detaching from the coast at 45 ° S forming a Panthalassa gyre (fig. 5.3A). High latitude/polar surface currents are weak in the Southern Hemisphere, reaching maximum velocities of $0.03\,\mathrm{m\,s^{-1}}$. In the Paleo Tethys Ocean a minor southward western boundary current is simulated, derived from both the Southern Hemisphere Panthalassa gyre and circumequatorial current.

The residual overturning circulation is dominated by the Northern Hemisphere circulation, and deep overturning in the partly-ventilated state is restricted to the Northern Hemisphere (fig. 5.4A). The circulation at the surface is near-symmetrical between hemispheres and mirrors the atmospheric circulation. Each hemisphere is dominated by two opposing shallow overturning cells; a tropical/subtropical circulation and a midlatitude circulation. In the tropics strong westward wind stress in the region surrounding the equator drives poleward surface Ekman transport in both hemispheres, resulting in Ekman upwelling on the equator. The surface water flows poleward, density increases due to evaporation exceeding precipitation, coupled with Ekman convergence, leading to warm saline waters sinking. The latitude of sinking differs between hemispheres; tropical water flows at the surface further poleward in the Northern Hemisphere, sinking at 50 ° N. Sinking is prominent on the eastern boundary of Siberia and extends eastward at this latitude away from the coastline where the velocity is more intense (figs. 5.3 and 5.5). The Northern Hemisphere tropical circulation also extends deeper forming a weak deep overturning circulation returning equatorward predominately between 1000 m to 3000 m. In comparison, this warm saline tropical water flows poleward at the surface in the Southern Hemisphere and sinks to a maximum depth of 1000 m at 30 ° S in the western Panthalassa.

In the midlatitude Northern Hemisphere, eastward wind stress drives equatorward surface Ekman transport at the surface (fig. 5.4A). As this sinks east of Siberia it flows northward at between 1000 m to 4000 m and is brought to the surface at 75 ° N north of Siberia through Ekman pumping due to converging Ekman transport associated with the polar

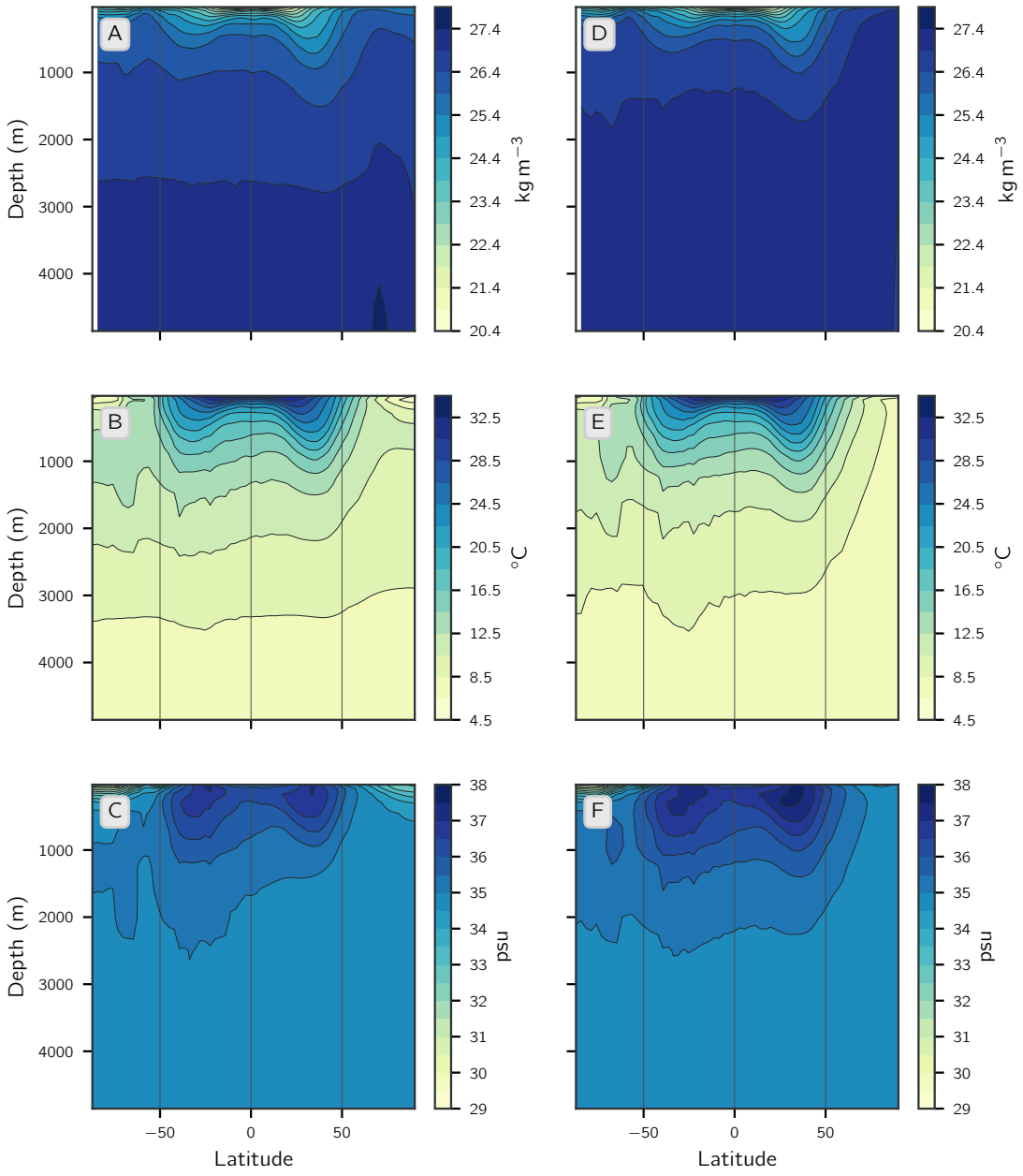

Figure 5.2: Zonal mean properties of the CGCM ocean; comparison of the partly-ventilated state (left) and the ventilated state (right). (A & D) potential density; (B & E) potential temperature; (C & F) salinity.

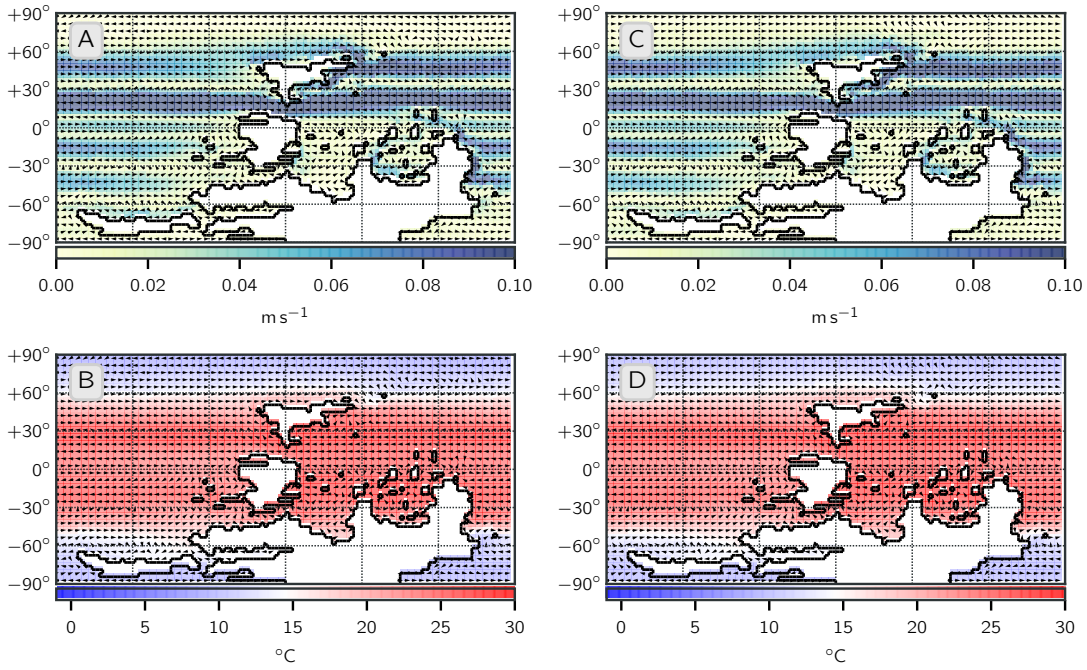

Figure 5.3: Comparison of the 100 year mean partly-ventilated state (left) and ventilated state (right) upper 500 m velocity vectors. (A & C) surface currents with colour shading representing surface velocity; (B & D) surface currents with colour shading representing surface temperature.

westward and midlatitude eastward wind-stresses. The circulation in the deep ocean is weak, transporting approximately 10 Sv. Further north there is a weak (∼10 Sv) polar circulation with sinking at the pole. These regions are lacking meridional boundaries, deep isopycnals are not ventilated to the surface, and this weak deep overturning is thought to be similar to the present-day Southern Ocean, where adiabatic upwelling and diapycnal mixing both contribute to return water to the surface (Watson et al., 2013; Silvester et al., 2014).

The circulation in the Southern Hemisphere follows a similar pattern of counter-rotating cells between the tropics and midlatitudes, although weaker, with the midlatitude circulation transporting a maximum of 20 Sv in the Southern Hemisphere versus 70 Sv in the north; shallower, reaching maximum depths of 1000 m; and shifted towards the equator (fig. 5.4A).

The polewards expansion of the tropical/subtropical overturning circulation in the Northern Hemisphere is linked to the position of the midlatitude zonal eastward wind stress being stronger and shifted slightly poleward in the Northern Hemisphere (fig. 5.1).

The Paleo Tethys Ocean circulation consists of a shallow wind-driven cell with southward transport at the surface, predominantly along the western boundary where this loses buoyancy through evaporation and increased salinity, sinking on the Paleo Tethys southern boundary to 1000 m. In the Rheic Ocean, the meridional circulation opposes that in the Paleo Tethys. There is no strong western boundary current to carry surface waters southward; instead the surface water flows equatorward sinking at 25 ° S to return southwards between 500 m to 1000 m. Both the Rheic and Paleo Tethys Ocean overturning circulations are weak, reaching a maximum of 6 Sv and 8 Sv, respectively.

5.2.2 Ventilated State

After 8500 years the ocean transitions to a ventilated state. The Northern Hemisphere high latitude fresh surface layer is absent and the polar region is well mixed (fig. 5.2). The stratification is collapsed and isopycnals outcrop from the deep ocean. Subtropical saline tongues extend deeper and are more saline in the ventilated state. The thermocline is shallower and deep water temperature reduced.

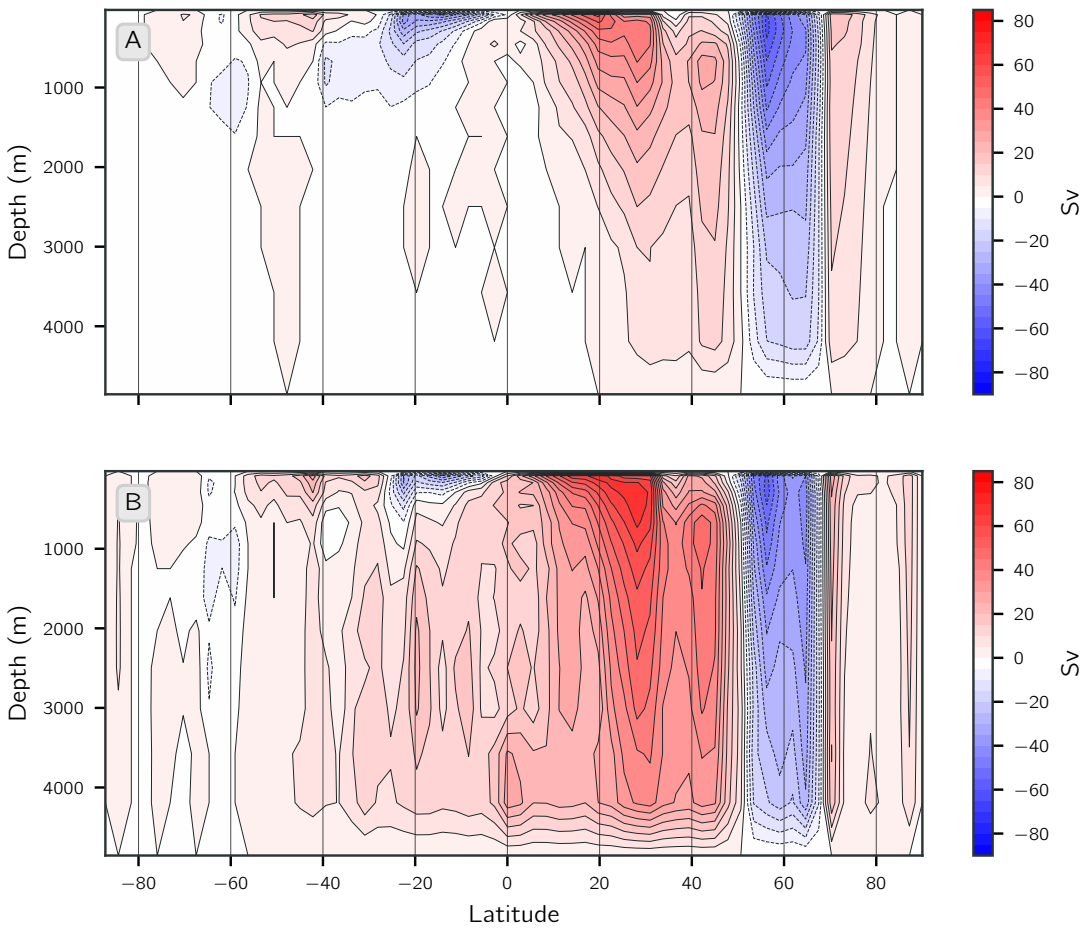

Figure 5.4: 100 year and zonal mean CGCM ocean residual overturning circulation; (A) partly-ventilated state; (B) ventilated state. Positive denotes clockwise circulation.

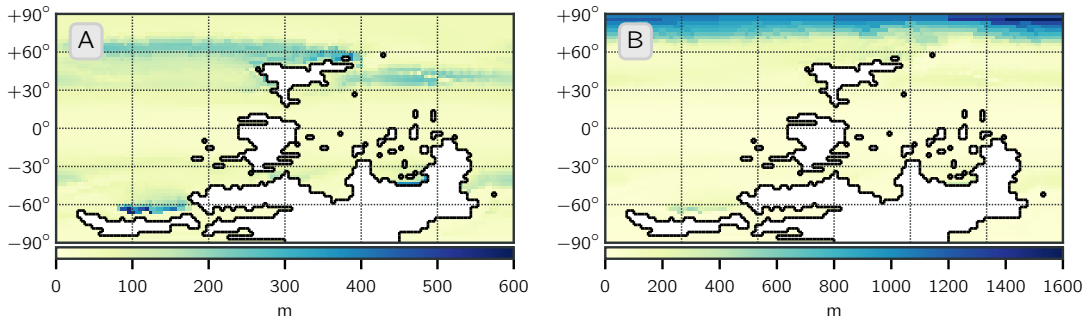

Figure 5.5: 100 year mean mixed layer depth in the CGCM; (A) partly-ventilated state; (B) ventilated state (note the different scales).

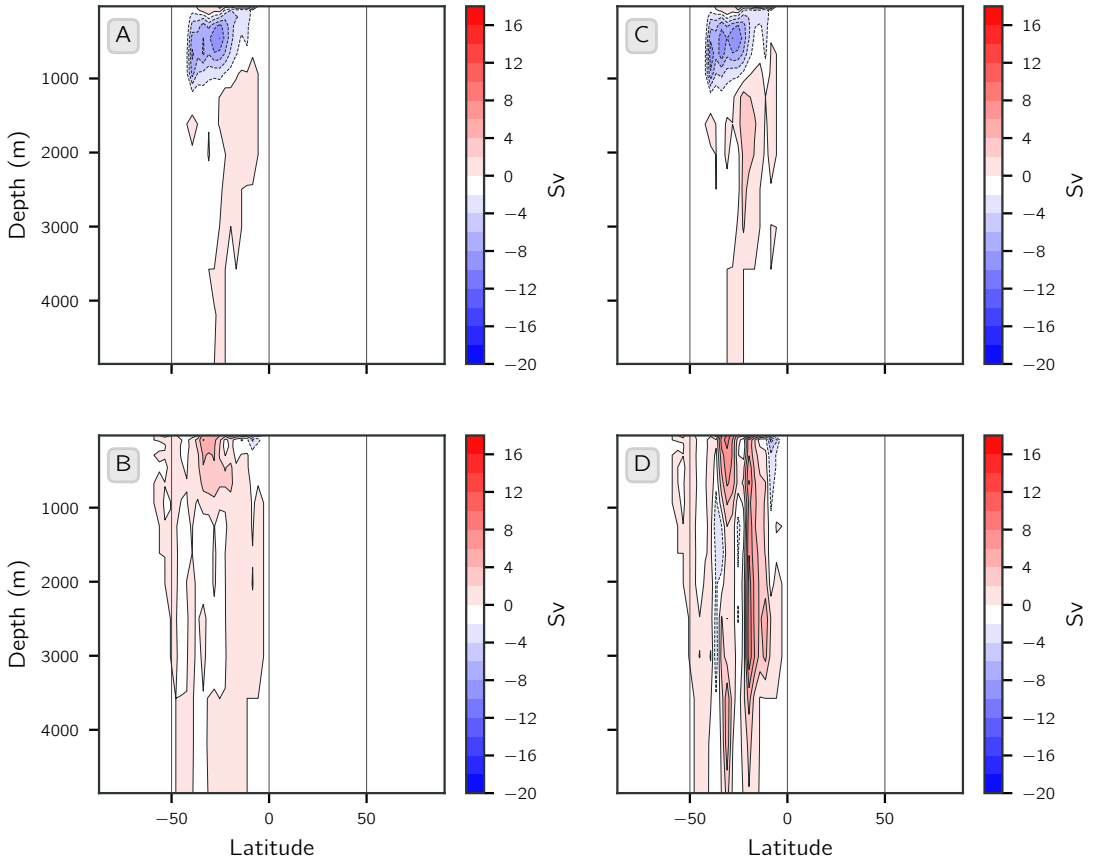

Figure 5.6: 100 year and zonal mean CGCM residual ocean overturning circulation in the Paleo Tethys Ocean (top) and Rheic Ocean (bottom); (A & B) partly-ventilated state; (C & D) ventilated state. Positive denotes clockwise circulation.

The upper 500 m ocean temperature in the Northern Hemisphere high latitudes decreases by approximately 0.2 °C and the deep ocean temperature decreases by 0.5 °C, while the global mean ocean temperature above 500 m is 0.05 °C lower and the deep ocean global mean temperature is reduced by 0.4 °C during the ventilated phase.

The global surface circulation in the ventilated state is similar to that in the partly-ventilated state except for the Northern Hemisphere polar region; there is no longer a polar westward current; instead the current is eastward from midlatitudes to the north pole. Diverging surface current vectors north east of Siberia results in upwelling at 80 ° N, allowing stronger, deeper overturning circulation and a ventilated deep ocean.

The strength of the overturning increases from 70 Sv to 80 Sv in the Northern Hemisphere tropics/subtropics (fig. 5.4). Buoyancy loss takes place in several regions in the mid and high-latitude Northern Hemisphere. First, the collapse of stratification in the ventilated phase causes deep convective mixing north of Siberia, allowing dense water formation. Figure 5.5B shows a significant increase in the mixed layer depth in the north pole region. Saline water flows poleward along the Panthalassa Western boundary and meets colder, more saline and consequently more dense water in comparison to the partly-ventilated state. The denser water results in a stronger deep water supply to the tropical to midlatitude circulation. The water then flows at depth further southwards into the Southern Hemisphere upwelling along the sloping northern boundary of China, Laurussia and Gondwana and on the southern boundary of the Rheic Ocean. In the ventilated state the overturning circulation extends to the seafloor and now circulates water from the deep ocean to the surface nearly globally. The Southern Hemisphere high latitudes are still not ventilated; a fresh surface layer restricts mixing in the region south of 60 ° S (figs. 5.2F and 5.4B).

The Rheic and Paleo Tethys ocean circulation is also increased slightly in the deep ocean (fig. 5.6). In the Paleo Tethys, there is a weak counter-rotating intermediate cell below the surface circulation, and the now deep Rheic overturning has increased in strength from 6 Sv to 10 Sv.

The overturning circulation is different to the present-day pattern. Similar to the present-day the Late Devonian ventilated state comprises a deep inter-hemispheric overturning cell associated with buoyancy loss, but while this buoyancy loss in the present-day is linked to buoyancy loss and sea-ice formation in marginal seas, the buoyancy loss in the Late Devonian takes place between the subtropics and mid-latitudes primarily due to evaporation increasing the surface salinity.

In the zonal mean there are strong westward currents that extend deeper in the subtropics either side of the eastward EUC (fig. 5.7). The Northern Hemisphere westward current, driven by strong easterly trade winds, extends to 1000 m water depth. Closer to the equator the surface westward current is shallow (20 m) and weak due to the weak equatorial atmospheric zonal easterlies. Below this surface current is the EUC; a relatively weak eastward current ($0.08\,\mathrm{m\,s^{-1}}$), between 20 m and 700 m. Figure 5.7A clearly shows how the surface wind pattern drives these currents. Figure 5.9 shows the zonal velocities along the equator in the ocean. The weak, shallow surface equatorial current results in a shallow sloping EUC, sloping upwards from ∼600 m at 120 °E to ∼300 m at 75 °W. Although the EUC extends deeper than the present-day Pacific EUC, the Late Devonian CGCM EUC is weaker, and upwelling of the EUC is weak in the east Panthalassa Ocean. The surface temperature difference between the east and west of the basin is only 2 °C (fig. 5.8).

5.2.3 Transition Partly-ventilated - Ventilated

The collapse in stratification, which leads to a transition to the ventilated phase takes place in the Northern Hemisphere high latitudes. Figure 5.10 clearly shows atmospheric freshwater supply to this region gradually declines throughout the partly-ventilated state, which is reflected in the ocean's freshwater content gradually decreasing north of 55 ° N (fig. 5.11B). A decrease in precipitation acts to reduce the freshness of the surface layer; this is visible in fig. 5.12. Over time the Northern Hemisphere fresh surface layer thins and becomes more saline. Coupled with decreasing high-latitude precipitation is the gradual accumulation of a warm, subsurface reservoir of heat, like in the OGCM simulation. As the heat content increases in the warm subsurface reservoir and precipitation at the surface decreases (fig. 5.12A), the vertical density difference decreases, leading to erosion of the

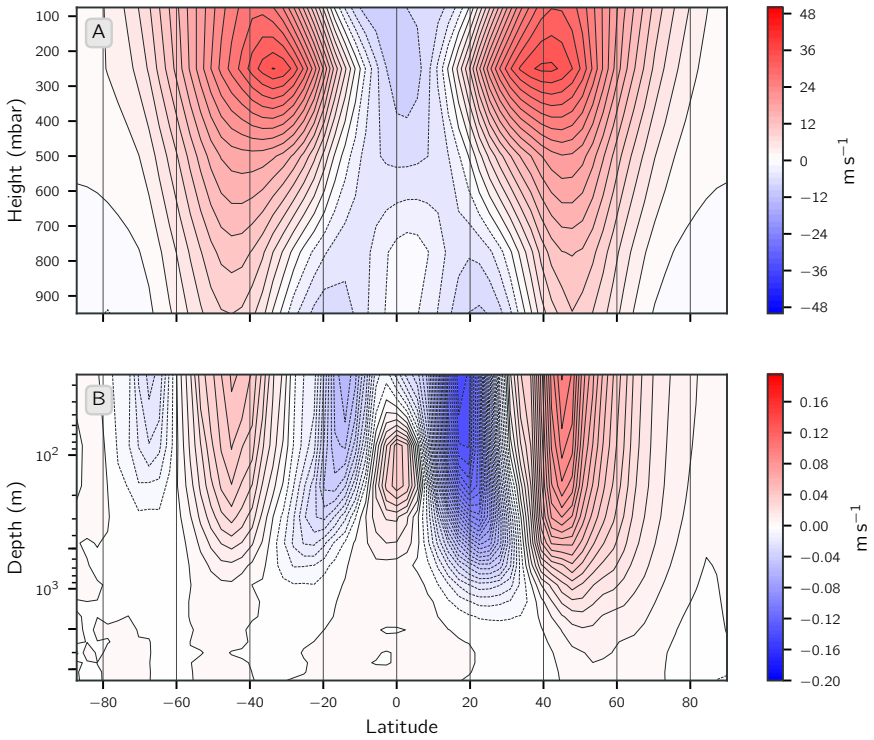

Figure 5.7: 100 year and zonal mean of (A) atmospheric zonal wind; (B) ocean zonal velocity during the ventilated state. Note the logarithmic depth scale in the ocean.

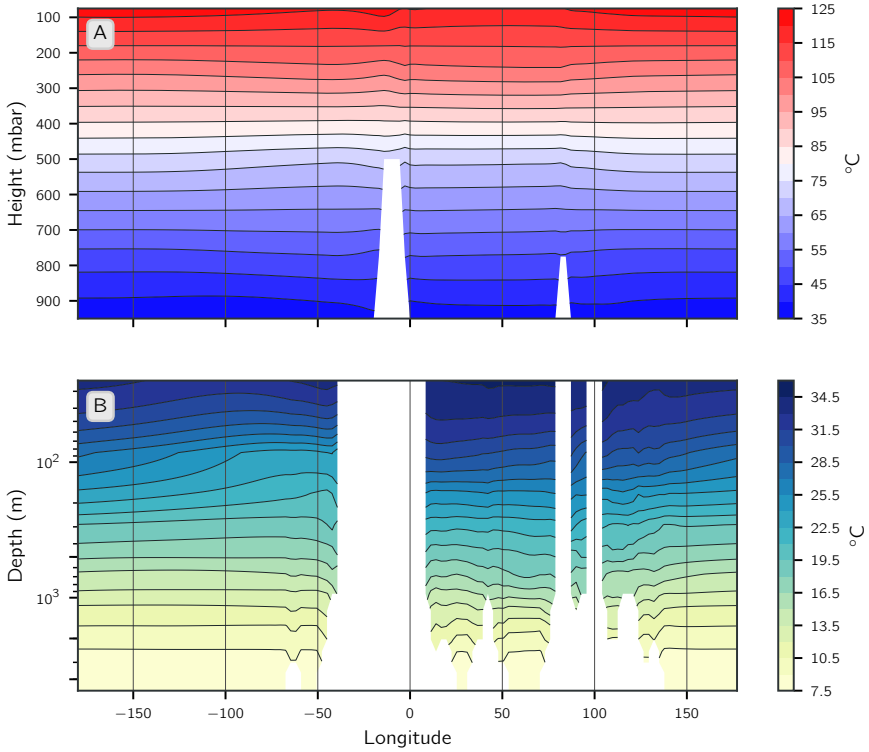

Figure 5.8: 100 year mean of potential temperature along the equator in the atmosphere (A) and ocean (B) during the ventilated state. Note the logarithmic depth scale in the ocean.

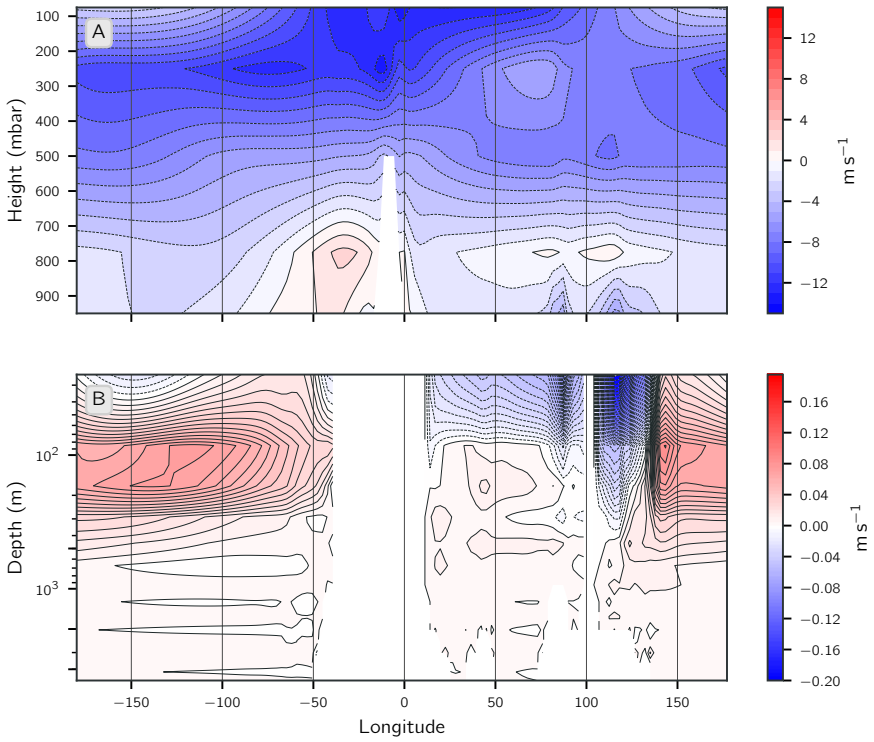

Figure 5.9: 100 year mean of equatorial (A) atmospheric zonal wind; (B) ocean zonal velocity during the ventilated state.

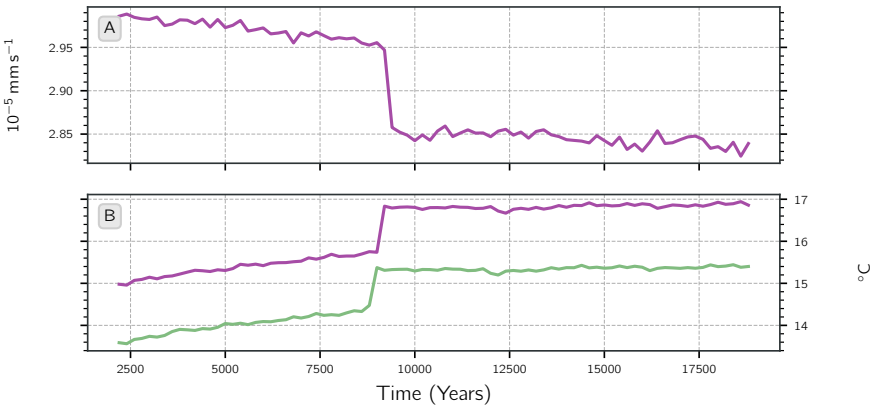

Figure 5.10: Time series of the atmosphere's role in the transition to ventilated ocean (A) freshwater supply to the region north of 55 ° N; (B) atmospheric surface temperature (*purple*) and SST (*green*) north of 55 ° N.

stratification. The warm reservoir of water in the subsurface is mixed to the surface and polar convective mixing is initiated, increasing the mixed layer depth (fig. 5.5). Following the erosion of stratification, the temperature remains fairly constant in the vertical and surface salinity gradually increases (fig. 5.12).

In the atmosphere, the transition to a ventilated ocean and increased SST is marked by a rapid increase in atmospheric surface temperature in the Northern Hemisphere high latitude region by 1 °C (fig. 5.13B). Following the surface temperature rise in the high latitude Northern Hemisphere, the temperature remains constant. Outside the Northern Hemisphere high latitudes the tropical/subtropical SST and atmospheric surface temperature rise slightly by 0.4 °C and Southern Hemisphere high latitudes begin to cool gradually by ∼0.3 °C over a 5000 year period. The surface atmospheric temperature is warmer than the surface ocean temperature in the Northern Hemisphere high latitudes, and this means heat flux is into the ocean, whereas in the Southern Hemisphere high latitudes the atmospheric surface temperature is colder than the oceanic surface temperature, and so heat flux is out of the ocean.

If this Southern Hemisphere cooling continued, the Southern Hemisphere could also become ventilated, similar to the north. Decreasing surface temperatures would reduce the vertical density gradient and could potentially lead to a Southern Hemisphere collapse in stratification, forming a strong, deep buoyancy driven overturning circulation. Yet, once

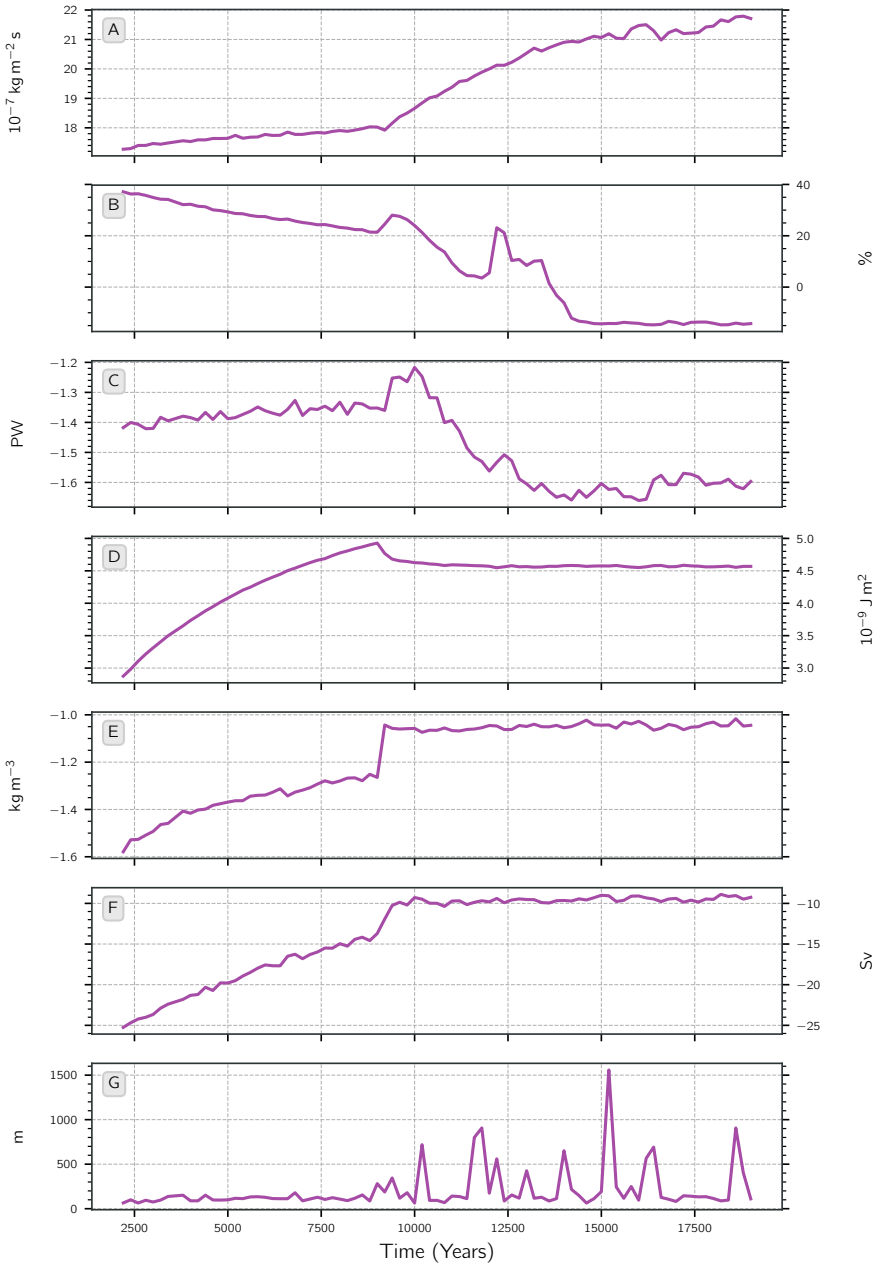

Figure 5.11: Time series of the CGCM ocean (A) salt transport along the section 55 ° N; (B) freshwater content north of 55 ° N; (C) heat transport along the section 55 ° N; (D) heat content below 200 m north of 55 ° N; (E) density difference north of 55 ° N between the surface and 800 m water depth; (F) mass transport along the section 55 ° N above 1000 m; (G) mixed layer depth north of 55 ° N.

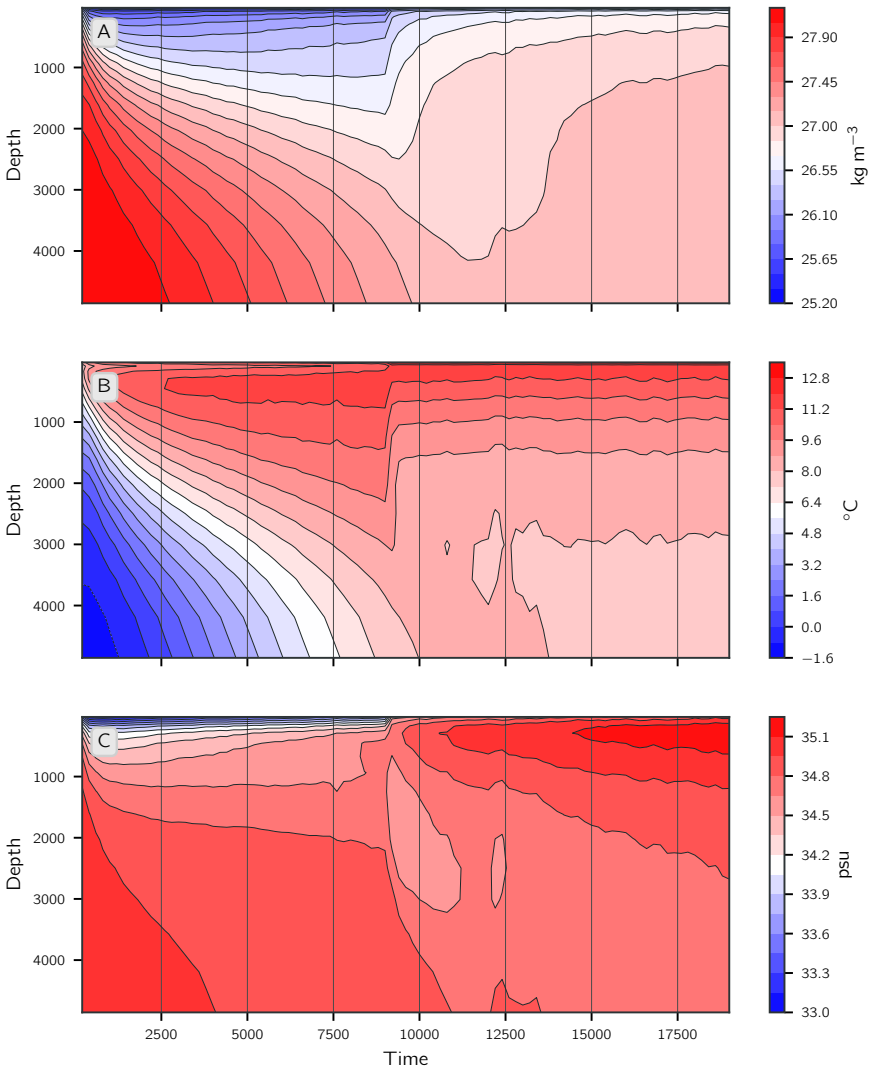

Figure 5.12: Time series of (A) mean potential density north of 55 ° N; (B) mean potential temperature north of 55 ° N; (C) mean salinity north of 55 ° N.

the climate has transitioned to the ventilated state, it remains ventilated for the remaining 11 500 years (i.e. the remainder of the simulation), and the Northern Hemisphere appears as though it would remain in this state if the model run were continued. Temperature does not change at all and salt transport into the region is increasing, gradually reducing the density gradient further. The stability shown in fig. 5.11 suggests the partly-ventilated state is in fact part of a long-term spin-up.

The atmospheric temperature change lags behind the ocean SST slightly and is a feedback on gradually increasing SST in the partly-ventilated phase through a gradual increase in atmospheric surface temperature and evaporation, causing the freshwater supply to the Northern Hemisphere to decrease (Increased SST causes increased precipitation, although this is outweighed by a greater increase in evaporation). This shows that through air-sea interactions, slight changes in the Northern Hemisphere evaporation-precipitation due to ocean surface conditions can keep the ocean in a ventilated state, suggesting this transition is in fact part of a long-term spin-up rather than two quasi stable states. This is different to the OGCM simulation which oscillated between a partly-ventilated and ventilated state due to fixed monthly atmospheric surface forcing.

5.3 Coupled Model Ocean Vs OGCM

The substantially stronger wind stress in the CGCM than the De Vleeschouwer study, which also resembles more the present-day zonal wind stress pattern, means the oceans overturning circulation is significantly different in the CGCM compared with the OGCM in both states. Both versions of the ocean circulation are strongly dependent on surface wind forcing, which differs considerably between models. Increased evaporation in the subtropical CGCM atmosphere causes greater surface salinity in both hemispheres than in the OGCM (figs. 5.14 and 5.15). Subsequently, buoyancy loss in the CGCM is greater which, coupled with increased wind stress driving enhanced Ekman downwelling, means the coupled ocean subtropical-midlatitude waters can mix to greater depths. Hence the different naming convention for equivalent ocean states: the OGCM shows no deep circulation in the unventilated state, whereas in the CGCM greater ocean salinity and wind stress allow deep water formation, restricted to the Northern Hemisphere, and a partly-ventilated deep ocean (figs. 3.3A and 5.4A).

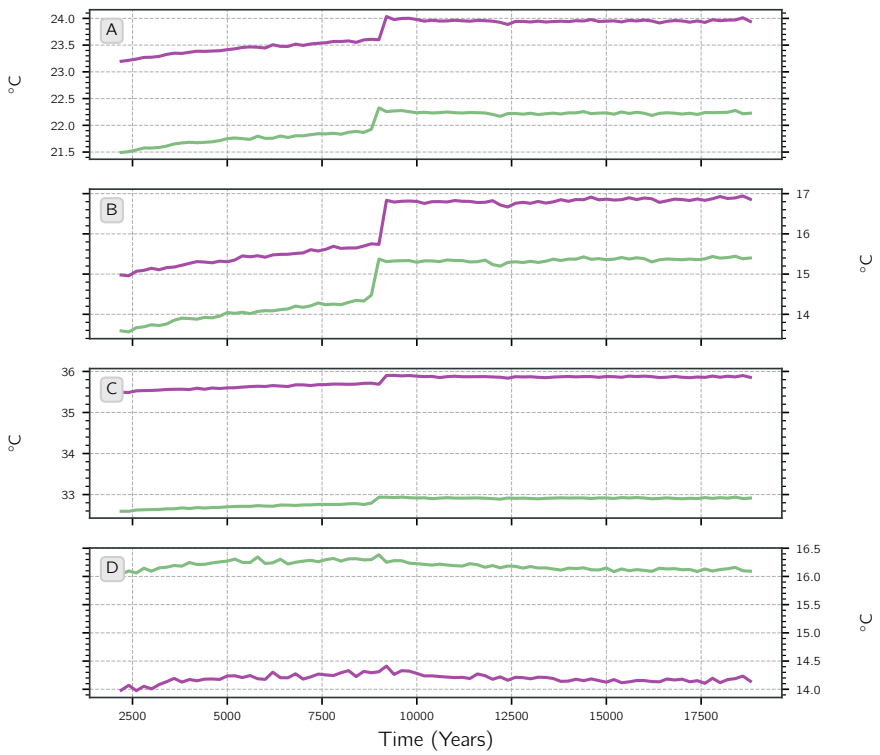

Figure 5.13: Time series of coupled model atmospheric surface temperature (purple line) and ocean SST (green line) for (A) global mean; (B) Northern Hemisphere mid (50°) to polar latitude mean; (C) tropical/subtropical mean; (D) Southern Hemisphere mid to polar latitude mean.

The strong trade winds and weak equatorial winds associated with the ITCZ in the CGCM also lead to a northward shift in the circumequatorial current, meaning the peak flow no longer interacts with the eastern boundary of Laurussia and the diverted flow into the Rheic Ocean is weaker. The northward shift of the current means greater interaction with the eastern boundary of Siberia, generating an intense north Panthalassa western boundary current and midlatitude gyre, which is also partially diverted north of Siberia (fig. 3.2 vs fig. 5.3A).

Both coupled and ocean only simulations highlight that the ocean circulation and properties are strongly dependent on the strength and meridional pattern of zonal wind stress, and the presence of a gateway allowing a circumnavigating current in the equatorial-subtropical region results in an ocean circulation dominated by the tropics and subtropics.

There is a saline tongue structure in each hemisphere of the CGCM, whereas this feature is only simulated in the Northern Hemisphere for the OGCM. During the unventilated/partly-ventilated ocean state the Northern Hemisphere warm subsurface reservoir is colder and slightly less saline in the CGCM, because the CGCM unventilated state is actually partly-ventilated. The Southern Hemisphere high latitude surface water shows colder regions (2 °C colder) extending to 700 m. During the ventilated state the region of Northern Hemisphere deep convection in the CGCM is 7 °C warmer, making the deep ocean significantly warmer than the OGCM simulation. The surface layer in the Northern Hemisphere polar regions is less saline, but overall the CGCM is more saline.

Generally, in both the unventilated/partly-ventilated and ventilated/ventilated states the coupled ocean is warmer, particularly in the subtropics, and more saline at the surface. Air-sea interactions in the CGCM simulation lead to a warmer ocean in both partly-ventilated and ventilated states; the subtropical warm lens extends deeper and is ∼8 °C warmer in this region when compared to the OGCM.

The CGCM does record two quasi-stable states of ocean circulation similar to the OGCM. However, the transition from unventilated to ventilated is more gradual in the coupled ocean, the ocean remains in the partly-ventilated state for a longer time initially with the same vertical mixing parameters and, most significantly, once the ocean transitions to a ventilated ocean state it remains in this state for the remainder of the simulation

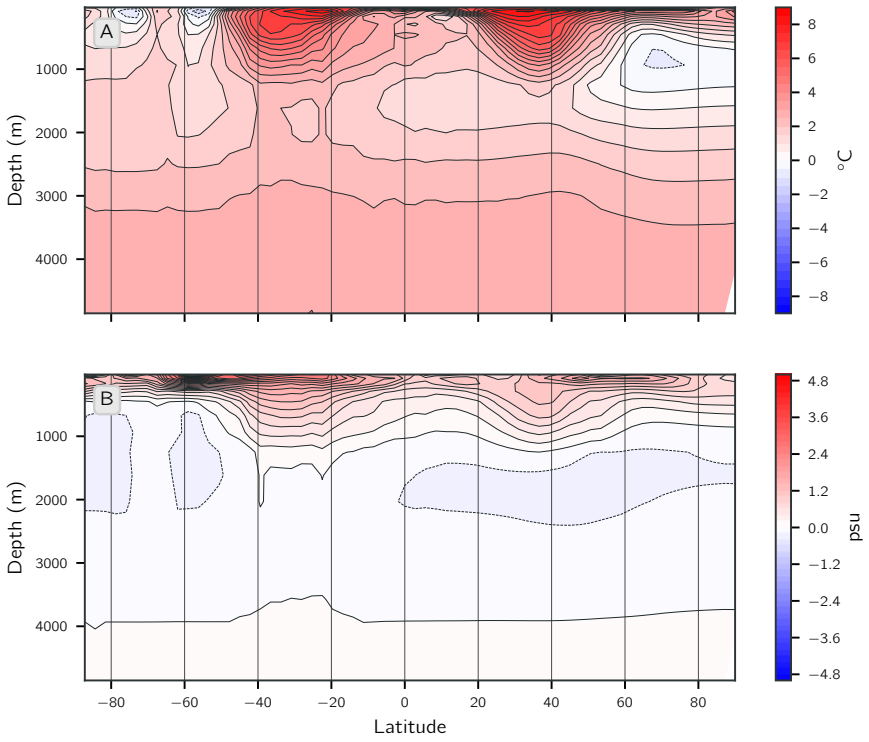

Figure 5.14: Zonal mean CGCM minus OGCM during the partly-ventilated/unventilated states for (A) zonal mean temperature and (B) zonal mean salinity.

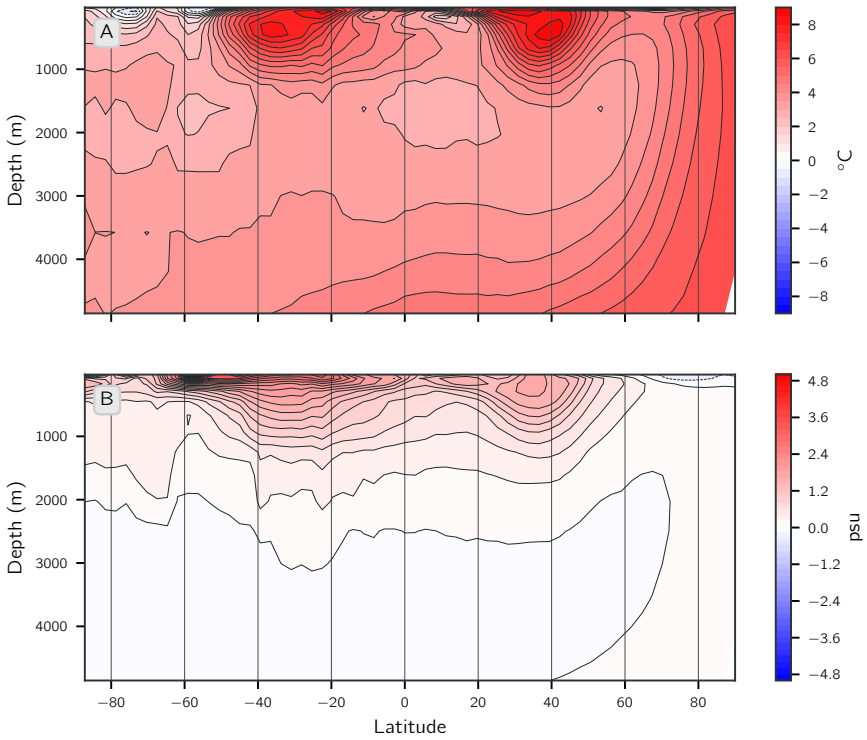

Figure 5.15: Zonal mean CGCM minus OGCM during the ventilated states for (A) zonal mean temperature and (B) zonal mean salinity.

(a further 12 000 years). It is interesting that both states, although slightly different to the OGCM, continue to exist in the face of the coupled feedbacks present in the Late Devonian CGCM simulation. It is clear that the unventilated state is plausible in the Late Devonian, although this will transition towards a stable ventilated state. The results of the CGCM suggest the climate would stay in the ventilated state, and so coupling an atmosphere and ocean climate does not allow oscillation between states. Potentially the unventilated state could be reinstated if the Late Devonian climate was perturbed externally, for example, through tectonic activity, volcanic activity or bolide impact. Interestingly, Late Devonian changes in climate correspond to the Viluy trap large igneous province volcanism on Siberia, beginning in the Frasnian and continuing to the Early Carboniferous. Siberia, located between the subtropical and high latitudes of the Northern Hemisphere, is highlighted in the OGCM and CGCM results as a key region for determining the global overturning circulation and strength of ventilation. Changes in the Northern Hemisphere climate due to volcanism could, therefore significantly affect the global ocean circulation and climate.

5.4 Atmosphere

The atmospheric circulation simulated using the MITgcm coupled atmosphere-ocean-ice model (CGCM) is described in detail here and comparisons made with the De Vleeschouwer et al. (2014) study, as well as a Late Devonian MITgcm atmospheric model with slab ocean (ASGCM).

5.4.1 Atmospheric Tropical Circulation

In the low latitudes, the Hadley circulation determines the structure of the convergence zones, and subsequently alters the pattern of precipitation. It also transports energy and angular momentum from the tropics to the subtropics. The Hadley circulation is a thermally driven circulation: warm equatorial air ascends high in the troposphere, flows polewards, descends in the subtropics and returns equatorwards at the surface (Hu et al., 2018). The descending branch of the Hadley circulation is at 30° north and south in the CGCM (figs. 5.16 and 5.17). The descending branch is a region of high pressure and low precipitation, and the climate there is characterised by arid to semi-arid conditions.

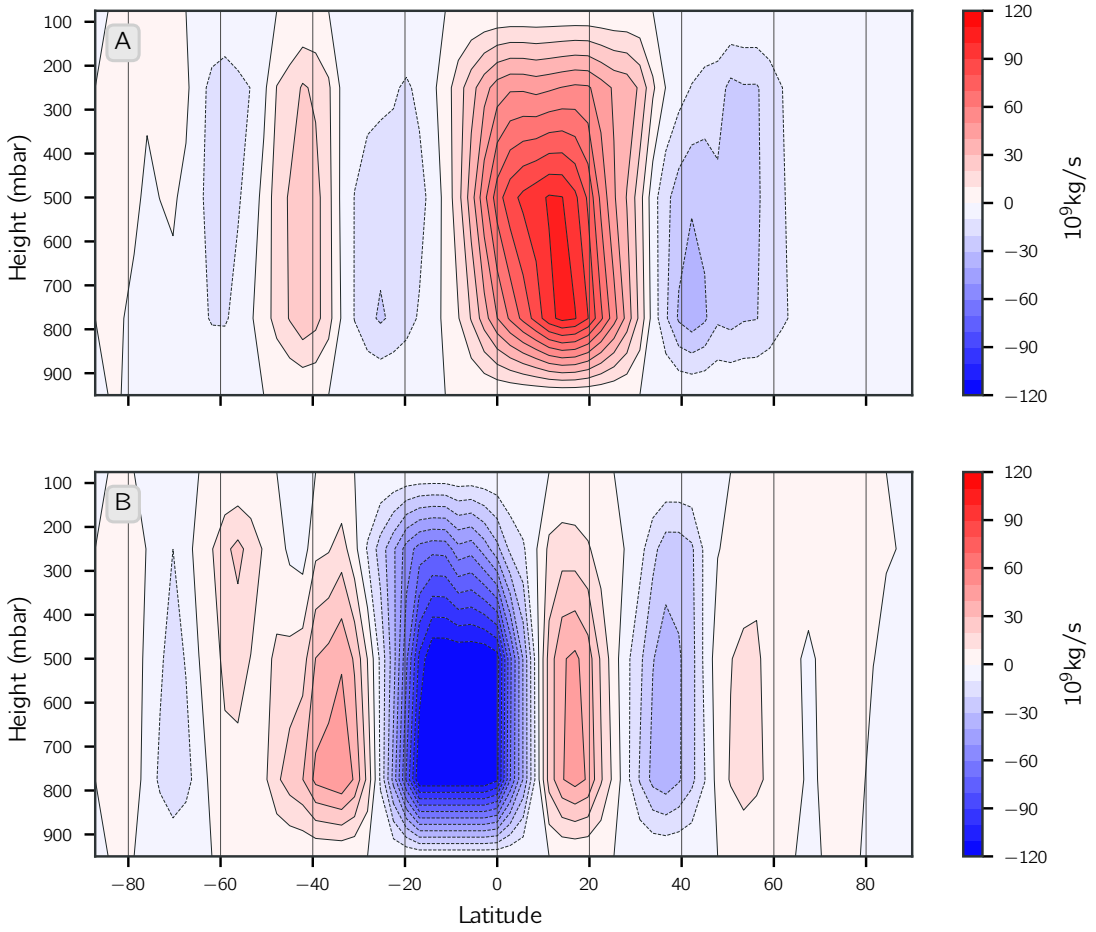

Figure 5.16: DJF comparison of atmospheric Eularian mean MOC. (A) CGCM; (B) ASGCM.

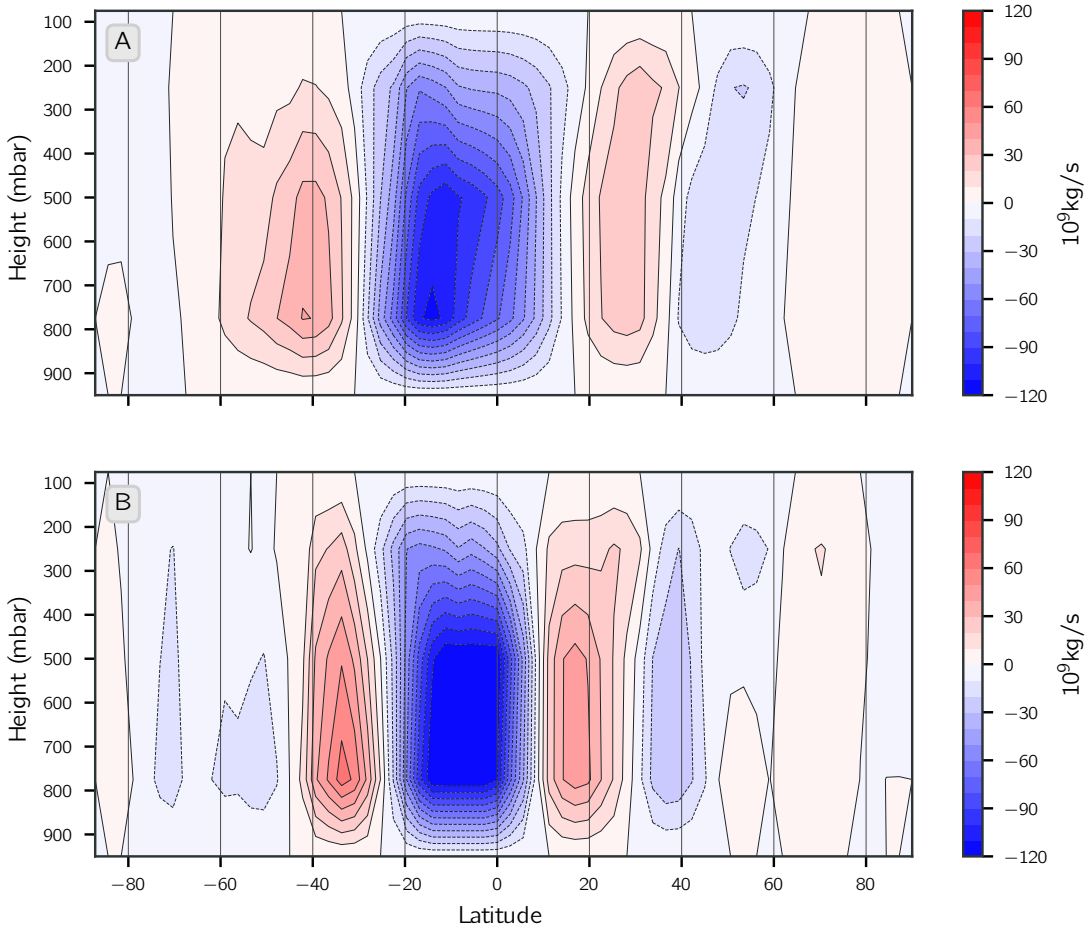

Figure 5.17: JJA comparison of atmospheric Eularian mean MOC. (A) CGCM; (B) ASGCM.

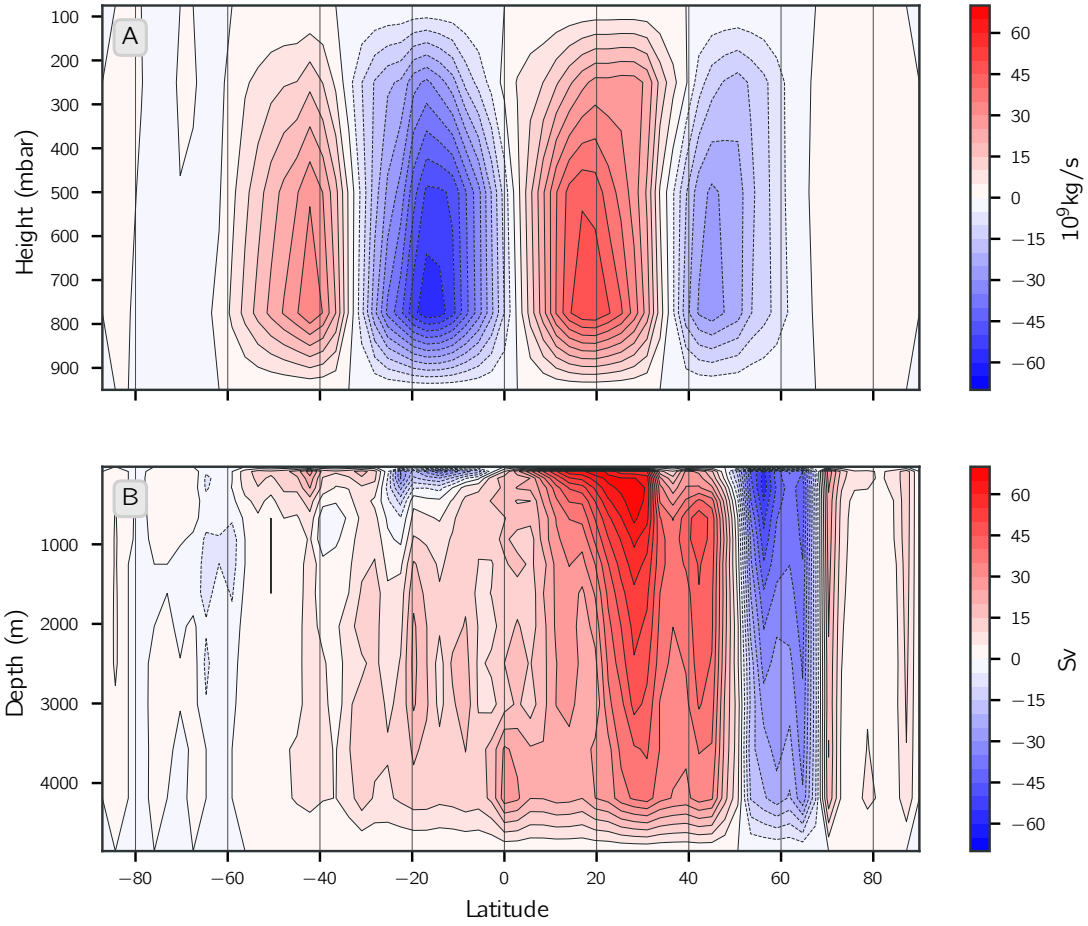

Figure 5.18: 100 year mean meridional overturning circulation in the atmosphere (A) and ocean (B) in the ventilated state of the CGCM. Positive denotes clockwise circulation.

Figure 5.18 clearly shows how the meridional overturning circulation of the ocean is affected by the atmospheric meridional overturning circulation, particularly the annual mean Hadley circulation here. The descending branch of the Hadley circulation results in dry conditions and evaporation, acting to increase the surface salinity, leading to buoyancy loss and sinking. In comparison, the Southern Hemisphere subtropical ocean overturning is weak and predominantly driven by atmospheric wind stress.

The ascending branch of the Hadley circulation determines the location of the ITCZ. Convergence of trade winds leads to strong convective cloud systems and heavy precipitation within the ITCZ (Hu et al., 2007). The meridional position of the ITCZ is linked with the atmospheric energy balance between the northern and Southern Hemispheres. In the present-day the Northern Hemisphere is warmer than the Southern Hemisphere

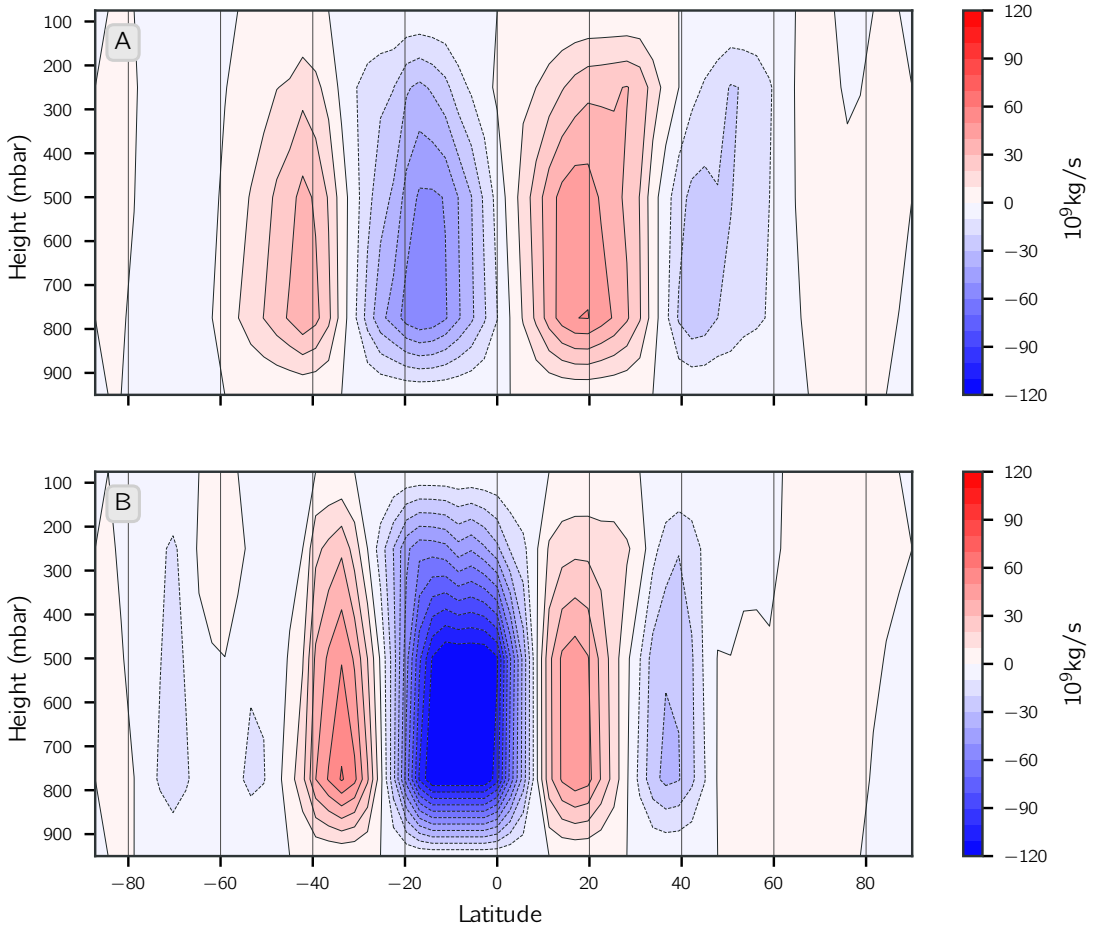

Figure 5.19: Annual mean comparison of atmospheric Eularian mean MOC. (A) CGCM; (B) ASGCM. Positive denotes clockwise circulation.

in the annual mean and, to compensate for the imbalance, the Hadley circulation and subsequently the ITCZ are centred north of the equator, allowing net southward energy transport across the equator. In the Late Devonian CGCM simulation the Northern Hemisphere atmosphere is marginally warmer, meaning energy must be transported southward. Thus the Southern Hemisphere Hadley circulation is stronger, and the ITCZ is centred just north of the equator (fig. 5.18).

The CGCM shows strong seasonality in the atmosphere, with the circulation varying seasonally; at each solstice, the tropics of the summer hemisphere receive more solar radiation than they radiate away locally. Seasonally, the ITCZ shifts towards the warmer, summer hemisphere (marked by weaker zonal wind and increased precipitation in figs. 5.20 and 5.21), with cross-equatorial flow transporting energy to the winter

hemisphere (Moreno-Chamarro et al., 2020). It is known from various present-day and palaeoclimate studies that the position of the ITCZ is affected by a combination of factors, including SST, vegetation, polar ice extent and low latitude orographic barriers. The spatial distribution of tropical SSTs plays an important role in the migration and position of the ITCZ. Coupling between SST and convection results in strong interactions of the ocean and the atmosphere, subsequently shaping the tropical climate, and its seasonal and inter-annual variations. For example, in the present-day central Pacific, SSTs at the equator are usually cooler than those away from the equator on both sides due to equatorial ocean upwelling. Since convection prefers warmer SSTs, the ITCZ shifts from one hemisphere to the other, instead of staying at the equator (Bjerknes, 1969). However, in the Indian Ocean and western Pacific warm-pool regions where maximum SST is at the equator, the ITCZ still prefers latitudes off the equator (Hu et al., 2007; Waliser and Jiang, 2015).

The tropical circulation simulated with the ASGCM is different. The annual mean Hadley circulation is more dominant in the Southern Hemisphere, and the circulation is similar to the Southern Hemisphere winter circulation, suggesting a lack of seasonality. Both DJF and JJA in the ASGCM have a stronger Southern Hemisphere Hadley circulation. The Southern Hemisphere summer is colder than the Northern Hemisphere winter, meaning cross-equatorial energy transport is required in all seasons to compensate for the imbalance. The ITCZ is positioned permanently just north of the equator and shows little variation seasonally. This highlights the importance of ocean dynamics in transporting heat out of the tropics polewards in the CGCM. The asymmetric Hadley circulation of the ASGCM circulation is similar to that simulated when cooling is applied to the Northern Hemisphere of the present-day Earth; the ITCZ shifts southwards, the northern trade winds are enhanced and southern trade winds weakened, and the Hadley circulation is latitudinally asymmetric with northern cell expansion and intensity increase and southern cell weakening (Braconnot et al., 2007; Broccoli et al., 2006; Zhang and Delworth, 2005). This annual asymmetric Hadley circulation with a dominant circulation in the cooler hemisphere, is a common feature of atmospheric slab ocean models, and is well-discussed in the literature (Chiang et al., 2003; Broccoli et al., 2006).

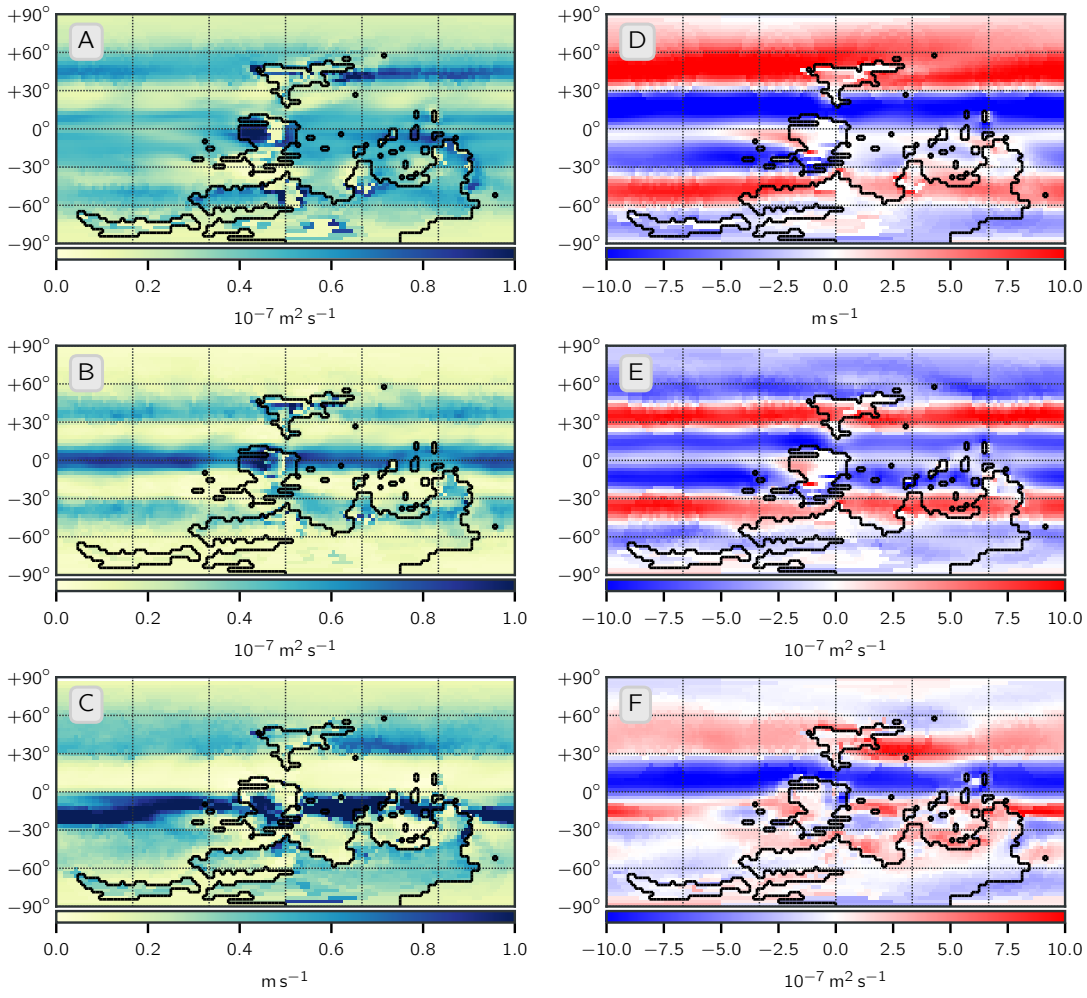

Figure 5.20: DJF comparison of, *top*, CGCM; *middle*, ASGCM; *bottom* De Vleeschouwer et al. (2014). (A - C) Precipitation; (D - F) zonal wind.

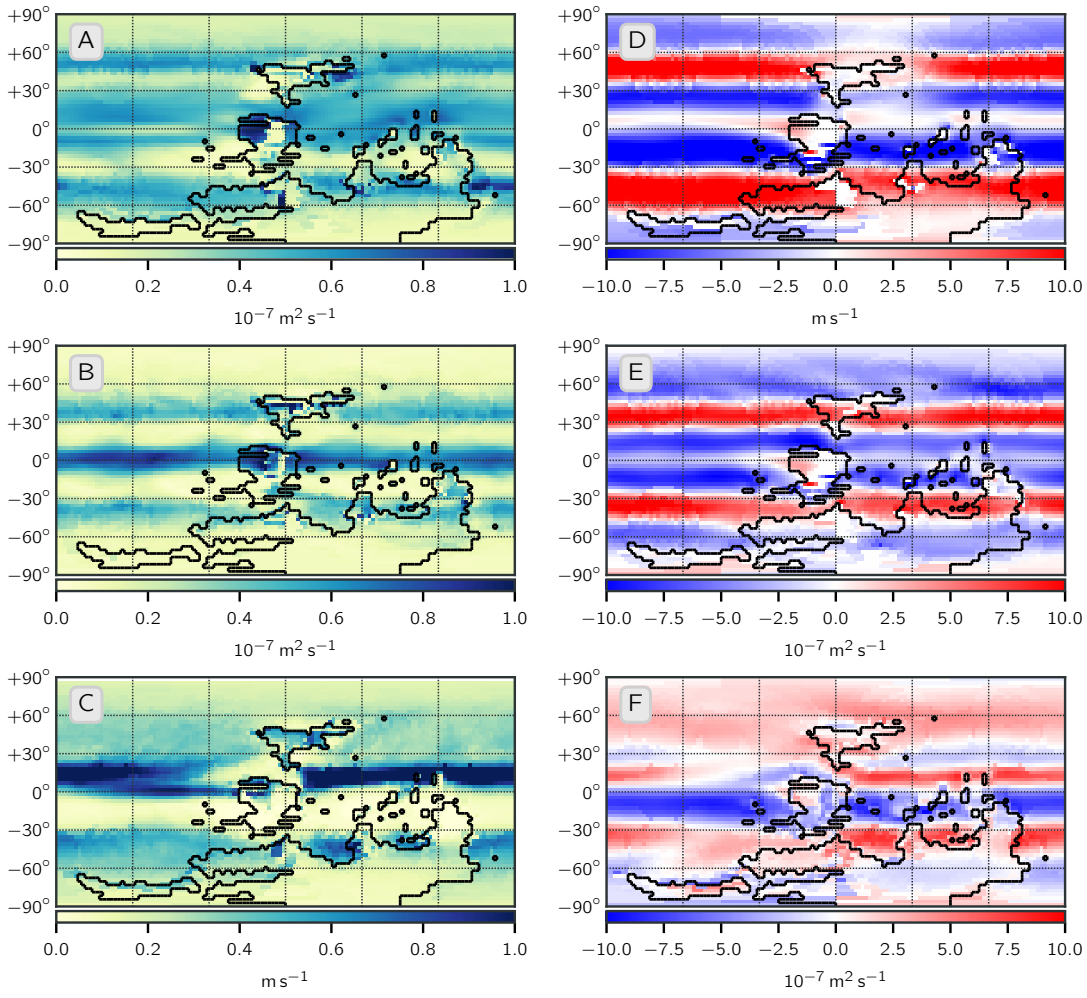

Figure 5.21: JJA comparison of, *top*, CGCM; *middle*, ASGCM; *bottom* De Vleeschouwer et al. (2014). (A - C) Precipitation; (D - F) zonal wind.

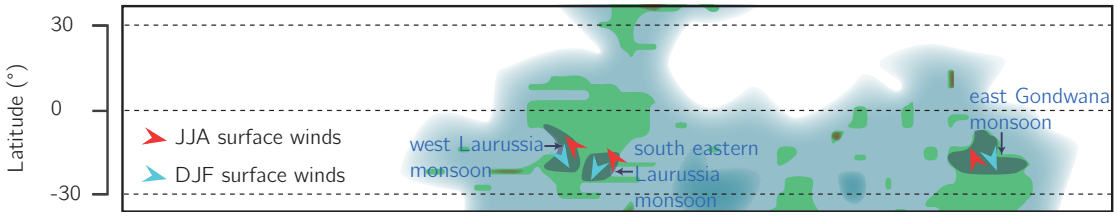

Figure 5.22: Locations of simulated Late Devonian monsoon systems, indicating the DJF and JJA surface wind directions.

Seasonally, the Southern Hemisphere winter cell still dominates in the ASGCM. This is due to a cooler Southern Hemisphere and increased equator-pole temperature gradient, so that the total atmospheric energy flux to the extratropics increases; the Northern Hemisphere demands more heat than the Southern Hemisphere (Broccoli et al., 2006). Green and Marshall (2017) emphasised annual cross-equator heat transport is stronger when an atmospheric slab ocean model is used.

5.4.2 Monsoons

Monsoon circulations are regional meridional circulations that oppose the Hadley circulation during the summer monsoon (Hu et al., 2018). The monsoonal region is delineated based on a significant change in the wind direction between winter and summer, with the direction of the prevailing wind within each season being reasonably steady, and maximum precipitation in the summer, followed by dryer conditions in winter (Chiang, 2009; Zhisheng et al., 2015). Three distinctive monsoon systems can be identified in the Late Devonian coupled climate (highlighted in figs. 5.22 and 5.23): east Gondwana, west Laurussia, and south eastern Laurussia monsoon systems.

The east Gondwana monsoon system is the region of land extending northwards close to the equator and separating the Panthalassa ocean and Paleo Tethys Ocean and is made up of present-day Australia and Antarctica. In the summer months (DJF) land-ocean temperature gradients result in north westerly air bringing warmer, equatorial winds to the continent. Surface temperatures reach 37 °C in February, followed by a peak precipitation of over 100 mm month^{-1} in April. In the winter months the wind shifts to an offshore south easterly, meaning moist, warm air is not being transported to the region and temperatures drops (fig. 5.24).

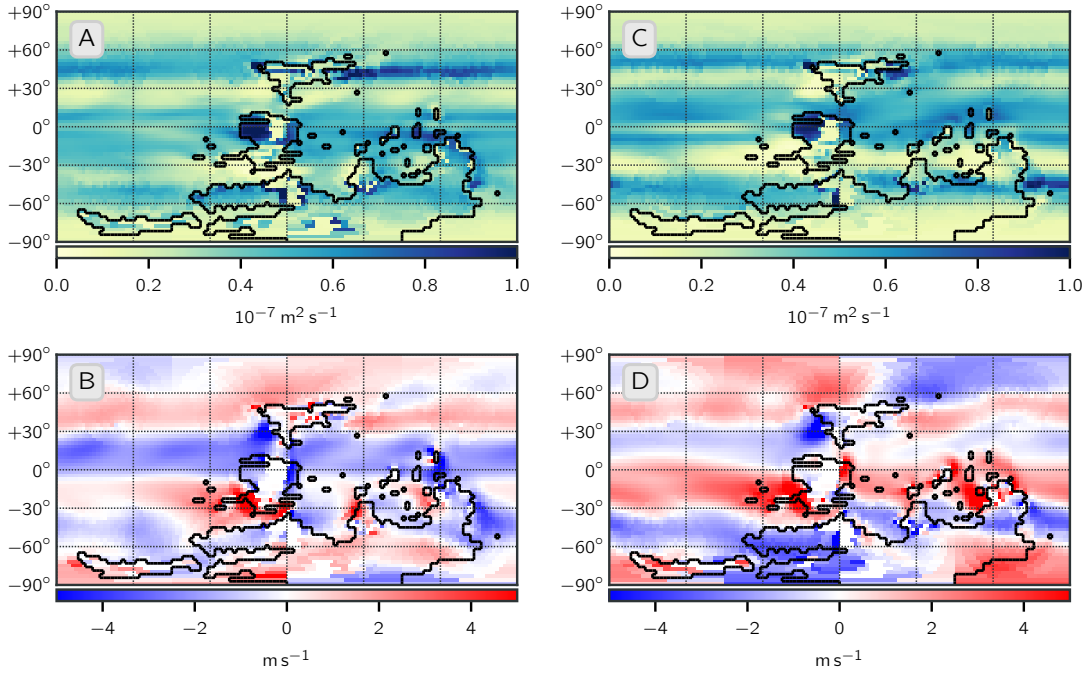

Figure 5.23: Comparison of DJF (left) and JJA (right) of CGCM atmosphere precipitation (A & C) and surface meridional wind (B & D).

The west Laurussia Monsoon is characterised by a shift from northerly winds in DJF to south easterly in JJA. Mean summer surface temperatures in the region reach 38.5 °C; the peak precipitation then lags behind due to moist processes and reaches ∼160 mm month^{-1} in March (fig. 5.24).

In DJF the southeast Laurussia monsoon system receives warm moist north westerly winds and the region receives a mean precipitation of 150 mm month^{-1}. In JJA the wind shifts to southerly and the surface temperature drops from 37 °C to 32 °C. As the moist processes adjust to changing winds and surface temperatures precipitation begins to fall.

5.4.3 Midlatitudes

Cyclones and anticyclones in the midlatitudes redistribute huge amounts of heat, moisture and angular momentum in Earth's extratropical atmosphere and form storm tracks. Midlatitude storm tracks are a key component of the general atmospheric circulation, determining weather and climate patterns (Mbengue and Schneider, 2018). Storm tracks are regions of high day-to-day variability, where fronts associated with perturbations are

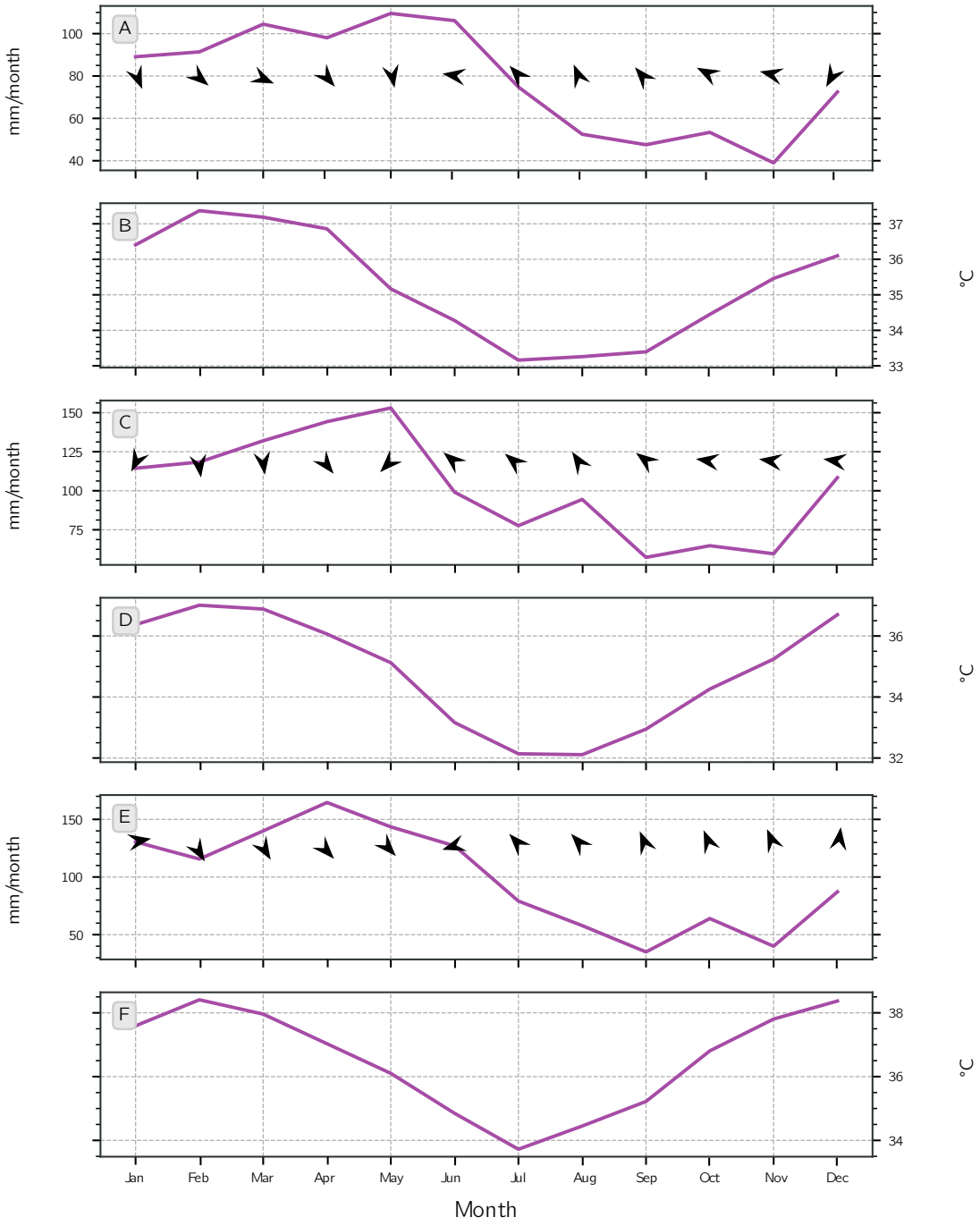

Figure 5.24: Monthly mean precipitation and 900 mbar wind vectors (A, C, & E), and surface temperature (B, D, & F) for Late Devonian Monsoon systems. (A, B), East Gondwana Monsoon region; (C & D) South East Laurussia Monsoon region; (E & F) West Laurussia Monsoon region.

linked with high precipitation. These perturbations, which explain the high-variability characteristic of the storm tracks, are manifestations of the baroclinic instability typical of the mean flow at midlatitudes. For the present-day, the east coasts of Asia and America are regions of high baroclinicity, and this is where meridional gradients in temperature are greatest due to contrasts between land and sea. Characteristics of storm tracks are dependent on the continent outlines, continental orography which can modify mean flow, and the surface temperature distribution (Kageyama et al., 1999).

Typically, storm tracks are diagnosed from either the zonal mean heat flux associated with transient eddies, geopotential height or the meridional velocity variance. These are computed from daily data. However, in this case it was not possible to output daily data for an extended time due to lack of computer resources. Alternatively, a more indirect indicator of storm tracks is the 900 mbar zonal wind velocity, since these low level winds exist due to momentum convergence in the storm track (figs. 5.20 and 5.21) and the atmospheric Eularian mean MOC. In the CGCM atmosphere, DJF Northern Hemisphere storm tracks are intense and extend from 35 °N to the poles. There is little variation zonally due to the Northern Hemisphere being mostly ocean, although there is disrupted flow across Siberia due to the Siberia mountain range, leading to greater precipitation on the leeward side. Precipitation is also greatest on the north western tip of Siberia. In the Northern Hemisphere summer the storm tracks narrow and polar easterlies exist. The zonal velocity is weaker surrounding Siberia and precipitation decreased.

In JJA at Southern Hemisphere midlatitudes there is a band of intense zonal velocity between 35 °S and 65 °S. Over central Gondwana weak westerly zonal winds extend further south to the pole. A mountain range in central Gondwana disrupts the zonal westerlies, causing zonally asymmetric zonal velocity in the polar region; in eastern high-latitude Gondwana westerly wind diverges from easterly wind in western high-latitude Gondwana/Panthalassa Ocean (fig. 5.21).

The location of midlatitude storm tracks is known in the present-day to be linked with the Hadley cell terminus, which shifts in tandem with storm tracks, and shifts in meridional SST gradient, since this gradient provides the energy for the storm tracks. The midlatitude storm tracks and the extent of Hadley circulation influence each other, but the causal link still remains unclear in the present literature. It is suggested the extent of

the Hadley cell may be controlled by measures of the baroclinicity, such as the subtropical static stability and meridional temperature gradients (Kang and Polvani, 2011; Ceppi and Hartmann, 2013; Mbengue and Schneider, 2018). During warm climates tropical static stability increases and the Hadley circulation expands, causing a poleward shift in the midlatitude storm tracks (Rojas et al., 2008; Mbengue and Schneider, 2018). The ASGCM climate is colder, seasonal sea-ice forms at the poles, and there is a greater meridional temperature gradient in the tropics-subtropics. The Hadley circulation is more intense and contracts towards the equator, causing an equatorward shift in midlatitude storm tracks.

5.4.4 Heat Transport

Total poleward heat transport H, is calculated from the top of the atmosphere radiation imbalance.

$$H(\phi) = \int_S^{\phi} \cos(\phi') R_{TOA} d\phi', \tag{5.1}$$

where

$$R_{TOA} = ASR - OLR \tag{5.2}$$

ASR is absorbed solar radiation, OLR is outgoing long wave radiation (also shown in figs. 5.25A and 5.26A).

ϕ is latitude, and R_{TOA} is the net radiation at the top of the atmosphere, defined as the difference between net ASR and OLR. The ASR is derived from solar radiation, and OLR is the total infrared radiation that exits the top of Earth's atmosphere, the majority emitted by the ocean surface and then by land (Gill, 1982).

This heat transport H is partitioned between the atmosphere and ocean. The ocean is not simulated in the ASGCM, but the energy budget for the ocean is calculated from residual heat fluxes,

$$H_O(\phi) = \int_S^\phi \cos(\phi') F_S d\phi' \tag{5.3}$$

where F_S represents the net upward energy flux at the Earth's surface;

$$F_S = Q_e + Q_b + Q_h + Q_s \tag{5.4}$$

in which Q_e is the rate of heat loss/gain by evaporation/condensation (latent heat flux); Q_b is the net longwave radiation at the ocean's surface; Q_s is net shortwave radiation at the ocean's surface; and Q_h is the sensible heat flux. Note that calculating ocean heat transport from heat fluxes assumes the ocean heat storage is negligible, which introduces some uncertainty.

The atmospheric contribution to poleward heat transport can then be written as:

$$H_A(\phi) = \int_S^\phi -\cos(\phi')(R_{TOA} + F_S) d\phi' \tag{5.5}$$

Figure 5.25B shows the total heat transport and the partitioning of heat transport between the ocean and the atmosphere in the CGCM, calculated from atmosphere-ocean heat fluxes.

The Northern Hemisphere ocean is more efficient at transporting heat poleward than the Southern Hemisphere. Southern Hemisphere ocean heat transport is weak across all latitudes, with peak transport of 0.6 PW in the tropics. Polewards of 50 ° S heat transport is very low.

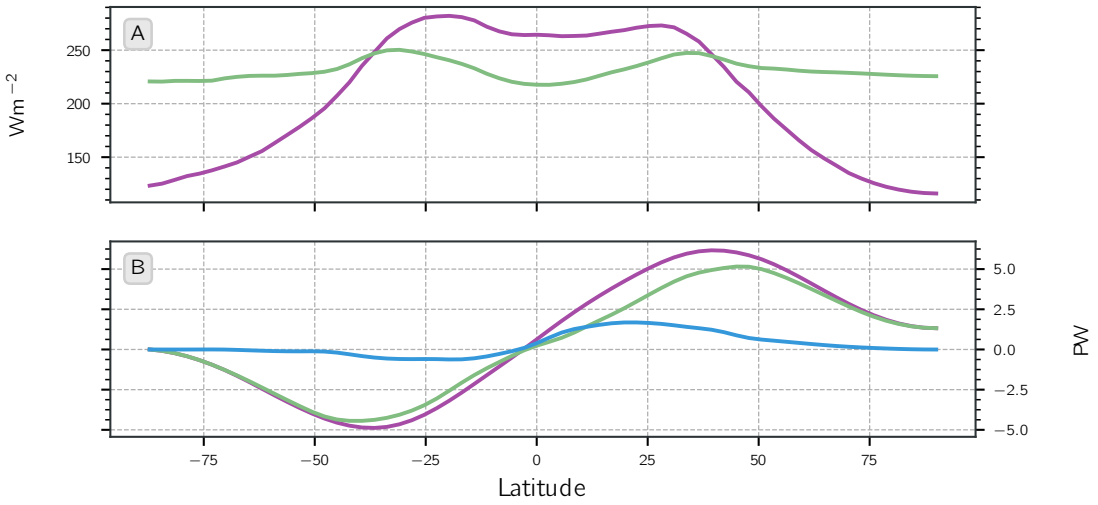

Figure 5.25: CGCM (A) Absorbed solar radiation (purple) and outgoing longwave radiation (green); (B) poleward energy transport calculated from top of the atmosphere energy budget and atmosphere-ocean heat fluxes. *Blue*, inferred ocean heat transport; *green*, inferred atmospheric heat transport; *purple*, total heat transport.

The Northern Hemisphere tropical/subtropical ocean is an active transporter of heat northwards, with peak transport of 2 PW in the region of 25 ° N. This active tropical and subtropical heat transport is linked to poleward Ekman transport, transporting warm water away from the equator.

The ocean plays a key role in transporting heat poleward out of the tropics, and the atmospheric midlatitudes transport large amounts of heat polewards. Peak atmospheric heat transport in the Northern Hemisphere is 6.2 PW at 45 ° N, whereas in the Southern Hemisphere peak heat transport is 5 PW in the region of 37 ° S. The atmosphere is responsible for transporting a large proportion of the total heat transport poleward in the Southern Hemisphere. However, total meridional heat transport is lower in the Southern Hemisphere compared to the Northern Hemisphere. This highlights the importance of a coupled atmosphere-ocean system to understand poleward heat transport effectively.

In comparison fig. 5.26 shows the heat transport calculated in the ASGCM simulation. The atmospheric heat transport reaches similar peak values between the ASGCM and CGCM, but the ASGCM peak is shifted towards the equator. The inferred ocean heat transport in the ASGCM is very different to the CGCM and is inconsistent with other atmospheric surface conditions of the ASGCM shown in fig. 5.1. It was expected that

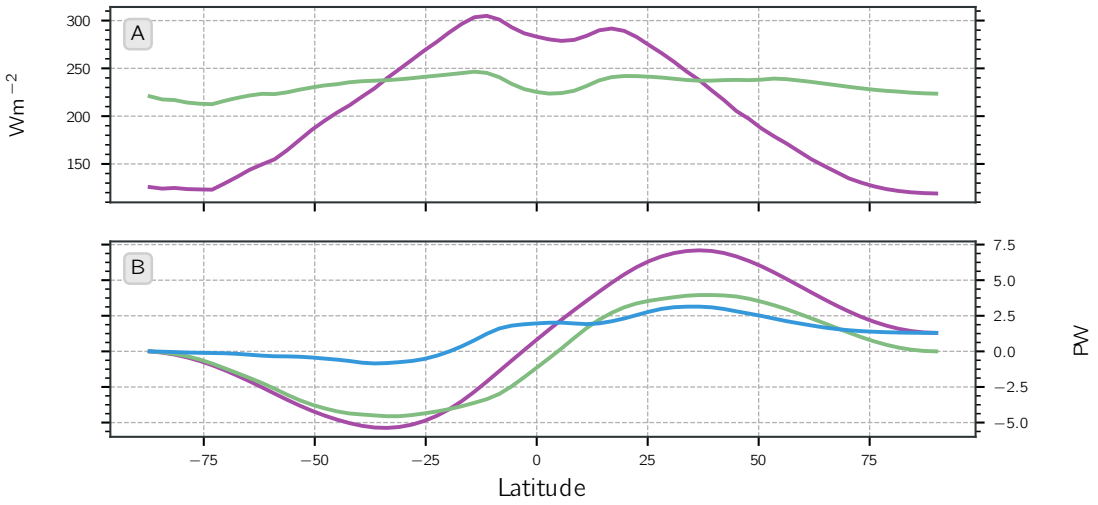

Figure 5.26: ASGCM (A) Absorbed solar radiation (purple) and outgoing longwave radiation (green); (B) poleward energy transport calculated from top of the atmosphere energy budget and atmosphere-ocean heat fluxes. *Blue*, inferred ocean heat transport; *green*, inferred atmospheric heat transport; *purple*, total heat transport.

the inferred ocean heat transport in the ASGCM would reach zero in the Northern Hemisphere, but fig. 5.26 shows the inferred ocean heat transport is imbalanced. Unfortunately, it is not known why this imbalance occurs. Poleward inferred ocean heat transport in the Southern Hemisphere ASGCM peaks at 0.6 PW in the subtropics; north of this peak heat transport switches to northward. Peak ocean heat transport is 3 PW at 35 ° N. This results in a climate which is efficient in transporting heat out of the tropics/subtropics to the midlatitudes. However, considering both figs. 5.1 and 5.26, the high latitudes are inefficient at transporting heat polewards, which leads to a large meridional temperature gradient and formation of sea-ice.

5.5 Impact of coupling to a Dynamic Atmosphere

The De Vleeschouwer et al. (2014) winds are inconsistent with those simulated in the ASGCM and CGCM atmospheres, and they are difficult to explain since exact details of the simulation are unknown. As a result, elements of the OGCM simulation forced by the weak De Vleeschouwer et al. (2014) wind stress forcing, are also not easily understood. The use of a coupled atmosphere-ocean-sea-ice model avoids introducing uncertainties in an ocean only model via the prescribed monthly atmospheric surface forcing. It is

interesting that both the OGCM and CGCM simulate a multi-state ocean with similarities in each state. However, the atmosphere-ocean feedbacks in the CGCM are clearly important in preventing a return from the ventilated state to the partly-ventilated state and an oscillation.

The ASGCM and CGCM are relatively similar, but key differences highlight the importance of coupling the atmosphere to a dynamic ocean. First, large equator-pole temperature gradients with high latitude sea-ice formation in the ASGCM (fig. 5.1), which is not observed in the geological record, shows how important the ocean dynamics are in transporting heat out of the tropics. The large equator-pole temperature gradient then affects atmospheric circulation. Considerable differences in land-ocean temperatures mean the ASGCM Southern Hemisphere summer is colder than the Northern Hemisphere winter, and cross-equatorial energy transport is required in all seasons to compensate for this imbalance. The ITCZ is positioned permanently just north of the equator and shows little variation seasonally. Greater meridional temperature gradients also cause an equatorward shift in midlatitude storm tracks. Consequently, the global atmosphere is MOC is significantly different to that in the CGCM atmosphere. Including a dynamic ocean means the ocean can transport heat polewards, while air-sea interactions allow the ocean to lose heat to the atmosphere and the meridional temperature gradient is reduced.

5.6 Implications for the Devonian

As with the OGCM, the Late Devonian coupled Frasnian-Famennian in the CGCM is characterised by two climate states; a partly-ventilated, (yet strongly stratified at high latitudes) ocean state; and a ventilated state with strong deep convective mixing. There is no oscillation between states in the CGCM simulation, although the existence of both states suggests the unventilated state is plausible.

Joachimski et al. (2009) reconstructed sea surface palaeotemperature throughout the Devonian low latitudes using brachiopod and conodont oxygen isotopes. The SST rose throughout the Frasnian, reaching a peak of 32 °C, declining at the F–F extinction by ∼1 °C. The sea surface temperatures simulated here are slightly greater in the low latitudes at ∼34 °C. But, similarly to the Joachimski et al. (2009) study, there is a global decrease in low latitude upper ocean temperature, although the change is not as significant, decreasing ∼0.3 °C between the partly-ventilated and ventilated states.

Figure 5.27 shows the simulated evaporation minus precipitation pattern and SST, with locations of Late Devonian palaeoclimate indicators from the geological record marked. Evaporite deposits are indicative of arid climates and are found in the Late Devonian geological record in east Panthalassa, east Siberia and the western Paleo Tethys; these all correlate with regions where evaporation exceeds precipitation. Coal is deposited in humid tropical wetland climates. Late Devonian coals of North America, located in west Laurussia, are formed in shrub-dominated peat wetlands. Forested wetland environments also appear for the first time in the Late Devonian in China. These early peats and forest mires represent the initiation of a new carbon sink, making changes to the Earth's global carbon cycle (Greb et al., 2006). Locations of coals correlate with regions of high precipitation and warm climate in the CGCM (fig. 5.27).

Reef development reached peak coverage during the Middle to Late Devonian when it is estimated reefs covered 10 times the modern day reef ecosystem area at $\sim 5 \times 10^6$ km. Locations of reef ecosystems are shown in fig. 5.27. The F-F extinction caused the collapse of stromatoporoid-tabulate coral ecosystems. Following this extinction microbial reefs became dominant, but were gradually replaced by stromatoporoid-tabulate coral again until the Hangenberg extinction when they were eliminated again (Yao et al., 2020). During

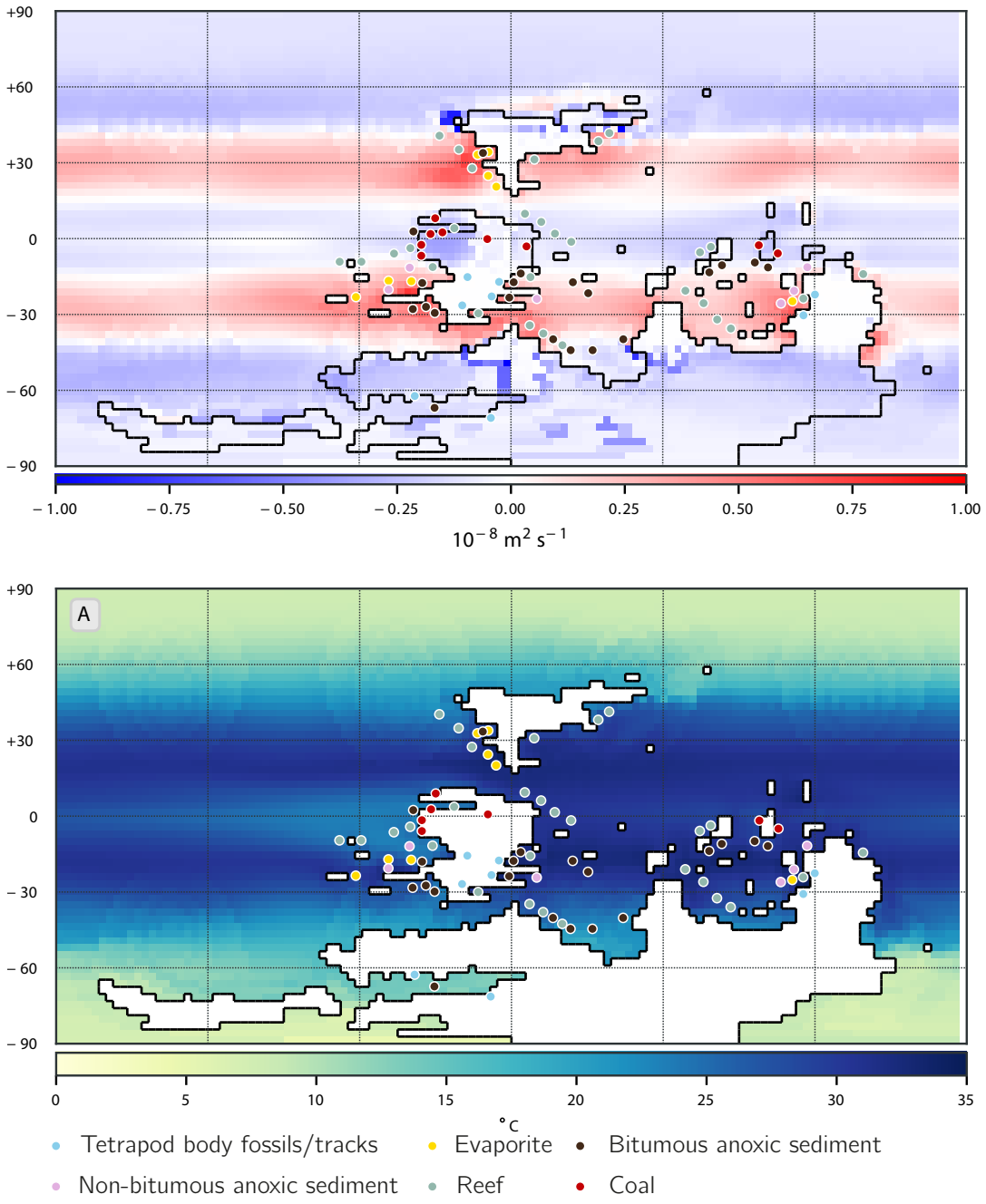

Figure 5.27: Modelled evaporation minus precipitation (A) and SST (B) comparison with approximate location of lithic indicators of palaeoclimate and primary tetrapod evolution sites. Adapted from Witzke (1990); Carmichael et al. (2019); Golonka (2020).

the Middle Devonian Eifelian-Givetian reefs are observed in the sedimentary record well into mid to high latitudes between 45 ° S and 60 ° N. Reefs in the Frasnian greenhouse climate were present, but did not reach as high latitudes, and extend between 45 ° N and 45 ° S in the geological record (Copper, 2002). Optimum water temperature for coral reefs in the present-day is between 23 °C and 29 °C, but some can tolerate temperatures as high as 40 °C. Due to weaker poleward ocean heat transport in the CGCM Southern Hemisphere, surface temperatures are cooler and reach the minimum optimum coral reef temperature at ∼40 ° S. This means the simulated surface temperature is too low for some mid-latitude Southern Hemisphere reefs observed Rheic Ocean. Potentially the Southern Hemisphere climate is slightly too cold in the CGCM simulation.

The largest Frasnian reef development is observed in the Canada basin, located on the equatorial eastern boundary of Panthalassa. The results of the CGCM show this region experienced upwelling of ∼24 °C waters (fig. 5.8), slightly cooler than in other equatorial regions, caused by the development of an east-west pressure gradient due to the strong continuous westward current, forming an ideal environment for reef development. Figure 5.28 shows dissolved O_2 during the partly-ventilated and ventilated ocean states. During the partly-ventilated state deep overturning circulation does not extend into the equatorial region or Southern Hemisphere (fig. 5.4), this means equatorial upwelling of O_2 is shallower and so the water upwelling to shallow reefs along the equator, and east Panthalassa region of the Canada basin is oxic and nutrient rich. In comparison during the ventilated state, a deep global overturning circulation extends into the Southern Hemisphere. Now upwelling of dysoxic/anoxic water along the equator is simulated, with waters with even less oxygen content upwelling in the Canada basin region due to the EUC. During the F–F extinction anoxic sediments are observed in this region, and reef ecosystems are eliminated.

Isotope research has highlighted regions of the Late Devonian ocean that were at least anoxic. These include: (1) the Paleo Tethys, in particular the northern region of the basin (Chen et al., 2013; Song et al., 2017), (2) the Rheic ocean, predominantly the western equatorial region; (3) regions of Panthalassa such as eastern equatorial Panthalassa (De Vleeschouwer et al., 2017). In these regions the simulated ocean circulation is weak during both ocean states, with slightly greater overturning strength in the ventilated

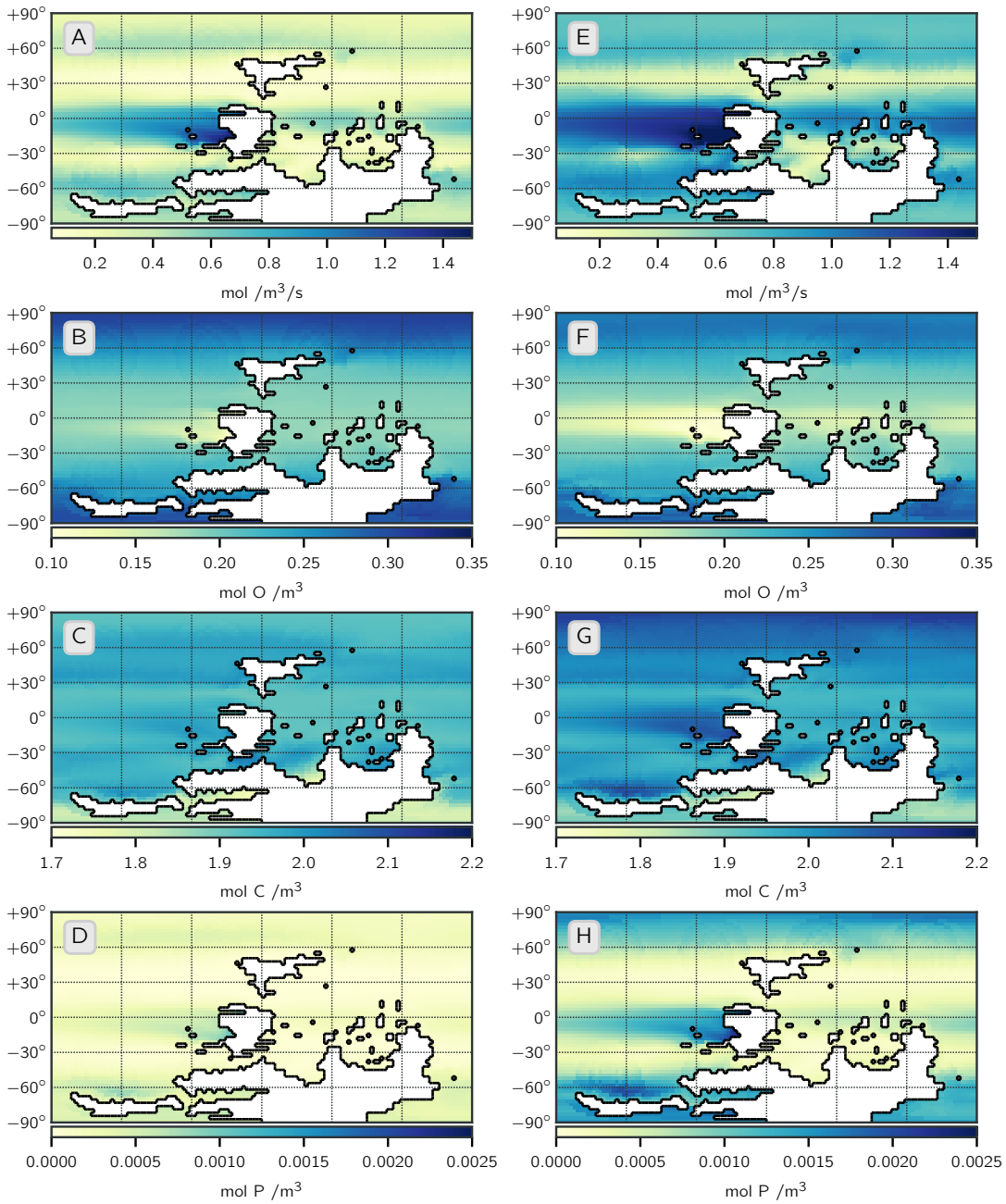

Figure 5.28: Coupled ocean 200 year mean surface biogeochemistry during both unventilated (left) and ventilated (right) states. (A & E) Biological productivity; (B & F) dissolved oxygen; (C & G) DIC; (D & H) PO_4.

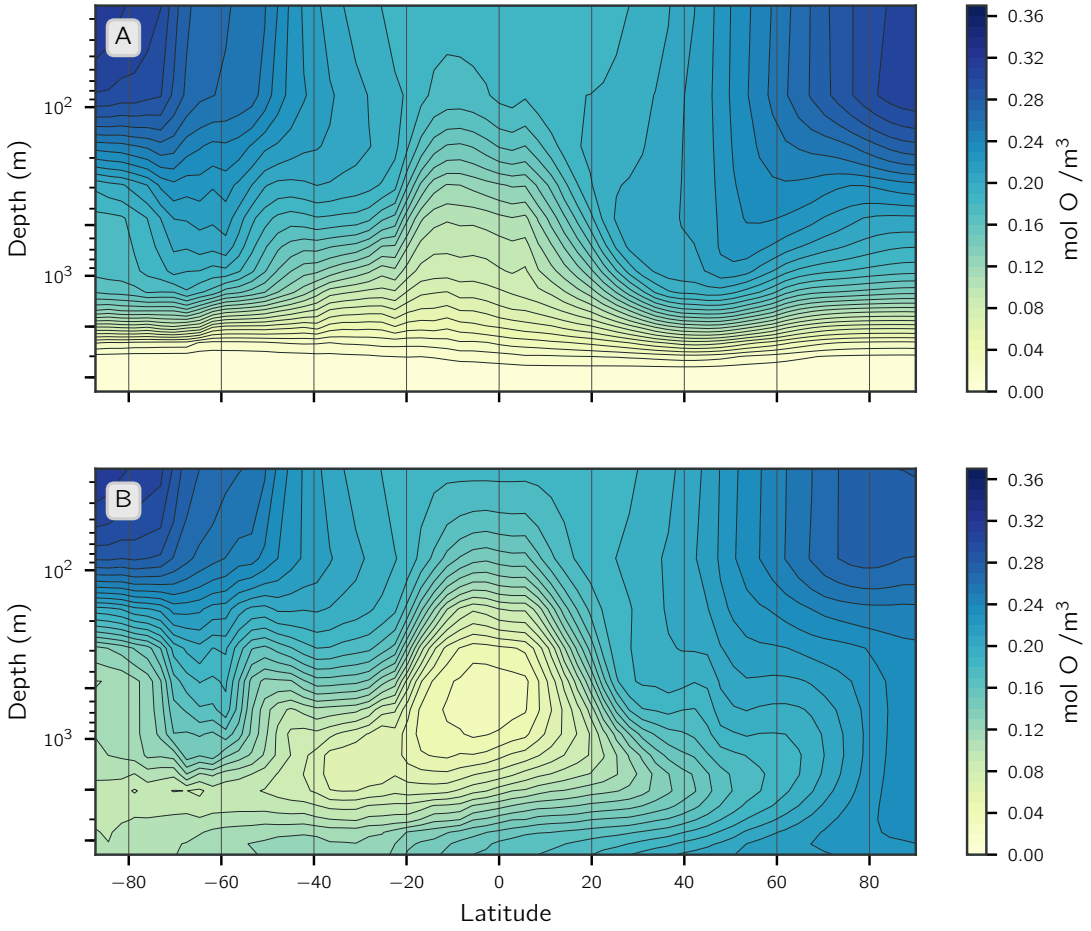

Figure 5.29: Coupled ocean 100 year, zonal mean dissolved oxygen during partly-ventilated (A) and ventilated (B) state.

state. Figure 5.29 shows the zonal mean dissolved oxygen concentration; during the partly-ventilated state the deep ocean is strongly depleted in oxygen. Oxygen depleted water is upwelled to shallow (∼200 m) regions in the tropics due to Ekman divergence. The simulated O_2 levels in the deep ocean are considered anoxic during the partly-ventilated state.

In both the Rheic Ocean and Paleo Tethys the ocean overturns to 1000 m water depth (fig. 5.6), and this is linked with the sinking of warm saline water. Below this upper ocean overturning the circulation and mixing are weak, and the ocean is strongly stratified, providing ideal conditions for the water to become stagnant and anoxic. Meyer and Kump (2008) suggested this resistance to vertical mixing is a dominant control in waters becoming anoxic/euxinic, coupled with efficient nutrient trapping. Figure 5.30 shows the

zonal mean O_2 for both the Rheic and Paleo Tethys Ocean. These are key in the geological record of anoxia. During the partly-ventilated state both basins are anoxic in the deep ocean, with the most oxic water extending up to ∼1000 m and ∼300 m depth in the Paleo Tethys and Rheic Ocean respectively on the southern boundaries. The vertical gradient in O_2 is greatest in the Paleo Tethys ocean, highlighting the strongly stratified state and lack of deep ocean mixing.

During the ventilated state the deep ocean remains anoxic in the Paleo Tethys Ocean, but the now slightly enhanced overturning mixes dysoxic/potentially anoxic water to the surface on the northern boundary. This upwelling of dysoxic/anoxic water is also seen on the Rheic Ocean northern boundary, although less significant. This is an interesting and important feature of the CGCM results, since ocean anoxia in the Late Devonian geological record is most commonly observed in the northern Paleo Tethys, surrounding South China, and northern Rheic, near east Laurussia. The results of the CGCM suggest that the hypothesis of deep anoxic/euxinic upwelling into shallow restricted northern regions in these two basins is possible as a 'kill' mechanism during the F–F.

The South China region of the Paleo Tethys, a key region in the literature for shallow and open ocean anoxia, positioned just south of the equator, experiences warm tropical climates. Annual mean SST is 34 °C in the CGCM simulation and ocean surface currents are moderate, flowing westward. Seasonally, the region experiences intense precipitation associated with the migration of the ITCZ in summer months, and in the winter precipitation is slightly reduced, approaching arid conditions further south in the open ocean regions of the Paleo Tethys (figs. 5.20 and 5.21). Ocean anoxia is also recorded in the eastern region of the Paleo Tethys in non-bituminous limestone or silt. This region, which is present-day Australia/Antarctic, would be subject to the East Gondwana monsoon climate, experiencing warm and intense seasonal precipitation between January-May, followed by colder (33 °C atmospheric temperature), dry periods. An East Gondwana monsoon is supported by studies of Early Forest soils across the Silurian and Devonian. Similarities between Middle/Late Devonian soils from Antarctica, and present-day northern India soils, which now support monsoon forests, are observed (Retallack, 1997).

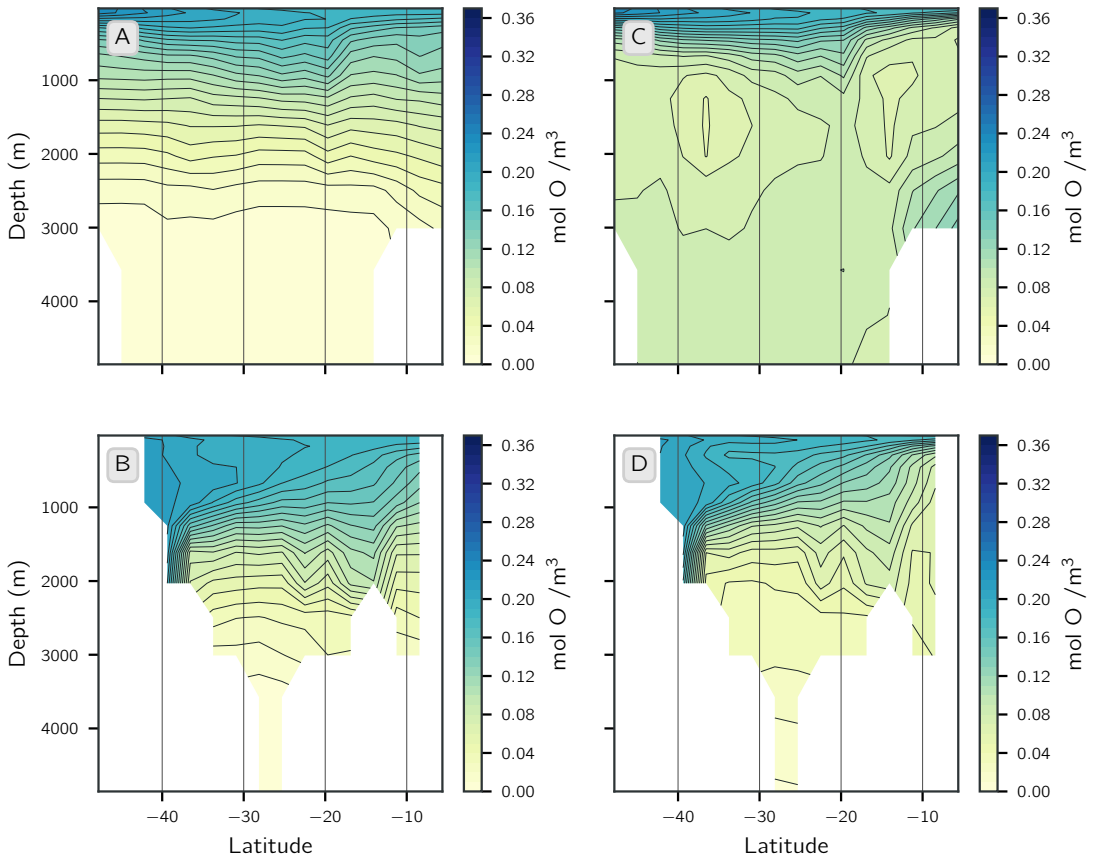

Figure 5.30: Coupled ocean 200 year, zonal mean dissolved O_2 during partly-ventilated (left) and ventilated (right) state. (A & C) Rheic Ocean; (B & D) Paleo Tethys Ocean.

Figure 5.28 shows surface biogeochemistry conditions simulated by the CGCM in both the partly-ventilated and ventilated states. Panels B and F clearly show the upwelling regions of dysoxic waters in the equatorial regions discussed above. However, the biological productivity, showing low productivity in the Paleo Tethys and Rheic basins is not realistic. The biogeochemistry package does not include nutrient influx from the land via river input, and so is primarily controlled through solar radiation and PO_4, which is controlled by the large scale pattern of vertical velocity. Regions of strong upwelling bring nutrients to the surface and promote biological productivity. In reality, the evolution of land plants in the Devonian would have led to increased terrestrial nutrient runoff, and potentially enhanced surface anoxia through eutrofication. The CGCM results show upper ocean overturning in the Rheic and Paleo Tethys Oceans was weak, even in the ventilated state (fig. 5.6). Weak mixing causing a strongly stratified ocean coupled with strong nutrient influx from land could enhance algal productivity, which consumes oxygen and increases hydrogen sulphide, leading to PZE.

DIC increases nearly globally at the surface in the ventilated state (fig. 5.28). Carbon is absorbed into the ocean more easily in colder, more alkaline surface conditions, and alkalinity correlates with the salinity pattern (Williams and Follows, 2011). During the ventilated state surface temperature decreases and surface salinity increases at all latitudes (fig. 5.2), but particularly the Northern Hemisphere, which consequently sees the largest increase in DIC between partly-ventilated and ventilated.

Figure 5.31 shows the locations of anoxia/euxinia based on the Late Devonian isotopic record, in relation to the simulated DO at a depth of 290 m. This depth corrosponds the typical depth of anoxic sediments observed during the F–F extiction. The figure clearly shows some key regions of where the simulated DO would be anoxic and correlates with the geological evidence. Specifically, eastern equatorial Panthalassa, the north east boundary of the Rheic Ocean and north Paleo Tethys Ocean.

The Devonian is a critical Period in Earth's history for the evolution of tetrapods. Stem tetrapod fish fossils are observed in the Paleo Tethys in the Early Devonian, and it is conjectured that surface ocean currents swept these early tetrapods towards the western boundary of the Rheic in the Middle-Late Devonian, where the fish-tetrapod transition is observed in the geological record (Clack, 2012). This is consistent with the simulated

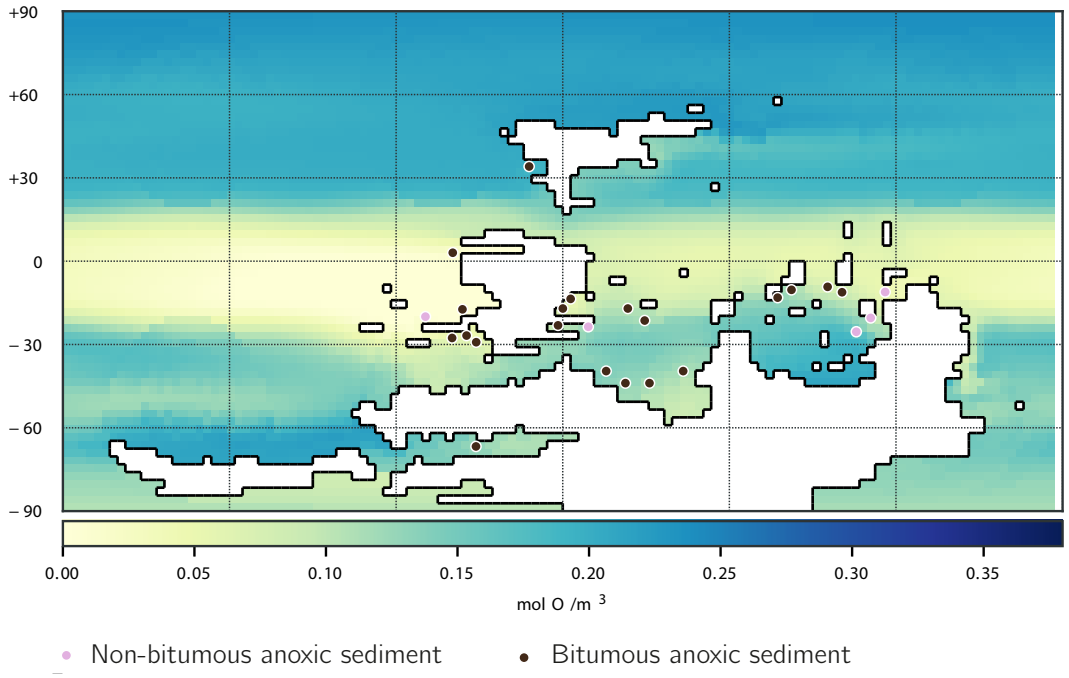

Figure 5.31: Coupled ocean 200 year mean dissolved O_2 during the ventilated state at a depth of 290 m, this corresponds to the average depth of isotopic evidence of anoxia/euxinia, the approximate location of which are marked on the map. Adapted from Witzke (1990); Carmichael et al. (2019); Golonka (2020).

surface ocean currents. Stem tetrapods and early tetrapods would have been exposed to warm saline surface conditions in these regions (fig. 5.3). Early tetrapod body fossils and trace fossils have been discovered in Middle Devonian North American and European sediments, which were part of east and west Laurussia. The climate model results suggest tetrapods would be living within a warm tropical/subtropical monsoonal climate, subject to the South East Laurussia monsoon. This is consistent with the interpretations of Late Devonian sediments which interpret a seasonally wet/arid climate for locations of Devonian tetrapods (Streel, 2000; Marshall et al., 2007; De Vleeschouwer et al., 2012, 2013; Narkiewicz and Retallack, 2014; Ahlberg, 2018). Research suggests the monsoon system here was weakest due to astronomical forcing at the F–F boundary and the driest climate persisted at this time (Kaiho et al., 2013). Increasing oxygen throughout the Devonian, coupled with increased aridity of tropical eastern Laurussia led to increased forest fires. Since this study only considers the climate under present-day astronomical forcing, it would be an interesting extension to the research to consider the Late Devonian climate under different combinations of eccentricity, obliquity and precession to test variations in the strength of monsoon systems, changes in snow/ice cover or even ocean overturning circulation.

Late Devonian tetrapods discovered at $\sim$70 °S indicate tetrapods were likely globally widespread outside of the tropical/subtropical climate zones (Gess and Ahlberg, 2018). The CGCM results indicate tetrapods in these latitudes would be subject to mild annual mean atmospheric temperatures of $\sim$10 °C. Tetrapods would experience large seasonal temperature variations from 20 °C in the summer to 0 °C in the winter. Conditions are not comparable to present-day climates at similar latitudes; the climate is significantly warmer and is more comparable to a present-day wet mid-latitude climate, like northern Scotland. Although a key difference would be the tetrapods experiencing darkness throughout the winter. Further evidence of a mild southern climate in this high latitude region is the migration of brachiopod species from a high-latitude Gondwana setting in the Late Devonian, to a low-latitude Laurussia setting in the end Devonian/Early Carboniferous as the global climate cooled and the southern high latitudes experienced glaciation (Scholze and Gess, 2017).

Poor poleward heat transport as simulated here in the Southern Hemisphere would cause gradual cooling of the polar region. Figure 5.13 clearly shows the Southern Hemisphere high latitude atmospheric surface temperature and SST decreases gradually following the transition to a ventilated ocean state. The Frasnian climate is described as a greenhouse climate, with evidence of glaciers recorded in the sedimentary record only in high altitude Gondwana (Eyles, 2008). The De Vleeschouwer et al. (2014) atmospheric results also support the formation of only high altitude glaciers, and in the CGCM sea-ice did not form. Current literature also suggests the Devonian oceans were absent of sea-ice. The early Famennian is then marked by glaciation, which is well-established by the late Famennian extending across the polar regions of Gondwana, with evidence of glacial marine environments (Isaacson et al., 2008). The earliest evidence of Northern Hemisphere polar sea-ice is recorded in the Early Carboniferous. Therefore, the simulated total heat transport supports a potential change to a glacial climate in the Southern Hemisphere.

5.7 Model Uncertainties

Feulner (2009) reviewed the capability of climate modelling to aid understanding of species extinction events, reviewing climate-modelling studies of extinction events in the Permian, Triassic/Jurassic, and Cretaceous. The review noted the importance of climate models in further considering the causes of mass extinctions and outlined a number of conditions which should be met when modelling palaeoclimates. These include; the use of an intermediate-complexity GCM, with a three-dimensional ocean component, coupled to an atmospheric component; realistic geography and topography for the time of the extinction event; approximations of continental vegetation and a marine carbon cycle. These conditions have been met in this study. However, modelling deep time palaeoclimates such as the Late Devonian still involves simplifications, leading to some limitations and uncertainties in the results. These uncertainties are discussed, and the key points that should be considered in future studies highlighted.

5.7.1 Atmospheric Component

The simplified atmospheric component of the model (Molteni, 2003) is a compromise between level of complexity and required computer resources. The simple 5-layer atmosphere can be coupled with different components of the climate system. In this study, coupling with the ocean and ice system is achieved and the model is run over long timescales using relatively few computer resources. However, in using an intermediate complexity atmosphere with just 5-layers there is a degree of simplification.

Brunetti and Vérard (2017) considered how to reduce long-term model drift in coupled climate model heat transport for both the Jurassic and present-day, finding that tuning of the Relative Humidity Threshold (RH) for low clouds (*RHCL2* in MITgcm) strongly impacts the degree of temperature drift. The results of the Brunetti and Vérard (2017) study were considered during the model setup; however, only limited tuning of the RH parameter was possible. To reduce uncertainty of the Late Devonian results, future studies could consider further tuning the RH parameter and increasing the vertical resolution of the atmosphere.

Large uncertainties in the initial boundary conditions also exist. Position and height of topography strongly impact the pattern of atmospheric circulation, and the oversimplification of a vegetation parameter which in turn sets the land surface albedo could pre-determine the climate in certain regions. Prior to coupling the atmospheric component with the dynamic ocean extensive testing on the impacts of changing vegetation parameter and topography was completed. This investigation found that the vegetation parameter had little impact on the atmospheric circulation, and for consistency the vegetation pattern implemented by De Vleeschouwer et al. (2014) was therefore used. The position of mountain ranges has a more significant impact on the atmospheric circulation, particularly on the zonal wind field and precipitation pattern. However, this model configuration implements a 'best guess' of the Late Devonian topography. The position of major mountain belts such as the Laurussia orographic barrier is widely agreed, although it is certain the topography implemented is an oversimplification. Further testing of the impacts of different topography using a coupled atmosphere-ocean-ice model is recommended.

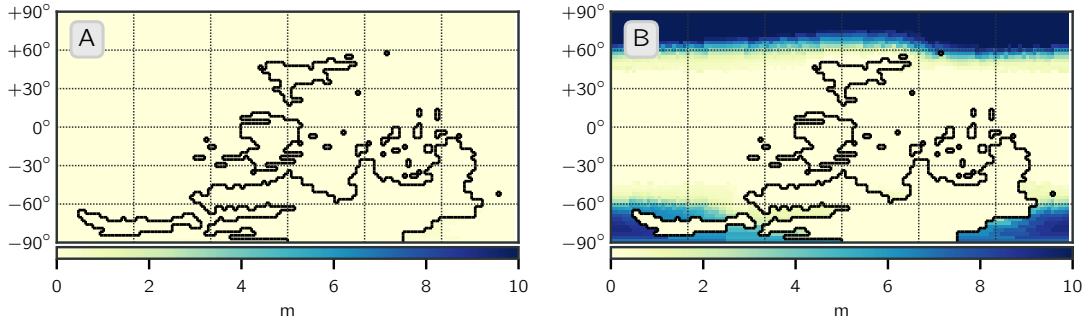

Figure 5.32: Comparison of annual mean coupled model sea-ice thickness with pCO_2 equal to (A) 2180 ppm; (B) 370 ppm.

5.7.2 Boundary Conditions

Orbital forcing is prescribed at present-day values, which may be a limitation. However, the De Vleeschouwer et al. (2014) study, considered the atmospheric circulation for a number of orbital forcing values, and chose a best fit obliquity of 23.5° (close to the present-day value). However, future studies could consider the coupled climate under different orbital forcing since these changes are one hypothesis for the cause of changing Late Devonian climate and the F–F extinction (De Vleeschouwer et al., 2012).

Atmospheric pCO_2 was also prescribed at the same level as De Vleeschouwer et al. (2014) (2180 ppm) for consistency; however, recent Phanerozoic atmospheric composition modelling suggests this was potentially slightly lower (Foster et al., 2017). Thus, an additional Late Devonian climate simulation was run under a significantly lower pCO_2 level of 370 ppm (close to the present-day level). The resulting climate is inconsistent with the geological record, with sea-ice extending to latitudes of 45° in both the northern and Southern Hemispheres. Sea-ice thickness is greatest in the Northern Hemisphere, reaching over 10 m thick over much of the high latitudes. This scenario is unlikely since there is no evidence of ice shelves in the Late Devonian Southern Hemisphere until the end Devonian, and before the F–F, reef coral is recorded at latitudes as far polewards as 50° in both hemispheres.

5.7.3 Ocean Component

Some uncertainties discussed regarding the OGCM still exist with the CGCM setup. The Late Devonian bathymetry is consistent between models and is once again a logical 'best guess' bathymetry. Continent configuration is based on Blakey (2018) reconstructions although other reconstructions exist which could be tested to determine sensitivity to continent outlines. The bathymetry includes a continental slope by increasing the depth by 1000 m per grid cell away from the continent until a maximum depth of 5000 m is reached. The deep ocean is flat with the exception of a ridge in the Northern Hemisphere where there are no meridional boundaries. Simulations with varying Northern Hemisphere ridge heights and seafloor ridges within all basins were conducted, and it was found this had little effect on the global overturning circulation; therefore it was decided the bathymetry used was the most conservative approach.

Diapycnal diffusivity is uniform across the ocean, although results of the OGCM simulations with spatially variable diapycnal diffusivity suggest that, without changing total energy available, there is little effect on the general ocean circulation. Implementing spatially varying diffusivities introduces further uncertainty, thus it was decided to use uniform diapycnal diffusivity in the CGCM run.

Similar to the OGCM the biogeochemistry package includes uncertainties in the initial concentration of tracers.

The biogeochemistry component could be considerably improved. No nutrient fluxes from the continent riverine input are considered. Recent global mapping of Late Devonian lithic types and environments by Golonka (2020) includes locations of major river and delta sediment, and so future studies could include mapping of major river input to the ocean which would promote primary production.

5.8 Summary

This chapter highlights the importance of using a coupled atmosphere-ocean-sea-ice model to consider palaeoclimates. The De Vleeschouwer et al. (2014) study imposed an ocean heat flux explicitly designed to match a fairly low meridional temperature gradient. Comparing the ASGCM model and CGCM highlight the ocean's importance and the CGCM results suggest that ocean heat transports do help reduce the gradient. Similar to the OGCM results presented in chapter 3, the CGCM experiments simulate two ocean states which show similarities to the OGCM, though with slight differences; a partly-ventilated state is equivalent to the OGCM unventilated state, but a deep subtropical-midlatitude circulation exists. There is also a ventilated state where deep convective mixing is present in the Northern Hemisphere, and the resulting deep overturning circulation extends to the midlatitudes of the Southern Hemisphere. The methods of transition between states are similar between the OGCM and CGCM experiments, but the CGCM does not oscillate between states due to important air-sea feedbacks, and we in fact suggest that this partly-ventilated state is part of the long-term spin-up of the model. However, further investigation by continuing to run the CGCM or perturbing this ventilated state could help understand this further.

The CGCM ventilated ocean state supports theories of deep ocean anoxia, and improvements in biogeochemical modelling will aid further understanding of the potential for shallow water anoxia in the Paleo Tethys and Rheic Ocean. The experiment also gives insight into the climate which animals such as tetrapods evolved within, and the study suggests movement onto land in warm, monsoonal climates, subject to intense seasonal rains followed by a dryer period. This is with the exception of the polar tetrapods recently identified in the geological record which would be living within a wet, mild coastal climate which rarely reached below 0 °C.

Chapter 6

Conclusions and Future Work

6.1 Conclusions

This thesis has presented results of various GCM simulations for the Late Devonian ocean, atmosphere, biogeochemistry and sea-ice to examine and explain the climate of the Late Devonian and the link to conditions in which animals lived, terrestrial vegetation evolved, and multiple pulses of extinction occurred. Three key stages were employed; (1), use De Vleeschouwer et al. (2014) Late Devonian atmospheric slab ocean model results to force an ocean only configuration of the MITgcm; (2), simulate the Late Devonian atmospheric circulation using the MITgcm intermediate complexity atmospheric slab ocean model and make comparisons to the De Vleeschouwer et al. (2014) study; (3), couple the Late Devonian MITgcm atmosphere and ocean components. Separating the project into these stages has been insightful and allowed us to make comparisons between the various approaches to understand deep-time palaeoclimates further.

In chapter 3, we present the OGCM results. Chapter 4 considers the impact of spatial variations in tidally-induced ocean diffusivity. The ASGCM and CGCM simulations are discussed in chapter 5. We then explore the key differences between each Late Devonian simulation in chapter 5. This proves an important step and provides a greater understanding of the limitations of each method when considering palaeoclimate modelling. The key results presented in this thesis include:

1. When simulating the ocean circulation forced by De Vleeschouwer et al. (2014) atmospheric surface conditions (i.e. the ocean circulation in the OGCM) the ocean oscillated between two states: (1) an unventilated, strongly stratified state, where the deep ocean is isolated from the surface; and (2) a ventilated state with a strong, deep global overturning circulation.

2. The biogeochemistry simulated in the OGCM shows the deep ocean does not receive surface refreshment of O_2 during the unventilated phase, potentially allowing the deep ocean to become anoxic.

3. The transition between states in the OGCM shows similarities to D-O cycles and the dynamics which could have led to oscillatory behaviour in the Late Devonian ocean are as follows: (1) a fresh surface layer at high northern latitudes restricts incoming warm subsurface water from coming into contact with the atmosphere, causing both gradual warming of the subsurface reservoir and weakening of stratification; (2) transition towards a ventilated phase caused by a reduced vertical density gradient as the heat content increases in the subsurface and the stratification weakens to the point of collapse; (3) a ventilated phase where deep water is formed in the high latitudes of the Northern Hemisphere, resulting in a deep global overturning circulation; (4) gradual return to an unventilated phase caused by a gradual decrease in convective mixing and re-accumulation of a fresh surface layer, and (5) return to a well stratified ocean with cold fresh surface and warm sub surface.

4. Allowing diapycnal diffusivity to vary spatially instead of using a uniform value alters the timescale of oscillation between the OGCM unventilated and ventilated states.

5. Implementing a spatially variable diapycnal diffusivity based on simulated Late Devonian tidal energy dissipation rates changes the timescale of oscillation. However, the total energy input is constant between the OGCM and OGCMmix simulations, and the tidal dissipation estimates are based on a model that does not include

interior ocean bathymetry, mixing away from the coastlines is strongly dependent on the very low background diffusivity. Including this form of spatially variable mixing, therefore introduces further uncertainties and questions, and for comparison with other studies, we decided to proceed with uniform diffusivity.

6. In a warm climate, if there are no meridional boundaries at high latitudes, weak wind stress, and precipitation exceeding evaporation, this leads to a weak and shallow ocean overturning circulation; the mechanical wind energy is not strong enough to mix through the stratification, and a fresh layer builds on the surface. If the surface layer can be mixed away, a buoyancy driven deep overturning circulation can be achieved. Therefore, the deep circulation is dependent on both the mechanical wind energy input and evaporation-precipitation in a warm climate.

7. Comparisons of the Late Devonian MITgcm atmospheric slab ocean model (AS-GCM) and the De Vleeschouwer et al. (2014) study show significant differences in the simulated atmospheric circulation. Atmospheric slab ocean models are notorious for large equator-pole temperature gradients, but the HadSM3 meridional gradient is shallower than the MITgcm model since the HadSM3 model imposed an artificial ocean heat flux designed to produce a low equator-pole gradient. It is nevertheless difficult to explain the extremely weak wind simulated by the HadSM3 model in the De Vleeschouwer study, and the MITgcm atmosphere simulates stronger wind with a similar structure and strength to the present-day.

8. Coupling of the atmosphere and ocean has proven essential. In terms of the ocean circulation, coupling with an intermediate complexity atmosphere removes uncertainty in the atmospheric surface forcing applied to an ocean only model, and considers important air-sea feedbacks. The impact of air-sea feedbacks on the atmospheric circulation is significant; the ocean is shown to play a key role in transporting heat polewards and reducing the meridional temperature gradient. Through more realistic simulation of the meridional temperature gradient, the general circulation of the atmosphere and the climate are significantly different.

9. Similar to the OGCM, the CGCM simulates two states of ocean circulation: (1) a partly-ventilated ocean state, where the Northern Hemisphere high latitudes is strongly stratified but weak Northern Hemisphere circulations nevertheless exists in the subtropics-midlatitudes, reaching the deep ocean; and (2) a ventilated state during which the Northern Hemisphere high latitudes is well-mixed and a strong deep overturning circulation exists with deep water formation in the Northern Hemisphere mid-high latitudes, and upwelling in Southern Hemisphere mid-latitudes.

10. The transition between unventilated/partly-ventilated and ventilated states in the OGCM and CGCM is similar; subsurface northward transport of warm water reduces the density gradient to the point of collapse, at which point the fresh surface layer is mixed and the deep ocean is ventilated. However, this process is slower in the CGCM, and air-sea interactions mean the vertical density gradient is reduced through both northward transport of warm subsurface water and reducing freshwater supply to the surface, gradually increasing surface salinity.

11. The CGCM remains in the ventilated state for the remainder of the model's run-time (11 500 years), and the results suggest the climate would stay in this state unless the Southern Hemisphere deep ocean also became locally ventilated. The wind stress is relatively weak in the high Northern Hemisphere and does not change between ocean states; air-sea feedbacks change the evaporation and precipitation over time which maintains Northern Hemisphere high latitude ventilation, unlike in the OGCM.

Comparisons between the different model results highlight the importance of using a coupled atmosphere-ocean-sea-ice model to simulate deep-time palaeoclimates. In chapter 5, we explored the results of the CGCM further, considering the results in comparison to the Late Devonian geological record. This is a powerful step in verifying the CGCM results, as well as aiding further understanding of unknown/controversial aspects of the Late Devonian. Key impacts and insights from the CGCM in terms of Late Devonian evolution and extinction events include:

1. The deep (below 2800 m) ocean of the CGCM in the partly-ventilated state is anoxic globally. Subsequently, during the transition to the ventilated state the deep Panthalassa Ocean is supplied with oxygenated water, and upwelling of dysoxic water occurs on the eastern equatorial Panthalassa boundary. This corresponds with locations of Late Devonian anoxic sediments and huge reef extinctions.

2. Simulated anoxic waters in the Paleo Tethys and Rheic oceans upwell to the surface on the northern boundaries of these basins. This corresponds to regions with sediments interpreted as anoxic in the Late Devonian geological record. If land-ocean nutrient fluxes were included in the biogeochemistry and resulted in increased surface biological productivity in these well stratified basins with the weak shallow circulation simulated, it is possible a combination of PZE and upwelling of anoxic deep water would make the ocean surface conditions for species uninhabitable and provide a potential 'kill mechanism' for the F–F extinction.

3. Lithic indicators of climate such as coals, evaporites and reefs, when mapped against simulated evaporation minus precipitation, and SST correlate with simulated climate conditions.

4. Although this study focuses on the Late Devonian, the simulated westward equatorial surface ocean current would be similar in the Middle Devonian, supporting the hypothesis that stem-tetrapods migrated towards Laurussia with the help of the surface ocean currents sweeping them westward.

5. The results of the CGCM suggest the majority of known Late Devonian tetrapod fossils were living within monsoonal regions, subject to intense rainy seasons in warm tropical climates followed by a less-wet/dry season.

6. The exception to Late Devonian tetrapods living within tropical monsoon climates is two tetrapod fossils observed in the higher latitudes of the Southern Hemisphere. These would be subject to similar climate conditions as the present-day mid-latitudes, with mild summers and cold/mild wet winters. The proximity to the coastline would ensure they did not get too cold, but in general the Late Devonian western Gondwana high latitudes do not fall below 0 °C.

7. The simulated poor poleward heat transport to the Southern Hemisphere high latitudes causes very gradual cooling of the region. The ocean is not ventilated at the surface here and, similar to the Northern Hemisphere, partly-ventilated state, deep convective mixing is not possible due to a fresh surface layer. The gradual cooling is in agreement with the geological record as the climate transitioned towards glaciation at the end of the Devonian. The Southern Hemisphere oceans could also become locally ventilated similar to the Northern Hemisphere, and potentially cause significant changes in ocean circulation and climate.

Similar to Feulner (2009), this study has highlighted the benefits and capabilities of GCMs for gaining insights into potential causes of extinction and the climate in which these events took place. A number of modelling requirements are outlined which both echo and build upon the points outlined by Feulner (2009) to achieve when modelling deep-time palaeoclimates, these include:

- At least an intermediate complexity atmospheric model coupled to a three-dimensional dynamic ocean and sea-ice model.
- Realistic continental outlines and topography on land for the time considered.
- Approximations of continental vegetation.
- A realistic pCO_2 value.
- Ocean biogeochemistry, modelling at least O_2, PO_4, biological productivity and DIC, preferably with land-ocean nutrient fluxes included.
- If possible, a 'best-guess' seafloor bathymetry should be implemented. Although, if deep ocean bathymetry is unknown, the logical positioning of some form of seafloor bathymetry is recommended (e.g. a small ridge in the region of no meridional boundaries).

- Spatially variable diapycnal mixing calculated from maps of tidal energy dissipation, produced using models with realistic seafloor bathymetry and continental slope. However, this should be implemented in secondary versions of the model, and compared to results of an equivalent model, with uniform diapycnal diffusivity, to diagnose the effects of a spatially variable diapycnal mixing on the ocean circulation.

- Use of a grid which allows modelling of ocean circulation in polar regions, such as the cube-sphere grid used here. The resolution of the model should be at least intermediate resolution of between 2° to 3°.

6.2 Future Work

This thesis has demonstrated the capabilities of climate models to aid greater understanding of Late Devonian climate, mass extinction and evolution. However, considering this time in Earth's history using GCMs has highlighted further considerations and potential avenues of research which would lead to greater insight into the causes of the F–F extinction and the transition towards an icehouse climate at the end of the Devonian. First, a general improvement to the coupled atmosphere-ocean setup would be to improve the land precipitation runoff mapping to direct precipitation through regions interpreted as fluvial by Golonka (2020). This may alter the overturning circulation as large amounts of less dense fresh water flow into restricted basins such as the Rheic and Paleo Tethys. Following this, land-ocean nutrient fluxes could be incorporated into the biogeochemistry component, which would improve the representation of surface biological productivity. Increasing the vertical resolution in the atmosphere would also more accurately represent clouds and radiation, which may have a significant impact on climate.

Including a spatially variable diapycnal diffusivity was shown to impact the global overturning circulation. However, barotropic tidal simulations with a realistic seafloor bathymetry are required to investigate further the impacts of spatially variable diapycnal diffusivity due to tidal energy dissipation on global overturning circulation. A team at the University

of Oxford are currently exploring how continental outlines and bathymetry affect the tides; once complete the resulting tidal energy dissipation estimates could be applied to a coupled atmosphere-ocean model to determine how the global overturning circulation changes under different spatially variable mixing coefficients.

Initially, while setting up the OGCM, different bathymetries were used to test the sensitivity of the large scale circulation to bathymetry. This included; changing the gradient of the continental slope, adding ridges in the interior ocean, and changing the height of the Northern Hemisphere high latitude meridional ridge. The preliminary results suggested this had little effect on the large scale ocean circulation. However, further testing could also use a more realistic seafloor bathymetry in either the OGCM or CGCM to further test sensitivities.

Results of the OGCM show that the ocean oscillated between unventilated and ventilated states. However, in the CGCM the ocean transitions from a partly-ventilated to a ventilated state, and stays in this state for the remaining 11 500 years. The results suggest this state would continue, and the partly-ventilated state is part of a long-term model spin-up. However, during the Late Devonian multiple pulses in ocean anoxia are recorded (Bond and Grasby, 2017), which are thought to represent perturbations in the climate, possibly due to volcanic activity in Viluy Traps and the PDD rift system of Siberia. LIP volcanism causes massive outgassing of CO_2 and SO_2, which would subsequently warm the climate (Macdonald et al., 2019; Percival et al., 2019). The current version of the CGCM does not vary pCO_2 over the course of the model simulation, and changes in ocean state are due solely to internal atmosphere-ocean dynamics. Further investigations and simulations perturbing the CGCM ventilated state with increased pCO_2 could provide insights into whether volcanism could force the ocean back towards the partly-ventilated state, and if so the quantities of magma extrusion and CO_2 outgassing required.

A second well regarded hypothesis for cycles in anoxic sediments and climate change is the astronomical forcing of the Late Devonian. The current model setup includes present-day astronomical forcing but could consider the Late Devonian coupled climate under different astronomical forcing to understand how this might affect the Late Devonian climate.

In the ventilated state the Southern Hemisphere is still strongly stratified with weak circulation and a fresh surface layer. The subsurface is warm and saline. The surface layer temperature is decreasing slightly. If the current CGCM simulation was continued, potentially the Southern Hemisphere high latitudes could become locally ventilated, and it would be interesting to see how the ocean circulation adjusts if there was a deep overturning circulation originating from the Southern Hemisphere. The model could also be perturbed in this region to understand what it would take to achieve Southern Hemisphere high latitude ventilation.

Finally, recent simulations of pCO_2 throughout the Palaeozoic suggest the Late Devonian atmospheric value was slightly lower than the 2200 ppm. Although we have also tested the climate using a minimum estimate of Late Devonian pCO_2, it is important to simulate the climate under a broader range, e.g. potentially a midpoint of the two simulations presented here. Further work would constrain uncertainties in the Late Devonian climate simulations, and potentially lead to an even greater understanding of extinction events and why the climate transitioned towards an icehouse climate at the end of the Devonian.

The Late Devonian has had little attention from the climate modelling community, despite being an important time in Earth's history for widespread evolution of land plants and the first land animals, tetrapods, all coexisting alongside multiple pulses in extinction. This thesis makes important steps to further considering the climate in which these major events in Earth's history took place, as well as highlighting gaps in the Late Devonian research community's knowledge which require further investigation.

References

Adcroft, A., Campin, J.-M., Hill, C. and Marshall, J. (2004), 'Implementation of an atmosphere–ocean general circulation model on the expanded spherical cube', *Monthly Weather Review* **132**(12), 2845–2863.

Ahlberg, P. E. (2018), 'Follow the footprints and mind the gaps: a new look at the origin of tetrapods', *Earth and Environmental Science Transactions of the Royal Society of Edinburgh* **109**(1-2), 115–137.

Algeo, T. J., Berner, R. A., Maynard, J. B. and Scheckler, S. E. (1995), 'Late devonian oceanic anoxic events and biotic crises:'rooted' in the evolution of vascular land plants', *GSA today* **5**(3), 45–66.

Algeo, T. J. and Scheckler, S. E. (1998), 'Terrestrial-marine teleconnections in the devonian: links between the evolution of land plants, weathering processes, and marine anoxic events', *Philosophical Transactions of the Royal Society of London B: Biological Sciences* **353**(1365), 113–130.

Balbus, S. A. (2014), 'Dynamical, biological and anthropic consequences of equal lunar and solar angular radii', *Proceedings of the Royal Society A: Mathematical, Physical and Engineering Sciences* **470**(2168).

Balter, V., Renaud, S., Girard, C. and Joachimski, M. M. (2008), 'Record of climate-driven morphological changes in 376 Ma devonian fossils', *Geology* **36**(11), 907.

Bambach, R. K., Knoll, A. H. and Wang, S. C. (2004), 'Origination, extinction, and mass depletions of marine diversity', *Paleobiology* **30**(4), 522–542.

Barash, M. S. (2016), 'Causes of the great mass extinction of marine organisms in the Late Devonian', *Oceanology* **56**(6), 863–875.

Baringer, M. O. and Price, J. F. (1997), 'Mixing and Spreading of the Mediterranean Outflow', *Journal of Physical Oceanography* **27**(8), 1654–1677.

Barreiro, M., Cherchi, A. and Masina, S. (2011), 'Climate sensitivity to changes in ocean heat transport', *Journal of Climate* **24**(19), 5015–5030.

Becker, R., Gradstein, F. and Hammer, O. (2012), The Devonian Period, *in* 'The Geologic Time Scale', Elsevier, pp. 559–601.

Berner, R. A. (2006), 'GEOCARBSULF: A combined model for Phanerozoic atmospheric O_2 and CO_2', *Geochimica et Cosmochimica Acta* **70**(23), 5653–5664.

Bice, K. L., Scotese, C. R., Seidov, D. and Barron, E. J. (2000), 'Quantifying the role of geographic change in cenozoic ocean heat transport using uncoupled atmosphere and ocean models', *Palaeogeography, Palaeoclimatology, Palaeoecology* **161**(3-4), 295–310.

Bjerknes, J. (1969), 'Atmospheric teleconnections from the equatorial Pacific', *Mon. Wea. Rev* **97**(3), 163–172.

Blakey, R. (2018), 'Global paleogeography'.

Blieck, A., Clement, G., Blom, H., Lelievre, H., Luksevics, E., Streel, M., Thorez, J. and Young, G. C. (2007), 'The biostratigraphical and palaeogeographical framework of the earliest diversification of tetrapods (Late Devonian)', *Geological Society, London, Special Publications* **278**(1), 219–235.

Boccaletti, G. (2005), 'The vertical structure of ocean heat transport', *Geophysical Research Letters* **32**(10).

Bond, D. P. and Grasby, S. E. (2017), 'On the causes of mass extinctions', *Palaeogeography, Palaeoclimatology, Palaeoecology* **478**, 3–29.

Bond, D., Wignall, P. B. and Racki, G. (2004), 'Extent and duration of marine anoxia during the Frasnian–Famennian (Late Devonian) mass extinction in Poland, Germany, Austria and France', *Geological Magazine* **141**(2), 173–193.

Braconnot, P., Otto-Bliesner, B., Harrison, S., Joussaume, S., Peterchmitt, J.-Y., Abe-Ouchi, A., Crucifix, M., Driesschaert, E., Fichefet, T., Hewitt, C. D., Kageyama, M., Kitoh, A., Loutre, M.-F., Marti, O., Merkel, U., Ramstein, G., Valdes, P., Weber, L., Yu, Y. and Zhao, Y. (2007), 'Results of PMIP2 coupled simulations of the Mid-Holocene and Last Glacial Maximum Part 2: feedbacks with emphasis on the location of the ITCZ and mid- and high latitudes heat budget', *Climate of the Past* **3**(2), 279–296.

Brandt, P., Funk, A., Tantet, A., Johns, W. E. and Fischer, J. (2014), 'The Equatorial Undercurrent in the central Atlantic and its relation to tropical Atlantic variability', *Climate Dynamics* **43**(11), 2985–2997.

Broccoli, A. J., Dahl, K. A. and Stouffer, R. J. (2006), 'Response of the ITCZ to northern hemisphere cooling', *Geophysical Research Letters* **33**(1).

Brugger, J., Hofmann, M., Petri, S. and Feulner, G. (2019), 'On the sensitivity of the devonian climate to continental configuration, vegetation cover, orbital configuration, CO 2 concentration, and insolation', *Paleoceanography and Paleoclimatology* **34**(8), 1375–1398.

Brunetti, M. and Vérard, C. (2017), 'How to reduce long-term drift in present-day and deep-time simulations?', *Climate Dynamics* .

Brunetti, M., Vérard, C. and Baumgartner, P. O. (2015), 'Modeling the Middle Jurassic ocean circulation', *Journal of Palaeogeography* **4**(4), 371–383.

Buggisch, W. (1991), 'The global Frasnian-Famennian» Kellwasser Event «', *Geologische Rundschau* **80**(1), 49–72.

Carmichael, S. K., Waters, J. A., Konigshof, P., Suttner, T. J. and Kido, E. (2019), 'Paleogeography and paleoenvironments of the Late Devonian Kellwasser event: A review of its sedimentological and geochemical expression', *Global and Planetary Change* **183**, 102984.

Carmichael, S. K., Waters, J. A., Suttner, T. J., Kido, E. and DeReuil, A. A. (2014), 'A new model for the kellwasser anoxia events (late devonian): Shallow water anoxia in an open oceanic setting in the central asian orogenic belt', *Palaeogeography, Palaeoclimatology, Palaeoecology* **399**, 394–403.

Ceppi, P. and Hartmann, D. L. (2013), 'On the Speed of the Eddy-Driven Jet and the Width of the Hadley Cell in the Southern Hemisphere', *Journal of Climate* **26**(10), 3450–3465.

Chen, D., Wang, J., Racki, G., Li, H., Wang, C., Ma, X. and Whalen, M. T. (2013), 'Large sulphur isotopic perturbations and oceanic changes during the Frasnian–Famennian transition of the Late Devonian', *Journal of the Geological Society* **170**(3), 465–476.

Chiang, J. C. (2009), 'The tropics in paleoclimate', *Annual Review of Earth and Planetary Sciences* **37**(1), 263–297.

Chiang, J. C. H., Biasutti, M. and Battisti, D. S. (2003), 'Sensitivity of the atlantic intertropical convergence zone to last glacial maximum boundary conditions', *Paleoceanography* **18**(4), n/a–n/a.

Clack, J. A. (2012), *Setting the Scene: The Devonian World*, 2 edn, Indiana University Press, chapter 4, pp. 101–141.

Copper, P. (1986), 'Frasnian/Famennian mass extinction and cold-water oceans', *Geology* **14**(10), 835.

Copper, P. (2002), 'Reef development at the Frasnian/Famennian mass extinction boundary', *Palaeogeography, Palaeoclimatology, Palaeoecology* **181**(1-3), 27–65.

Crasquin, S. and Horne, D. J. (2018), 'The palaeopsychrosphere in the Devonian', *Lethaia* **51**(4), 547–563.

Dansgaard, W., Johnsen, S. J., Clausen, H. B., Dahl-Jensen, D., Gundestrup, N. S., Hammer, C. U., Hvidberg, C. S., Steffensen, J. P., Sveinbjornsdottir, A. E., Jouzel, J. and Bond, G. (1993), 'Evidence for general instability of past climate from a 250-kyr ice-core record', *Nature* **364**(6434), 218–220.

Davies, N. S. and Gibling, M. R. (2010), 'Paleozoic vegetation and the Siluro-Devonian rise of fluvial lateral accretion sets', *Geology* **38**(1), 51–54.

De Vleeschouwer, D., Crucifix, M., Bounceur, N. and Claeys, P. (2014), 'The impact of astronomical forcing on the Late Devonian greenhouse climate', *Global Planet. Change* **120**, 65–80.

De Vleeschouwer, D., Rakociński, M., Racki, G., Bond, D. P., Sobień, K. and Claeys, P. (2013), 'The astronomical rhythm of Late-Devonian climate change (Kowala section, Holy Cross Mountains, Poland)', *Earth and Planetary Science Letters* **365**, 25–37.

De Vleeschouwer, D., Silva, A. C. D., Boulvain, F., Crucifix, M. and Claeys, P. (2012), 'Precessional and half-precessional climate forcing of Mid-Devonian monsoon-like dynamics', *Climate of the Past* **8**(1), 337–351.

De Vleeschouwer, D., Silva, A.-C. D., Sinnesael, M., Chen, D., Day, J. E., Whalen, M. T., Guo, Z. and Claeys, P. (2017), 'Timing and pacing of the Late Devonian mass extinction event regulated by eccentricity and obliquity', *Nature Communications* **8**(1).

Dokken, T. M., Nisancioglu, K. H., Li, C., Battisti, D. S. and Kissel, C. (2013), 'Dansgaard-Oeschger cycles: Interactions between ocean and sea ice intrinsic to the Nordic seas', *Paleoceanography* **28**(3), 491–502.

Domeier, M. and Torsvik, T. H. (2014), 'Plate tectonics in the late Paleozoic', *Geoscience Frontiers* **5**(3), 303–350.

Donnadieu, Y., Pierrehumbert, R., Jacob, R. and Fluteau, F. (2006), 'Modelling the primary control of paleogeography on Cretaceous climate', *Earth and Planetary Science Letters* **248**(1-2), 426–437.

Döös, K., Nycander, J. and Coward, A. C. (2008), 'Lagrangian decomposition of the deacon cell', *Journal of Geophysical Research* **113**(C7).

Döös, K. and Webb, D. J. (1994), 'The Deacon Cell and the Other Meridional Cells of the Southern Ocean', *Journal of Physical Oceanography* **24**(2), 429–442.

Dopieralska, J. (2009), 'Reconstructing seawater circulation on the Moroccan shelf of Gondwana during the Late Devonian: Evidence from Nd isotope composition of conodonts', *Geochemistry, Geophysics, Geosystems* **10**(3).

Drenkard, E. J. and Karnauskas, K. B. (2014), 'Strengthening of the Pacific Equatorial Undercurrent in the SODA Reanalysis: Mechanisms, Ocean Dynamics, and Implications', *Journal of Climate* **27**(6), 2405–2416.

Dufour, C. O., Morrison, A. K., Griffies, S. M., Frenger, I., Zanowski, H. and Winton, M. (2017), 'Preconditioning of the Weddell Sea Polynya by the Ocean Mesoscale and Dense Water Overflows', *Journal of Climate* **30**(19), 7719–7737.

Dutkiewicz, S., Follows, M. J. and Parekh, P. (2005), 'Interactions of the iron and phosphorus cycles: A three-dimensional model study', *Global Biogeochemical Cycles* **19**(1).

Egbert, G. D. and Ray, R. D. (2001), 'Estimates of m2tidal energy dissipation from TOPEX/poseidon altimeter data', *Journal of Geophysical Research: Oceans* **106**(C10), 22475–22502.

Eldevik, T., Risebrobakken, B., Bjune, A. E., Andersson, C., Birks, H. J. B., Dokken, T. M., Drange, H., Glessmer, M. S., Li, C., Nilsen, J. E. Ø., Otterå, O. H., Richter, K. and Skagseth, Ø. (2014), 'A brief history of climate – the northern seas from the last glacial maximum to global warming', *Quaternary Science Reviews* **106**, 225–246.

Eyles, N. (2008), 'Glacio-epochs and the supercontinent cycle after ∼3.0 ga: Tectonic boundary conditions for glaciation', *Palaeogeography, Palaeoclimatology, Palaeoecology* **258**(1-2), 89–129.

Ferrari, R. and Ferreira, D. (2011), 'What processes drive the ocean heat transport?', *Ocean Modelling* **38**(3-4), 171–186.

Ferrari, R., Mashayek, A., McDougall, T. J., Nikurashin, M. and Campin, J.-M. (2016), 'Turning ocean mixing upside down', *Journal of Physical Oceanography* **46**(7), 2239–2261.

Ferreira, D. and Marshall, J. (2015), 'Freshwater transport in the coupled ocean-atmosphere system: a passive ocean', *Ocean Dynamics* **65**(7), 1029–1036.

Feulner, G. (2009), 'Climate modelling of mass-extinction events: a review', *International Journal of Astrobiology* **8**(03), 207.

Foster, G. L., Royer, D. L. and Lunt, D. J. (2017), 'Future climate forcing potentially without precedent in the last 420 million years', *Nature Communications* **8**, 14845.

Freeman, E., Skinner, L., Tisserand, A., Dokken, T., Timmermann, A., Menviel, L. and Friedrich, T. (2015), 'An atlantic–pacific ventilation seesaw across the last deglaciation', *Earth and Planetary Science Letters* **424**, 237–244.

Gent, P. R. and McWilliams, J. C. (1990), 'Isopycnal mixing in ocean circulation models', *Journal of Physical Oceanography* **20**(1), 150–155.

Gent, P. R., Willebrand, J., McDougall, T. J. and McWilliams, J. C. (1995), 'Parameterizing eddy-induced tracer transports in ocean circulation models', *Journal of Physical Oceanography* **25**(4), 463–474.

Gess, R. and Ahlberg, P. E. (2018), 'A tetrapod fauna from within the Devonian Antarctic Circle', *Science* **360**(6393), 1120–1124.

Gill, A. E. (1982), *Atmosphere-ocean dynamics*, Elsevier.

Golonka, J. (2020), 'Late devonian paleogeography in the framework of global plate tectonics', *Global and Planetary Change* **186**, 103129.

Gough, D. O. (1981), Solar interior structure and luminosity variations, *in* 'Physics of Solar Variations', Springer Netherlands, pp. 21–34.

Greb, S. F., DiMichele, W. A. and Gastaldo, R. A. (2006), Evolution and importance of wetlands in earth history, *in* 'Wetlands through Time', Geological Society of America.

Green, B. and Marshall, J. (2017), 'Coupling of trade winds with ocean circulation damps ITCZ shifts', *Journal of Climate* **30**(12), 4395–4411.

Green, J. A. M., Green, C. L., Bigg, G. R., Rippeth, T. P., Scourse, J. D. and Uehara, K. (2009), 'Tidal mixing and the meridional overturning circulation from the last glacial maximum', *Geophysical Research Letters* **36**(15).

Green, J., Huber, M., Waltham, D., Buzan, J. and Wells, M. (2017), 'Explicitly modelled deep-time tidal dissipation and its implication for lunar history', *Earth and Planetary Science Letters* **461**, 46–53.

Hansen, B. and Østerhus, S. (2000), 'North Atlantic–Nordic Seas exchanges', *Progress in Oceanography* **45**(2), 109–208.

Hansen, J., Russell, G., Rind, D., Stone, P., Lacis, A., Lebedeff, S., Ruedy, R. and Travis, L. (1983), 'Efficient three-dimensional global models for climate studies: Models i and II', *Monthly Weather Review* **111**(4), 609–662.

Hartmann, D. L. (2015), *Global physical climatology*, Vol. 103, Newnes.

Hu, Y., Huang, H. and Zhou, C. (2018), 'Widening and weakening of the Hadley circulation under global warming', *Science Bulletin* **63**(10), 640–644.

Hu, Y., Li, D. and Liu, J. (2007), 'Abrupt seasonal variation of the ITCZ and the Hadley circulation', *Geophysical Research Letters* **34**(18).

Huang, C., Joachimski, M. M. and Gong, Y. (2018), 'Did climate changes trigger the Late Devonian Kellwasser Crisis? Evidence from a high-resolution conodont δ18OPO4 record from South China', *Earth and Planetary Science Letters* **495**, 174–184.

Huang, R. X. (2010), *Ocean circulation: wind-driven and thermohaline processes*, Cambridge University Press.

Huber, M. and Sloan, L. C. (2001), 'Heat transport, deep waters, and thermal gradients: Coupled simulation of an Eocene greenhouse climate', *Geophysical Research Letters* **28**(18), 3481–3484.

Hüneke, H. (2006), 'Erosion and deposition from bottom currents during the Givetian and Frasnian: Response to intensified oceanic circulation between Gondwana and Laurussia', *Palaeogeography, Palaeoclimatology, Palaeoecology* **234**(2-4), 146–167.

Isaacson, P., Díaz-Martínez, E., Grader, G., Kalvoda, J., Babek, O. and Devuyst, F. (2008), 'Late Devonian–earliest Mississippian glaciation in Gondwanaland and its biogeographic consequences', *Palaeogeography, Palaeoclimatology, Palaeoecology* **268**(3-4), 126–142.

Joachimski, M., Breisig, S., Buggisch, W., Talent, J., Mawson, R., Gereke, M., Morrow, J., Day, J. and Weddige, K. (2009), 'Devonian climate and reef evolution: Insights from oxygen isotopes in apatite', *Earth and Planetary Science Letters* **284**(3-4), 599–609.

Joachimski, M. M., Ostertag-Henning, C., Pancost, R. D., Strauss, H., Freeman, K. H., Littke, R., Damste, J. S. S. and Racki, G. (2001), 'Water column anoxia, enhanced productivity and concomitant changes in δ 13 c and δ 34 s across the frasnian–famennian boundary (kowala–holy cross mountains/poland)', *Chemical Geology* **175**(1), 109–131.

Johnson, G. C., Sloyan, B. M., Kessler, W. S. and McTaggart, K. E. (2002), 'Direct measurements of upper ocean currents and water properties across the tropical Pacific during the 1990s', *Progress in Oceanography* **52**(1), 31–61.

Kageyama, M., Valdes, P. J., Ramstein, G., Hewitt, C. and Wyputta, U. (1999), 'Northern Hemisphere Storm Tracks in Present Day and Last Glacial Maximum Climate Simulations: A Comparison of the European PMIP Models', *Journal of Climate* **12**(3), 742–760.

Kaiho, K., Yatsu, S., Oba, M., Gorjan, P., Casier, J.-G. and Ikeda, M. (2013), 'A forest fire and soil erosion event during the Late Devonian mass extinction', *Palaeogeography, Palaeoclimatology, Palaeoecology* **392**, 272–280.

Kang, S. M. and Polvani, L. M. (2011), 'The Interannual Relationship between the Latitude of the Eddy-Driven Jet and the Edge of the Hadley Cell', *Journal of Climate* **24**(2), 563–568.

Katz, E. (1977), 'Zonal pressure-gradient along equatorial Atlantic', *Journal of Marine Research* **35**(2), 293–307.

Kump, L. R. and Pollard, D. (2008), 'Amplification of Cretaceous Warmth by Biological Cloud Feedbacks', *Science* **320**(5873), 195–195.

Lakin, J. A., Marshall, J. E. A., Troth, I. and Harding, I. C. (2016), 'Greenhouse to icehouse: a biostratigraphic review of latest Devonian–Mississippian glaciations and their global effects', *Geological Society, London, Special Publications* **423**(1), 439–464.

Lauderdale, J. M., Garabato, A. C. N., Oliver, K. I. C., Follows, M. J. and Williams, R. G. (2013), 'Wind-driven changes in southern ocean residual circulation, ocean carbon reservoirs and atmospheric CO2', *Climate Dynamics* **41**(7-8), 2145–2164.

Laurent, L. S. and Garrett, C. (2002), 'The role of internal tides in mixing the deep ocean', *Journal of Physical Oceanography* **32**(10), 2882–2899.

Liu, J. and Luo, G. (2019), 'Intensified ocean deoxygenation during the end devonian mass extinction', *Geochemistry, Geophysics, Geosystems* **20**(12), 6187–6198.

Liu, J., Tian, J., Liu, Z., Herbert, T. D., Fedorov, A. V. and Lyle, M. (2019), 'Eastern equatorial pacific cold tongue evolution since the late miocene linked to extratropical climate', *Science Advances* **5**(4).

Lucas, S. G. (2015), 'Thinopusand a critical review of devonian tetrapod footprints', *Ichnos* **22**(3-4), 136–154.

Lumpkin, R. and Speer, K. (2007), 'Global ocean meridional overturning', *Journal of Physical Oceanography* **37**(10), 2550–2562.

Macdonald, F. A., Swanson-Hysell, N. L., Park, Y., Lisiecki, L. and Jagoutz, O. (2019), 'Arc-continent collisions in the tropics set earth's climate state', *Science* .

Marcott, S. A., Clark, P. U., Padman, L., Klinkhammer, G. P., Springer, S. R., Liu, Z., Otto-Bliesner, B. L., Carlson, A. E., Ungerer, A., Padman, J., He, F., Cheng, J. and Schmittner, A. (2011), 'Ice-shelf collapse from subsurface warming as a trigger for heinrich events', *Proceedings of the National Academy of Sciences* **108**(33), 13415–13419.

Marshall, J. (2007), 'Mean climate and variability of the atmosphere and ocean on an aquaplanet', *Journal of the Atmospheric Sciences* **64**(12), 4270–4286.

Marshall, J., Adcroft, A., Hill, C., Perelman, L., Heisey, C. et al. (1997b), 'A finite-volume, incompressible navier stokes model for studies of the ocean on parallel computers', *Journal of Geophysical Research: Oceans* **102**(C3), 5753–5766.

Marshall, J., Donohoe, A., Ferreira, D. and McGee, D. (2013), 'The ocean's role in setting the mean position of the inter-tropical convergence zone', *Climate Dynamics* **42**(7-8), 1967–1979.

Marshall, J. E. A., Astin, T. R., Brown, J. F., Mark-Kurik, E. and Lazauskiene, J. (2007), 'Recognizing the kačák event in the devonian terrestrial environment and its implications for understanding land–sea interactions', *Geological Society, London, Special Publications* **278**(1), 133–155.

Marshall, J., Hill, C., Perelman, L., Adcroft, A. et al. (1997a), 'Hydrostatic, quasi-hydrostatic, and nonhydrostatic ocean modeling', *Journal of Geophysical Research: Oceans* **102**(C3), 5733–5752.

Marshall, J. and Plumb, R. A. (2007), *Atmosphere, ocean and climate dynamics: an introductory text*, Vol. 21, Academic Press.

Marshall, J. and Speer, K. (2012), 'Closure of the meridional overturning circulation through Southern Ocean upwelling', *Nature Geoscience* **5**(3), 171–180.

Martin, J. H., Knauer, G. A., Karl, D. M. and Broenkow, W. W. (1987), 'VERTEX: carbon cycling in the northeast Pacific', *Deep Sea Research Part A. Oceanographic Research Papers* **34**(2), 267–285.

Mbengue, C. and Schneider, T. (2018), 'Linking hadley circulation and storm tracks in a conceptual model of the atmospheric energy balance', *Journal of the Atmospheric Sciences* **75**(3), 841–856.

McPhaden, M. J. and Taft, B. A. (1988), 'Dynamics of seasonal and intraseasonal variability in the eastern equatorial pacific', *Journal of Physical Oceanography* **18**(11), 1713–1732.

McWilliams, J. C. and Danabasoglu, G. (2002), 'Eulerian and eddy-induced meridional overturning circulations in the tropics', *Journal of Physical Oceanography* **32**(7), 2054–2071.

Meijers, A. J., Bindoff, N. L. and Roberts, J. L. (2007), 'On the total, mean, and eddy heat and freshwater transports in the southern hemisphere of a $1/8 \times 1/8$ global ocean model', *Journal of Physical Oceanography* **37**(2), 277–295.

Meincke, J. (1997), 'The Arctic Ocean–Nordic Seas thermohaline system', *ICES Journal of Marine Science* **54**(3), 283–299.

Meyer, K. M. and Kump, L. R. (2008), 'Oceanic euxinia in earth history: Causes and consequences', *Annual Review of Earth and Planetary Sciences* **36**(1), 251–288.

Meyers, G. (1979), 'Annual variation in the slope of the 14 C isotherm along the equator in the Pacific Ocean', *Journal of Physical Oceanography* **9**(5), 885–891.

Molteni, F. (2003), 'Atmospheric simulations using a GCM with simplified physical parametrizations. i: model climatology and variability in multi-decadal experiments', *Climate Dynamics* **20**(2), 175–191.

Moreno-Chamarro, E., Marshall, J. and Delworth, T. L. (2020), 'Linking ITCZ migrations to the AMOC and north atlantic/pacific SST decadal variability', *Journal of Climate* **33**(3), 893–905.

Munk, W. H. (1966), 'Abyssal recipes', *Deep Sea Research and Oceanographic Abstracts* **13**(4), 707–730.

Munk, W. and Wunsch, C. (1998), 'Abyssal recipes II: energetics of tidal and wind mixing', *Deep Sea Research Part I: Oceanographic Research Papers* **45**(12), 1977–2010.

Naeher, S. and Grice, K. (2015), 'Novel 1 h -pyrrole-2,5-dione (maleimide) proxies for the assessment of photic zone euxinia', *Chemical Geology* **404**, 100–109.

Narkiewicz, M. and Retallack, G. J. (2014), 'Dolomitic paleosols in the lagoonal tetrapod track-bearing succession of the Holy Cross Mountains (Middle Devonian, Poland)', *Sedimentary Geology* **299**, 74–87.

Niedźwiedzki, G., Szrek, P., Narkiewicz, K., Narkiewicz, M. and Ahlberg, P. E. (2010), 'Tetrapod trackways from the early Middle Devonian period of Poland', *Nature* **463**(7277), 43–48.

Peltier, W. R. and Vettoretti, G. (2014), 'Dansgaard-Oeschger oscillations predicted in a comprehensive model of glacial climate: A "kicked" salt oscillator in the Atlantic', *Geophysical Research Letters* **41**(20), 7306–7313.

Percival, L., Selby, D., Bond, D., Rakociński, M., Racki, G., Marynowski, L., Adatte, T., Spangenberg, J. and FÃűllmi, K. (2019), 'Pulses of enhanced continental weathering associated with multiple Late Devonian climate perturbations: Evidence from osmium-isotope compositions', *Palaeogeography, Palaeoclimatology, Palaeoecology* **524**, 240–249.

Petersen, S. V., Schrag, D. P. and Clark, P. U. (2013), 'A new mechanism for Dansgaard-Oeschger cycles', *Paleoceanography* **28**(1), 24–30.

Philander, S. G. H. (1973), 'Equatorial undercurrent: Measurements and theories', *Reviews of Geophysics* **11**(3), 513.

Philander, S. G. H. (1980), 'The equatorial undercurrent revisited', *Annual Review of Earth and Planetary Sciences* **8**(1), 191–204.

Pohl, A., Donnadieu, Y., Hir, G. L. and Ferreira, D. (2017), 'The climatic significance of Late Ordovician-early Silurian black shales', *Paleoceanography* **32**(4), 397–423.

Poulsen, C. J. and Zhou, J. (2013), 'Sensitivity of Arctic Climate Variability to Mean State: Insights from the Cretaceous', *Journal of Climate* **26**(18), 7003–7022.

Qie, W., Algeo, T. J., Luo, G. and Herrmann, A. (2019), 'Global events of the Late Paleozoic (Early Devonian to Middle Permian): A review', *Palaeogeography, Palaeoclimatology, Palaeoecology* **531**, 109259.

Qvarnström, M., Szrek, P., Ahlberg, P. E. and Niedźwiedzki, G. (2018), 'Non-marine palaeoenvironment associated to the earliest tetrapod tracks', *Scientific Reports* **8**(1).

Rasmussen, T. L. and Thomsen, E. (2004), 'The role of the North Atlantic Drift in the millennial timescale glacial climate fluctuations', *Palaeogeography, Palaeoclimatology, Palaeoecology* **210**(1), 101–116.

Redi, M. H. (1982), 'Oceanic isopycnal mixing by coordinate rotation', *Journal of Physical Oceanography* **12**(10), 1154–1158.

Retallack, G. J. (1997), 'Early forest soils and their role in devonian global change', *Science* **276**(5312), 583–585.

Richardson, P. L. (2008), 'On the history of meridional overturning circulation schematic diagrams', *Progress in Oceanography* **76**(4), 466–486.

Rojas, M., Moreno, P., Kageyama, M., Crucifix, M., Hewitt, C., Abe-Ouchi, A., Ohgaito, R., Brady, E. C. and Hope, P. (2008), 'The southern westerlies during the last glacial maximum in PMIP2 simulations', *Climate Dynamics* **32**(4), 525–548.

Sadatzki, H., Dokken, T. M., Berben, S. M. P., Muschitiello, F., Stein, R., Fahl, K., Menviel, L., Timmermann, A. and Jansen, E. (2019), 'Sea ice variability in the southern Norwegian Sea during glacial Dansgaard-Oeschger climate cycles', *Science Advances* **5**(3).

Sallan, L. C. and Coates, M. I. (2010), 'End-devonian extinction and a bottleneck in the early evolution of modern jawed vertebrates', *Proceedings of the National Academy of Sciences* **107**(22), 10131–10135.

Saltzman, M. R. (2003), 'Late paleozoic ice age: Oceanic gateway or pCO2?', *Geology* **31**(2), 151.

Schmittner, A. and Egbert, G. D. (2014), 'An improved parameterization of tidal mixing for ocean models', *Geoscientific Model Development* **7**(1), 211–224.

Schmittner, A., Green, J. A. M. and Wilmes, S.-B. (2015), 'Glacial ocean overturning intensified by tidal mixing in a global circulation model', *Geophysical Research Letters* **42**(10), 4014–4022.

Scholze, F. and Gess, R. W. (2017), 'Oldest known naiaditid bivalve from the high-latitude Late Devonian (Famennian) of South Africa offers clues to survival strategies following the Hangenberg mass extinction', *Palaeogeography, Palaeoclimatology, Palaeoecology* **471**, 31–39.

Sessford, E., Jensen, M., Tisserand, A., Muschitiello, F., Dokken, T., Nisancioglu, K. and Jansen, E. (2019), 'Consistent fluctuations in intermediate water temperature off the coast of Greenland and Norway during Dansgaard-Oeschger events', *Quaternary Science Reviews* **223**, 105887.

Silvester, J. M., Lenn, Y.-D., Polton, J. A., Rippeth, T. P. and Maqueda, M. M. (2014), 'Observations of a diapycnal shortcut to adiabatic upwelling of Antarctic Circumpolar Deep Water', *Geophysical Research Letters* **41**(22), 7950–7956.

Smith, R. S., Dubois, C. and Marotzke, J. (2006), 'Global climate and ocean circulation on an aquaplanet ocean–atmosphere general circulation model', *Journal of Climate* **19**(18), 4719–4737.

Song, H., Song, H., Algeo, T. J., Tong, J., Romaniello, S. J., Zhu, Y., Chu, D., Gong, Y. and Anbar, A. D. (2017), 'Uranium and carbon isotopes document global-ocean redox-productivity relationships linked to cooling during the Frasnian-Famennian mass extinction', *Geology* **45**(10), 887–890.

Stigall, A. L. (2012), 'Speciation collapse and invasive species dynamics during the Late Devonian 'Mass Extinction'', *GSA Today* **22**(1), 4–9.

Stossel, I., Williams, E. A. and Higgs, K. T. (2016), 'Ichnology and depositional environment of the Middle Devonian Valentia Island tetrapod trackways, south-west Ireland', *Palaeogeography, Palaeoclimatology, Palaeoecology* **462**, 16–40.

Streel, M. (2000), 'Late Frasnian–Famennian climates based on palynomorph analyses and the question of the Late Devonian glaciations', *Earth-Science Reviews* **52**(1-3), 121–173.

Talley, L. D. (2003), 'Shallow, intermediate, and deep overturning components of the global heat budget', *Journal of Physical Oceanography* **33**(3), 530–560.

Talley, L. D., Pickard, G. L., Emery, W. J. and Swift, J. H. (2011), *Descriptive Physical Oceanography*, Elsevier LTD, Oxford.

Tansley, C. E. and Marshall, D. P. (2001), 'On the dynamics of wind-driven circumpolar currents', *Journal of Physical Oceanography* **31**(11), 3258–3273.

Torsvik, T. H. and Cocks, L. R. M. (2004), 'Earth geography from 400 to 250 ma: a palaeomagnetic, faunal and facies review', *Journal of the Geological Society* **161**(4), 555–572.

Torsvik, T. H., der Voo, R. V., Preeden, U., Niocaill, C. M., Steinberger, B., Doubrovine, P. V., van Hinsbergen, D. J., Domeier, M., Gaina, C., Tohver, E., Meert, J. G., McCausland, P. J. and Cocks, L. R. M. (2012), 'Phanerozoic polar wander, palaeogeography and dynamics', *Earth-Science Reviews* **114**(3-4), 325–368.

Waliser, D. and Jiang, X. (2015), Tropical meteorology and climate: Intertropical Convergence Zone, *in* 'Encyclopedia of Atmospheric Sciences', Elsevier, pp. 121–131.

Waterhouse, A. F., MacKinnon, J. A., Nash, J. D., Alford, M. H., Kunze, E., Simmons, H. L., Polzin, K. L., Laurent, L. C. S., Sun, O. M., Pinkel, R., Talley, L. D., Whalen, C. B., Huussen, T. N., Carter, G. S., Fer, I., Waterman, S., Garabato, A. C. N., Sanford, T. B. and Lee, C. M. (2014), 'Global patterns of diapycnal mixing from measurements of the turbulent dissipation rate', *Journal of Physical Oceanography* **44**(7), 1854–1872.

Watson, A. J., Ledwell, J. R., Messias, M.-J., King, B. A., Mackay, N., Meredith, M. P., Mills, B. and Garabato, A. C. N. (2013), 'Rapid cross-density ocean mixing at mid-depths in the Drake Passage measured by tracer release', *Nature* **501**(7467), 408–411.

Weaver, C. P. (2003), 'Efficiency of storm tracks an important climate parameter? The role of cloud radiative forcing in poleward heat transport', *Journal of Geophysical Research* **108**(D1).

Weber, T. and Thomas, M. (2017), 'Tidal dynamics and their influence on the climate system from the Cretaceous to present day', *Global and Planetary Change* **158**, 173–183.

White, D. A., Elrick, M., Romaniello, S. and Zhang, F. (2018), 'Global seawater redox trends during the Late Devonian mass extinction detected using U isotopes of marine limestones', *Earth and Planetary Science Letters* **503**, 68–77.

Whiteside, J. H. and Grice, K. (2016), 'Biomarker records associated with mass extinction events', *Annual Review of Earth and Planetary Sciences* **44**(1), 581–612.

Wilde, P. and Berry, W. (1984), 'Destabilization of the oceanic density structure and its significance to marine "extinction" events', *Palaeogeography, Palaeoclimatology, Palaeoecology* **48**(2-4), 143–162.

Williams, R. G. and Follows, M. J. (2011), *Ocean dynamics and the carbon cycle: Principles and mechanisms*, Cambridge University Press.

Willis, K. and McElwain, J. (2013), *The Evolution of Plants*, Oxford University Press.

Wilmes, S.-B. and Green, J. A. M. (2014), 'The evolution of tides and tidal dissipation over the past 21,000 years', *Journal of Geophysical Research: Oceans* **119**(7), 4083–4100.

Wilmes, S.-B., Schmittner, A. and Green, J. A. M. (2019), 'Glacial ice sheet extent effects on modeled tidal mixing and the global overturning circulation', *Paleoceanography and Paleoclimatology* .

Wilson, M. and Lyashkevich, Z. M. (1996), 'Magmatism and the geodynamics of rifting of the pripyat-dnieper-donets rift, east european platform', *Tectonophysics* **268**(1-4), 65–81.

Winton, M. (2000), 'A reformulated three-layer sea ice model', *Journal of Atmospheric and Oceanic Technology* **17**(4), 525–531.

Witzke, B. J. (1990), 'Palaeoclimatic constraints for palaeozoic Palaeolatitudes of Laurentia and Euramerica', *Geological Society, London, Memoirs* **12**(1), 57–73.

Wunsch, C. (2017), *Ocean Mixing*, Oxford University Press.

Wunsch, C. and Ferrari, R. (2004), 'Vertical mixing, energy and the general circulation of the oceans', *Annual Review of Fluid Mechanics* **36**(1), 281–314.

Yao, L., Aretz, M., Wignall, P. B., Chen, J., Vachard, D., Qi, Y., Shen, S. and Wang, X. (2020), 'The longest delay: Re-emergence of coral reef ecosystems after the Late Devonian extinctions', *Earth-Science Reviews* **203**, 103060.

Zhang, J. and Steele, M. (2007), 'Effect of vertical mixing on the Atlantic Water layer circulation in the Arctic Ocean', *Journal of Geophysical Research* **112**(C4).

Zhang, R. and Delworth, T. L. (2005), 'Simulated tropical response to a substantial weakening of the atlantic thermohaline circulation', *Journal of Climate* **18**(12), 1853–1860.

Zhang, R., Follows, M. J., Grotzinger, J. P. and Marshall, J. (2001), 'Could the Late Permian deep ocean have been anoxic?', *Paleoceanography* **16**(3), 317–329.

Zhisheng, A., Guoxiong, W., Jianping, L., Youbin, S., Yimin, L., Weijian, Z., Yanjun, C., Anmin, D., Li, L., Jiangyu, M., Hai, C., Zhengguo, S., Liangcheng, T., Hong, Y., Hong, A., Hong, C. and Juan, F. (2015), 'Global monsoon dynamics and climate change', *Annual Review of Earth and Planetary Sciences* **43**(1), 29–77.

Zhu, M., Ahlberg, P. E., Zhao, W. and Jia, L. (2002), 'Palaeontology: First Devonian tetrapod from Asia', *Nature* **420**(6917), 760–761.